Doctoral Thesis

Budding yeast protein phosphatase 4 promotes meiotic chromosome axis formation through Hop1 assembly

Ke Li

Laboratory of Genome and Chromosome functions
Department of Biological Science
Graduate School of Science
Osaka University

1. Content

1. Content 2

2. Abbreviation list 6

3. Abstract 8

4. Introduction 11

4.1. Significance of meiotic recombination 11

4.2. Architecture of the meiotic chromosome axis 12

4.3. Role of Hop1-Red1 complex in meiotic DSB formation 14

4.4. Molecular mechanism of meiotic recombination 15

4.5. Homologous axes are required for homolog synapsis 17

4.6. Down-regulation of axial Hop1 by AAA+ ATPase Pch2 18

4.7. Cooperation of PP4 and Mec1^{ATR}/Tel1^{ATM} kinases in DNA damage response 20

4.7.1. Mec1/Tel1 kinases and PP4 in mitosis 21

4.7.2. Mec1/Tel1 kinases and PP4 in meiosis 22

4.8. Purpose of my research 23

5. Materials and Methods 25

5.1. Strains 25

5.2. Spore viability and the distribution of viable spores 25

5.3. Meiosis time course analysis 25

5.4. Checking meiosis progress by DAPI staining 26

5.5. Meiotic nuclear spread by liposol method 27

5.6. Immunostaining of meiotic chromatin spread 27

5.7. Cytological analysis 28

5.8. Protein preparation 29

5.9. Western blotting 30

5.10. Genome DNA preparation 31

5.11. Southern blotting 32

5.12. Immunoprecipitation 34

6. Results 36

6.1. Novel role of PP4 activity in promoting Hop1 and Red1 loading by directly regulating Hop1 in a Mec1/Tel1 independent manner. 36

6.1.1. The *pph3-H112N* and *pph3Δ* mutants were equally delayed in meiosis progress. 36

6.1.2. Reduced spore viability in the *pph3* mutants 37

6.1.3. The *pph3* mutants showed delayed but longer observation of γH2A signal in meiosis. 38

6.1.4. Wild type level of Hop1 expression with delay in both phosphorylation and dephosphorylation of Hop1-pT318 in *pph3* mutants .. 38

6.1.5. Significant delay in Hop1 loading onto leptotene chromatin in the *pph3* mutants 39

6.1.6. Significant delay in loading of Red1, but not Rec8, onto leptotene chromatin in the *pph3* mutants 42

6.1.7. Wild type levels of expression of Red1 and Rec8 proteins in *pph3* mutants 43

6.1.8. Physical interaction of PP4 complex with Hop1 *in vivo* 44

6.1.9. Significantly delayed Hop1 loading caused by PP4 dysfunction even in *spo11-Y135F* mutation background 45

6.1.10. Meiosis-specific knockdown of Mec1/Tel1 kinases in the *pCLB2-MEC1 tel1Δ* background 46
6.1.11. Significantly delayed Hop1-Red1 loading caused by PP4 dysfunction in the *pCLB2-MEC1 tel1Δ* background 47
6.1.12. Defective assembly of Hop1 on meiotic chromatin in the *pph3Δ pch2Δ* mutant 48
6.1.13. Obvious Red1-related reduction in Rec8 linearization in the *pph3Δ pch2Δ* mutant 50
6.1.14. A genetic interaction between *PPH3* and *HOP1* 51
6.2. PP4 dysfunction causes ZMM protein-related decrease in crossover formation. 53
6.2.1. Synergistic defect in meiotic prophase I in the *pph3Δ pch2Δ* mutants 53
6.2.2. The *pph3* mutants showed a Mec1/Tel1-independent delay in the formation of meiotic DSBs 53
6.2.3. Delayed assembly of Rad51 onto meiotic chromatin in the *pph3* mutants 55
6.2.4. The comparable numbers of Rad51 foci per cell in the *pph3Δ pch2Δ* mutant and *pch2Δ* mutant 56
6.2.5. Pch2-independent decrease in assembly of Zip3 on chromatin in *pph3* mutants 57
6.2.6. Decreased crossover formation and increased noncrossover formation in meiotic recombination in the *pph3* mutants 58
7. Discussion 61
7.1. Novel role of PP4 activity in the formation of chromosome axis: promoting the loading of Hop1-Red1 complex onto chromatin by direct

regulating Hop1 62

7.2. Influences of defective Hop1-Red1 loading on meiotic recombination in the *pph3* mutants 64

7.3. Requirement of PP4 activity for efficient meiotic recombination depending on Mec1/Tel1 kinases 65

7.4. Defect and checkpoint activity in meiotic prophase I in the *pph3Δ pch2Δ* mutant 67

8. Acknowledgements 71

9. Tables 72

10. References 76

11. Figures and legends 93

2. Abbreviation list

APS: Ammonium peroxydisulfate

ATM: Ataxia-telangiectasia-mutated

ATR: ATM and Rad3-related

BPB: Bromophenol blue

BSA: Bovine serum albumin

CI: Confidence interval

CO: Crossover

DAPI: 6'-diamidino-2-pheylindole

DDR: DNA damage response

dHJ: double Hoilliday Junction

D-loop: Displacement-loop

DSB: Double strand break

DTT: Dithiothreitol

EDTA: Ethylenediaminetetraacetic acid

EtOH: Ethanol

HD: Heteroduplex

HEPES: 4-(2-hydroxyethel)-1-piperazineethanesulfonic acid

HR: Homologous recombination

IH: Inter-homologue

IS: Inter-sister

MES: 2-(*N*-morpholino) ethane sulfonic acid

MI: Meiosis-I

MII: Meiosis-II

NCO: Noncrossover

NHEJ: Non-homologous end joining

PFA: Paraformaldehyde

PPP: Phosphoprotein phosphatase

PSP: Protein serine/threonine phosphatase

RPA: Replication protein A

SC: Synaptonemal complex

SD: Standard deviation

SDS: Sodium dodecyl sulfate

SEI: Single end invasion

SEM: Standard error of the mean

SIC: Synapsis initiation complex

SUMO: Small -ubiquitin like modifier

S. V.: Spore viability

TAE: Tris acetate EDTA

TBS: Tris-buffered saline

TBST: Tris-buffered saline with Tween 20

TCA: Trichloroacetic acid

TE: Tris-EDTA

TEMED: N, N, N', N', tetramethyl ethylenediamine

Tris: Trishydroxymethylaminomethane

XC: Xylene cyanol

ZMM: Zip-Msh-Mer

3. Abstract

Meiosis consists of one round of DNA replication followed by two rounds of chromosome segregation, which produces four haploid gametes from one diploid cell. Meiotic crossover formation between homologs generates a physical connection called chiasma which is essential for the first round of homologous chromosomes segregation (meiosis I), and simultaneously increases genetic diversity in gametes. Crossover formation requires a meiosis-specific chromosome axis-loop structure, providing a scaffold for Spo11-dependent meiotic DNA double-strand break (DSB) formation to initiate crossover. During the onset of meiotic prophase I, meiotic chromatins are folded into a dense array of loops emanating from proteinaceous linear architecture called the meiotic chromosome axis. Therefore, the establishment of chromosome axes by hierarchical assemblies of axial components is significant for axis formation. In budding yeast, Rec8, Red1 and Hop1 are essential axial components. Rec8 generates fundamental structure for the loading of the Hop1-Red1 complex to form the meiotic chromosome axis. The Hop1-Red1 complex, the main regulator of meiotic recombination, exhibits dynamical distribution on chromosome axes involved in the recruitment of Spo11-accessory proteins to promote meiotic DSB formation. $Mec1^{ATR}$/$Tel1^{ATM}$ kinases, functioning as sensors in the DNA damage response pathway, phosphorylate Hop1 proximity to DSB site to activate meiotic DSB dependent checkpoint. Protein phosphatase 4 (PP4) counteracts $Mec1^{ATR}$/$Tel1^{ATM}$ kinases and dephosphorylates Hop1 to inactivate the meiotic checkpoint and promote the transition to meiosis I. In addition, it is also reported that PP4 is possible to be a component of the meiotic chromosome structure. Therefore, I would like to reveal if PP4 functions independently of meiotic DSB

formation in meiotic prophase I.

PP4 is a stable complex consisting of a Pph3 catalytic subunit and a Psy2 regulatory subunit. To avoid the structural effect of Pph3 protein absence, a catalytic-dead allele *pph3-H112N* was also analyzed besides the *pph3* null allele (*pph3Δ*) to elucidate the enzymatic necessity of PP4. In this study, I found the *pph3Δ* and *pph3-H112N* mutants showed delayed phosphorylation and dephosphorylation of Hop1 with the wild-type level of expression of Hop1 protein. Using immunostaining analysis, I revealed that the *pph3-H112N* and *pph3Δ* mutants show a significant delay in Hop1 and Red1 loading onto meiotic chromatin, but not in Rec8 loading. It suggested that the delayed phosphorylation of Hop1 was caused by delayed assembly of Hop1 protein onto chromatin. This delayed Hop1-Red1 loading caused by PP4 dysfunction was still observed in meiotic DSBs deficient mutation (*spo11-Y135F*) background, indicating the function of PP4 in Hop1 loading is meiotic-DSB independent. Moreover, the significant delay in Hop1 loading was not rescued in a $Mec1^{ATR}$/$Tel1^{ATM}$ meiosis-specific knockdown background (*pCLB2-MEC1 tel1Δ*), indicating this PP4 function is free from the $Mec1^{ATR}$/$Tel1^{ATM}$ activity. Co-immunoprecipitation analysis revealed that PP4 physically interacts with Hop1, but not with Red1 or Rec8. This suggests PP4 directly promotes recruitment onto chromatin or stabilization of Hop1 protein on chromosome axes. In addition, the deletion of the *PCH2* gene, which is required for Hop1 removal from the synapsed regions of chromosome axis, failed to restore Hop1 loading in the *pph3* mutants, indicating PP4 function is required for timely assembly of Hop1 protein onto chromatin.

Based on these results, I showed a novel role of PP4 activity which is completely distinguished from the known function of PP4 as a counteractor of $Mec1^{ATR}$/$Tel1^{ATM}$ kinases. That is during the onset of meiotic prophase I, PP4

promotes the loading of Hop1-Red1 onto chromatin which is required for the timely formation of meiotic DSBs and entire homolog synapsis. The comparable phenotype of *pph3-H112N* mutant and *pph3Δ* mutant indicates the requirement of PP4 catalysis, rather than structure, in this novel role. Therefore, I would like to propose a model that PP4 physically interacts and dephosphorylates Hop1 to promote efficient loading of Hop1-Red1 and form an axis-loop structure. In this model, Hop1 just after translation is phosphorylated possibly may explain the suppression of inappropriate binding Hop1 onto chromatin. I would like to discuss this novel role of PP4 activity in the regulation of meiotic chromosome morphogenesis in detail.

4. Introduction

4.1. Significance of meiotic recombination

The balance between genome integrity and genome diversity is maintained to allow adaptation to changing environments, which is crucial for the survival of species. Mostly eukaryotes reproduce sexually requiring gametes, which are generated through meiosis from diploid germ cells. Meiosis is an evolutionarily significant program of cell division in eukaryotes. Budding yeast, a model organism with a short life cycle, can survive in both haploid and diploid states. One diploid yeast cell can produce four haploid cells through meiosis, while two haploid yeast cells (respective mating type a and α) can mate to restore the diploidy state containing 16 pairs of homologous chromosomes. In this research, I utilized budding yeast to reveal the mechanism of meiosis.

The progress of meiosis is involved in only one round of DNA replication followed by two rounds of chromosome segregation **(Figure 1)**. The first round of chromosome segregation, termed meiosis I, occurs between homologous chromosomes. The second round, termed meiosis II, occurs between replicated sister chromatids. Meiosis II is similar to mitotic cell division. Meiosis is generally initiated from the G1 phase and starts with a specific pre-meiotic S-phase (Holm et al., 1979) during which DNA replication proceeds. The diploidy cell undergoes an extended meiotic prophase I when an inter-homologous physical connection called chiasma is formed. The chiasma is produced by repairing meiotic programmed double-strand breaks (DSBs) through crossover recombination between homologous chromosomes. Over 100 DSBs per yeast cell are progammedly induced during meiotic prophase I distributing along meiotic chromosomes. The formation of an obligate chiasma on each bivalent

chromosome is a prerequisite for the faithful execution of meiosis I. The regulation of obligate crossover formation, termed crossover assurance, prevents the mis-segregation of homologous chromosomes in meiosis I, which results in non-gametogenesis, aneuploidy, and a high rate of descendant mortality.

The proper formation of meiotic crossover requires a meiosis-specific structure called the meiotic chromosome axis (**Figure 2**). This meiotic chromosome axis is a linear proteinaceous architecture that begins to form at the onset of meiotic prophase. The chromosome axis orchestrates meiotic chromatin into a dense array of loops. The chromatin loops emanating from the axial element generate an axis-loop structure that provides a scaffold for the formation of meiotic DSBs. The chromatin regions attached to the axial element are poorly accessible, in contrast the chromatin loop regions are high accessible to DSB formation to initiate crossover recombination. Moreover, the axes of homologous chromosome, termed the homologous axes, are required for homolog synapsis that accompanies crossover recombination.

4.2. Architecture of the meiotic chromosome axis

The meiotic chromosome axis comprises the hierarchical assemblies of multiple axial components (**Figure 2A**). In particular, these include meiosis-specific proteins Rec8 and Hop1, a Hop1 partner protein Red1, and a serine/threonine kinase Mek1 (Leem & Ogawa, 1992; Rockmill & Roeder, 1991). The kleisin subunit Rec8 of the cohesin complex bundles sister chromatids following DNA replication (Klein et al., 1999; Watanabe & Nurse, 1999). Hop1 contains a HORMA domain in the N-terminal region from amino acid (a.a.) 1 to 255), which was named after three proteins sharing the same domain: Hop1, Rev7, and Mad2 (Hollingsworth & Byers, 1989; Hollingsworth et al., 1990).

The HORMA domain is involved in the regulation of checkpoint signaling. Structural analyses reveal that the HORMA domain in Hop1 physically interacts with Red1 (Rockmill & Roeder, 1988) through a short domain called closure motif (a.a. 340~362) (Woltering et al., 2000) (**Figure 2B**). A limited sequence homologous closure motif is also conserved in the Hop1 C-terminus (a.a. 585~605). This motif is possibly involved in the self-assembly of Hop1 though a transient and modest interaction with the HORMA domain (Aravind & Koonin, 1998; Hollingsworth & Ponte, 1997; Schwacha & Kleckner, 1994; Smith & Roeder, 1997; West et al., 2018). A coiled-coil domain conserved in the C-terminus of Red1 is also involved in Red1 self-assembly.

In the pre-meiotic S-phase, the Rec8-cohesin complex binds to regions of replicated DNA. Upon the onset of the meiotic prophase, Rec8 becomes enriched in intergenic regions of convergent genes. The coincident close contacts of these regions represent the fundamental basis of chromatin loops (**Figure 2A**) (Kugou & Ohta, 2009; Muller et al., 2018; Panizza et al., 2011; Schalbetter et al., 2019; Sun et al., 2015). Rec8 is a linker factor that is involved in the association between the cohesion of sister chromatids with the formation of chromosome axis. Rec8 on chromatin functions as a platform that determines the localization of Red1 and Hop1 on chromatin (Panizza et al., 2011; Sun et al., 2015). Red1 and Hop1 form a complex that is recruited to chromatin through an interaction between Rec8 and Red1 (Sun et al., 2015). Loading of the Hop1-Red1 complex mediated by Rec8 onto chromatin forms an axial element that generates a stable axis-loop structure.

In the absence of Rec8, although the axis-loop structure cannot be established, the Hop1-Red1 complex still loads on chromatin at a reduced level (Panizza et al., 2011). The latter finding indicates the loading of the Hop1-Red1

complex occurs in a cohesion-independent manner. Moreover, the formation of the Hop1-Red1 complex through the interaction between the HORMA domain and the closure motif is a prerequisite for initial loading of Hop1, but not Red1, onto chromatin. Hop1 fails to load onto chromatin in the absence of Red1 *in vivo*, even though Hop1 can bind to DNA *in vitro* (Chen et al., 2014). Localization of Red1 on chromatin is not influenced by the absence of Hop1 *in vivo* (Sun et al., 2015). Both *red1* and *hop1* mutants exhibit a partial and defective axis-like structure (Klein et al., 1999), but normal loading of Rec8 on chromatin (Sun et al., 2015). Interestingly, *rec8* mutants show a relatively mild reduction in the formation of meiotic DSBs, which reduces dramatically in *hop1* or *red1* mutants, resulting in extremely low spore viability (Hollingsworth & Byers, 1989; Klein et al., 1999; Rockmill & Roeder, 1988). These findings suggest that the loading of Hop1-Red1 complex on chromatin is regulated precisely, which is required for the formation of meiotic DSBs (Blat et al., 2002; Mao-Draayer et al., 1996; Schwacha & Kleckner, 1997; Woltering et al., 2000).

4.3. Role of Hop1-Red1 complex in meiotic DSB formation

The loading of the Red1-Hop1 complex is strongly correlated with the distribution of axial Rec8 (Sun et al., 2015). Hop1 and Red1 exert multiple functions in meiotic prophase I. These functions include promoting meiotic DSB formation, raising inter-homolog bias during repair template search and homolog synapsis (Blat et al., 2002; Hollingsworth & Byers, 1989; Klein et al., 1999; Mao-Draayer et al., 1996; Rockmill & Roeder, 1988; Roeder, 1990; Schwacha & Kleckner, 1997).

The Hop1-Red1 complex plays a significant role in meiotic DSB formation (**Figure 2C**). Meiotic DSBs are frequently induced in chromatin loop regions,

rather than regions attaching the axial element (Panizza et al., 2011; Sommermeyer et al., 2013). Hop1 recruits Spo11-accessory proteins that comprise the RMM complex (Rec114-Mei4-Mer2) to the axial element through an interaction with Mer2 (Zhang et al., 2020). The RMM complex prefers to bind on regions of the axial element where are enriched in Hop1 and Red1. The RMM complex then recruits Spp1 and Spo11 to promote meiotic DSB formation (Karányi et al., 2018; Prieler et al., 2005; Sommermeyer et al., 2013; Yadav & Claeys Bouuaert, 2021). Spp1 is a subunit of the Set1 histone-methyltransferase complex that catalyzes methylation of histone H3 at lysine 4 (H3K4). Spp1 contains a PHD finger domain, which can recognize the trimethylation of histone H3 lysine 4 (H3K4me3) in the chromatin loop by the Set1 complex, and tether the H3K4me3 region to the axial element (Borde et al., 2009; Sollier et al., 2004; Sommermeyer et al., 2013). Spo11 is a topoisomerase-like protein that cleaves DNA at the H3K4me3 region to generate DSB (Li et al., 2006; Sasanuma et al., 2007). In *hop1* and *red1* mutants, the formation of meiotic DSBs is markedly reduced, which results in low spore viability (Hollingsworth & Byers, 1989; Hollingsworth et al., 1990; Rockmill & Roeder, 1988).

Since meiotic DSBs are induced, the regulation of Hop1 and Red1 by $Mec1^{ATR}$/$Tel1^{ATM}$ kinases raises an inter-homologous bias in recombination template search (**Figure. 4**), which is essential for crossover formation. This aspect is discussed in detail in section **4.7.2**. Next, the molecular mechanisms of crossover recombination are considered.

4.4. Molecular mechanism of meiotic recombination

Programmed DSBs induced by Spo11 initiate meiotic crossover **(Figure 3)** (Keeney et al., 1997; Klapholz et al., 1985). The ends of a DSB site are

recognized by the MRX complex and resected by exonucleases, such as Exo1 (Gobbini et al., 2016; Mimitou & Symington, 2009; Zhu et al., 2008). The multi-stage resection generates extensive 3'-single strand DNA (ssDNA) overhang ends (Bonetti et al., 2010; Manfrini et al., 2010). Recombinase Rad51 (in both mitosis and meiosis) and Dmc1 (only in meiosis) bind to the 3'-ssDNA overhangs to form filaments which proceed the recombination template search. Rad51 filaments are mediated by many accessory proteins. In mitosis, Rad51 filaments drive the recombination template search between sister chromatids followed by ssDNA invasion. In meiosis, the activity of Rad51 is down-regulated through Hed1 and Mek1 activity (Busygina et al., 2008; Callender et al., 2016; Tsubouchi & Roeder, 2006). Recombination template search between homologous chromosomes is catalyzed by Dmc1 filaments, rather than by Rad51, to promote inter-homologous recombination (Liu et al., 2014). Binding of Dmc1 to 3'-ssDNA overhangs requires Rad51 and Mei5-Sae3 (Ferrari et al., 2009; Hayase et al., 2004). The invasion of the 3'-ssDNA overhang end into homologous double-strand DNA (dsDNA) catalyzed by Rad51 and Dmc1 generates an unstable recombination intermediate joint termed the displacement-loop (D-loop) (Paques & Haber, 1999; Petukhova et al., 2000; Shinohara et al., 2000).

DNA synthesis that proceeds from the invading 3'-ssDNA overhang end in stable the D-loop structure establishes a single end invasion structure (SEI). The second end capture of the 3'-ssDNA overhang advances the generation of another recombination intermediate designated the double Holliday Junction (dHJ). The dHJ is specifically resolved into reciprocal genetic exchanged production accompanied by the formation of the chiasma structure, which is defined as crossover recombination (Abdullah et al., 2004; Hunter & Kleckner, 2001; Novak et al., 2001). The major formation of crossovers in budding yeast

depends on the recruitment of Zip-Msh-Mer (ZMM) proteins on the recombination site to stabilize the D-loop structure. ZMM proteins is a generic term for multiple regulators involved in crossover assurance and interference. If the newly synthesized DNA stretch rewinds easily from the D-loop without ZMM proteins, it will be repaired through the synthesis-dependent strand annealing pathway without chiasma formation, which is defined as noncrossover recombination (McMahill et al., 2007).

ZMM proteins include Zip1 (Storlazzi et al., 1996; Sym et al., 1993), Zip2 (Chua & Roeder, 1998), Zip3 (Agarwal & Roeder, 2000), Zip4 (Tsubouchi et al., 2006), Msh4 (Novak et al., 2001; Ross-Macdonald & Roeder, 1994), Msh5 (Hollingsworth et al., 1995), Spo16 (Shinohara et al., 2008), and Mer3 (Nakagawa & Kolodner, 2002; Nakagawa & Ogawa, 1999). Among ZMM proteins, the assembly of Zip3 on recombination site is required for the recruitment of other ZMM proteins, especially Msh4 and Msh5. Msh4 and Msh5 form a heterodimer, which stabilizes D-loop structure to promote crossover formation (Agarwal & Roeder, 2000; Jessop et al., 2006; Novak et al., 2001; Ross-Macdonald & Roeder, 1994; Shinohara et al., 2008). We have demonstrated that a DNA damage checkpoint factor termed the 9-1-1 clamp (Rad17-Ddc1-Mec3) is involved in the recruitment of Zip3 (Shinohara et al., 2015). The 9-1-1 clamp is stimulated to load on the region adjacent to ssDNA and dsDNA. The assemblies of ZMM proteins are completely abolished in *9-1-1* mutants with a physical interaction between Zip3 and the 9-1-1 clamp. The finding suggests that the 9-1-1 clamp recruits ZMM proteins to promote crossover formation.

4.5. Homologous axes are required for homolog synapsis

As crossover recombination proceeds, homologous chromosomes are

synapsed on a genome-wide scale. Homolog synapsis indicates the physical connection through polymerization of the transverse filament Zip1 protein that contacts the two juxtaposed homologous chromosomes axes (**Figure 4**). Polymerization of Zip1 is initiated from the DSB site underwent crossover recombination in a zipper-like fashion, since ZMM proteins load and stabilize the D-loop structure. Polymerization of Zip1 completes throughout all bivalent chromosomes in the pachytene stage (Novak et al., 2001; Shinohara et al., 2015; Shinohara et al., 2008; Sym et al., 1993). Therefore, ZMM proteins are also termed the synapsis initiation complex. The tripartite proteinaceous structure constituted by homologous axial elements and a transverse element is called synaptonemal complex. Accompanied by the polymerization of Zip1, only axial Hop1 is evicted from the synapsed axial region, while Rec8 and Red1 remain on the axial element (Borner et al., 2008; San-Segundo & Roeder, 1999). In the pachytene stage, synaptonemal complexes are established throughout entire chromosomes when homologous chromosomes prepare to segregate in meiosis I. Therefore Hop1 displays a more dynamic loading on chromatin than Rec8 and Red1, which is regulated precisely. Homolog synapsis requires homologous chromosome axes. Homolog synapsis fails to proceed in *rec8*, *hop1*, and *red1* mutants (Hollingsworth & Byers, 1989; Klein et al., 1999; Rockmill & Roeder, 1988) meanwhile the formation of chromosome axis is intact in the absence of Zip1 or Zip3 (Herruzo et al., 2016; Zhu et al., 2010).

4.6. Down-regulation of axial Hop1 by AAA+ ATPase Pch2

The assembly and disassembly of Hop1 on chromosome axes are regulated appropriately and simultaneously to coordinate meiotic recombination and homolog synapsis. Since the onset of meiotic prophase, Hop1 and Red1 load on

chromatin to form axis-loop structure. This structure is required for the formation of meiotic DSB that initiates crossover recombination and homolog synapsis depending on ZMM proteins. As homolog synapsis proceeds, the regulation of Hop1 disassembly is enhanced to evict Hop1 from the axial element. While the regulatory factor of Hop1 loading onto chromatin is still unclear, an AAA+ ATPase termed Pch2 disassembles axial Hop1 from the synapsed axial elements (**Figure 5**) (Chen et al., 2014; Raina & Vader, 2020; San-Segundo & Roeder, 1999; West et al., 2018).

Pachytene checkpoint protein 2 (Pch2) is a hexametric ATPase that is conserved in mammals as TRIP13 (Eytan et al., 2014; Wojtasz et al., 2009). Pch2 is originally defined as a checkpoint mediator that prevent the segregation of homologous chromosomes when homolog synapsis is defective (Borner et al., 2008; San-Segundo & Roeder, 1999; Wu & Burgess, 2006). The absence of Pch2 rescues meiotic prophase arrest caused by incomplete synapsis in *zip1* mutant, but spore viability is reduced in *pch2 zip1* mutant. Recently, it is reported that the regulation of meiotic checkpoint (activation or inactivation) by Pch2 depends on both homolog synapsis level and the dynamic ratio of free Hop1 and axial Hop1 (Raina & Vader, 2020).

Importantly, Hop1 is completely absent from ribosomal DNA (rDNA) regions where Pch2 is only observed, but *pch2* null mutant undergoes obviously Hop1 assembly in rDNA regions. Moreover, the deletion of *PCH2* also prevents the eviction of axial Hop1, producing a complete linear morphology of Hop1 throughout all chromosome axes at pachytene (San-Segundo & Roeder, 1999), which is similar with Rec8 and Red1. In addition, biochemical analysis demonstrates that Pch2 binds Hop1 in a nucleotide-dependent fashion, while Pch2 displaces Hop1 from large DNA substrates. Both steps require ATP binding

and hydrolysis (Chen et al., 2014). The HORMA domain of Hop1 adopts two distinct conformational states. The closed one interacts with the closure motif. The relatively extended one disengages closure motif. This conformational change of HORMA domain is supposed to be regulated by Pch2 (Chen et al., 2014; West et al., 2018). Therefore, Pch2 possibly removes axial Hop1 by disrupting the interaction between the HORMA domain and the closure motif.

4.7. Cooperation of PP4 and Mec1^{ATR}/Tel1^{ATM} kinases in DNA damage response

To maintaining genome stability and integrity, DNA damage checkpoints and signaling cascades are highly conserved in eukaryotes. In budding yeast, Mec1, a homologue of ATR kinase, and Tel1, a homologue of ATM kinase, principally function as sensors in the DNA damage response pathway (Durocher & Jackson, 2001). Both Mec1 and Tel1 are serine/threonine kinases that share a target of consensus sequence, termed as [T/S] Q motif (Traven & Heierhorst, 2005). Multiple targets are phosphorylated by Mec1 and Tel1 kinases to activate checkpoint (arrest cell cycle) and promote DNA damage repair.

Protein phosphatase 4 (PP4) is a representative member of phosphoprotein phosphatases (PPPs), which generally consist of one catalytic subunit and multiple regulatory subunits determining substrate specificity. Pph3 is a catalytic subunit that associates with the regulatory subunit Psy2 to form the stable PP4 complex. PP4 is a protein serine/threonine phosphatase, which counteracts Mec1/Tel1 activity to promote checkpoint recovery in both mitosis and meiosis (Falk et al., 2010; Hoffmann et al., 1994; Hustedt et al., 2015; Keogh et al., 2006; Lai et al., 2011; O'Neill et al., 2007).

4.7.1. Mec1/Tel1 kinases and PP4 in mitosis

Exogenous and endogenous damage to DNA are constantly caused by ultraviolet light and oxygen free radicals. In mitosis, one DSB is sufficient to activate DNA damage checkpoint to arrest the cell cycle (van den Berg et al., 2018). Improper repair of DNA damage markedly increases the risk to genetic integrity.

Basic histone octamers consisting of H2A, H2B, H3, and H4 subunits associate and compact eukaryotic nuclear DNA generating nucleosomes to form chromatin (Luger et al., 1997). In budding yeast, a well-known Mec1/Tel1 consensus phosphorylation site in DNA damage response is defined as serine 129 of histone H2A (H2A-S129). Phosphorylated H2A-pS129 is usually termed γ-H2A (**Figure 6A**). It is also conserved as γ-H2AX in mammals (Chowdhury et al., 2008; Freeman & Monteiro, 2010; Nakada et al., 2008; O'Neill et al., 2007). Once DNA damage occurs, Mec1 together with binding partner Ddc2 is activated to approach damage site, and phosphorylates the adjacent H2A-S129. The γ-H2A at the damage site is required for efficient DNA damage repair (Downs et al., 2000). Moreover, Tel1 is functionally redundant with Mec1 in DNA damage response (Mantiero et al., 2007; Usui et al., 2001). The activated Mec1 and Tel1 cooperatively channel signal cascades of checkpoint until DNA damage repair is completed (Branzei & Foiani, 2006).

PP4 counteracts Mec1 and Tel1 activity in DNA damage response by dephosphorylating multiple targets of Mec1 and Tel1, including γ-H2A, when DNA damage is repaired (**Figure 6A**). Whereas it is recently reported that Mec1 itself is a target of PP4. PP4 physically interacts with Mec1 through an interaction between Ddc2 and Psy2. This interaction is required for the robust activation of Mec1 in the DNA damage response. Mec1 is activated inadequately in the

absence of PP4, resulting in an inefficient DNA damage repair (Hustedt et al., 2015).

4.7.2. Mec1/Tel1 kinases and PP4 in meiosis

Besides activating the meiotic checkpoint, Mec1/Tel1 kinases play multiple additional roles in meiotic recombination. These roles include promoting meiotic DSB formation, raising inter-homolog bias (Carballo et al., 2008; Cheng et al., 2013; Grushcow et al., 1999; Hong & Roeder, 2002), and crossover control which decides orientation of COs that provides sufficient spacing from each other (Shinohara et al., 2019). Hop1 contains multiple [T/S] Q consensus sites and is a meiosis-specific target of Mec1/Tel1. Axial Hop1 proximate to DSB site is phosphorylated by activated Mec1/Tel1 (**Figure 6B**). Among these target phosphorylation sites in Hop1, phosphorylation at threonine 318 (Hop1-pT318) activates $Mek1^{Rad53/Chk2}$, a meiotic paralog of the DNA damage effector kinase (Börner et al., 2008; Niu et al., 2005). These interactions generate a Red1 dependent inter-homologous bias during recombination template search in meiotic recombination (Carballo et al., 2008; Chuang et al., 2012). The failure in the phosphorylation at Hop1-T318 by Mec1/Tel1 provokes rapid Dmc1-independent inter-sister recombination. In addition, this phosphorylation at Hop1-T318 is also slightly involved in the formation of meiotic DSBs (Chuang et al., 2012).

PP4 catalyzes the dephosphorylation of Hop1-pT318 after meiotic recombination completes (Herruzo et al., 2016; Lo et al., 2014) (**Figure 6B**). This PP4 catalyzed dephosphorylation is related to meiotic checkpoint inactivation and promotes the transition to meiosis I. PP4 also promotes the pairing of centromeres by dephosphorylating Zip1-pS75 in an Mec1 dependent manner.

This role of Zip1 is distinct from the polymerization in homolog synapsis. The absence of Pph3 protein also produces a delay in pre-meiotic S-prophase and decreased crossover formation (Falk et al., 2010).

4.8. Purpose of my research

Mec1 plays multiple additional roles in meiotic recombination. These include promoting DSB formation, generating inter-homologous bias during recombination template search (Carballo et al., 2008; Chuang et al., 2012), and regulating crossovers distribution (Shinohara et al., 2019), as discussed above. The *pph3* mutant shows a complicated phenotype that includes delayed initiation of meiotic recombination, inefficient meiotic recombination, and decreased crossover formation. The molecular mechanisms of PP4 in meiosis remain mostly unclear, which is valuable to verify.

The establishment of chromosome axis architecture must be appropriately regulated for crossover recombination and homolog synapsis. How the chromosome axis is formed and the nature of the regulator(s) of the loading of axial components onto chromatin remain poorly understood. Concerning the loading of Hop1 on chromatin, the biochemical analyses have revealed that it may be involved in the regulation of post-transcriptional modification of Hop1 (West et al., 2018). Moreover, the Hop1 protein harbors multiple phosphorylation sites, which may indicate a possible role of phosphorylation in the regulation of Hop1 loading.

Here, I identified a novel role of PP4 activity in promoting the establishment of chromosome axis, which is required for the timely formation of meiotic DSBs to initiate meiotic recombination. The data demonstrate that PP4 promotes the efficient loading of Hop1 and Red1 through a direct interaction with Hop1 in a

Mec1/Tel1 kinases independent manner. Defective Hop1 assembly caused by the deletion of *PPH3* was observed even in the *pch2Δ* background. This finding reveals PP4 promotes the loading of Hop1 onto chromatin directly, rather than stabilize the binding of Hop1 on the axial element. The present study also revealed decreased Zip3 assembly relating to the localization of Hop1 on axial elements in the *pph3* mutants. The collective results suggest a relationship between the distribution of axial components and ZMM proteins-dependent crossover formation.

5. Materials and Methods

5.1. Strains

All strains used in this research were originated from the *Saccharomyces. cerevisiae* SK1 strains, NKY 1303/1543 (Storlazzi et al., 1996). *PSY2-13MYC* was constructed through a PCR-based tagging method (Bähler et al., 1998; Shinohara et al., 2015). *pph3-H112N* was constructed via two-step gene replacement. The genotype of strains used in the study are mentioned in Table 3 which are provided from Dr. M Shinohara.

5.2. Spore viability and the distribution of viable spores

Parental strains (*MATa / MATα*) were streaked together on YPAD (1% Bacto Yeast Extract, 2% Bacto Peptone, 2% Glucose, 0.004% Adenine, 1.6% Agar) plate over 6 hours at 30˚C. Then transferred the cells on SPM plate (0.3% CH_3COOK, 0.02% Raffinose) and incubated them at 30˚C overnight. Then suspended the cells in 200 μl of ZK buffer (25 mM Tris-HCl (7.5), 0.8 M KCl, 0.1 mg ml^{-1} Zymolyase 100T, 0.2% Glucose) and incubated at room temperature for 30 min. Added 100 μl of Distilled water into the culture. Dissected spores from one ascus manually using Zeiss Axioskop 40 microscope on DISS plate (1% Bacto Yeast Extract, 2% Bacto Peptone, 2% Glucose, 0.004% Adenine, 2.4% Bacto Agar) and Incubated at 30˚C for 2 day. Then counted the number of viable spores to evaluate spore viability. (Challa et al., 2019) More than 40 spores for each strain were analyzed.

5.3. Meiosis time course analysis

Spread diploid yeast cells stocking at -80˚C on YPG plate (1% Bacto Yeast

Extract, 2% Bacto Peptone, 2% glycerol, 1.6% Agar) and incubated at 30˚C for 6 hours. Then single colonies of each yeast strain were streaked out on YPAD plate and incubated for 2 days at 30˚C. One single diploid colony was inoculated into 3 ml of liquid YPAD medium (1% Bacto Yeast Extract, 2% Bacto peptone, 2% Glucose, 0.004% Adenine) then incubated at 30˚C for 24 hour while stirring. 2 ml of liquid YPAD culture was transferred into 200 ml of SPS medium (0.5% Bacto Yeast Extract, 1% Bacto peptone, 0.17% Yeast Nitrogen Base, 1% Potassium acetate, 0.5% Ammonium sulfate, 1.02% Potassium hydrogen phthalate). Then incubated at 30˚C with 230 rpm for 17 hours using Innova 44 shaker. The cells were transferred into a 500 ml centrifuge bottle and harvested by centrifugation at 6000 rpm for 5 min at 4˚C. Washed these cells with 30 ml of cold sterilized distilled water by 3 times. These yeast cells were suspended into 250 ml of SPM medium (0.3% Potassium acetate, 0.02% Raffinose) then incubated and shook at 30˚C with 230 rpm to initiate meiosis. The cells were collected at each meiotic time point.(Shinohara et al., 2003)

5.4. Checking meiosis progress by DAPI staining

Mixed 0.5 ml of SPM culture at each meiotic time point collected from **5.3.** with 0.5 ml of 100% cold EtOH. The cells were harvested by centrifuging at 5000 rpm for 1 min at 4˚C. Washed these cells with 500 μl of 1 M cold sorbitol twice. Then suspended cells into 50 μl of 1 M sorbitol containing DAPI (1 μg ml^{-1}). Applied 5 μl of suspension on slide glass and the nuclei of cells were observed with fluorescence microscope. Counted the number of cells exhibiting one nucleus, two and four nuclei respectively.

5.5. Meiotic nuclear spread by liposol method

5 ml of SPM culture from **5.3.** were collected at each time point. Then harvested cells by centrifuging at 3000 rpm for 2 min at room temperature in 15 ml screw cap tube. Suspended cells into 1 ml of ZK buffer with DTT (25 mM Tris-HCl (pH 7.5), 0.8 M KCl, 20 mM ml^{-1} DTT) by glass pasteur and incubated at room temperature for 2 min. Harvested cells by centrifuging at 3000 rpm for 2 min at room temperature and suspended cells into 1 ml of ZK buffer (25 mM Tris-HCl (pH 7.5), 0.8 M KCl, 0.1 mg ml^{-1} Zymolyase 100T, 0.2% Glucose) by glass pasteur. Incubated the suspension at 30˚C for 30 min. Then harvested cells by centrifuging at 2500 rpm for 2 min and washed the cells with 1 ml of cold MES/Sorbitol (1 M Sorbitol, 0.1 M MES (pH 6.5), 1 mM EDTA, 0.5 mM $MgCl_2$). Suspended the cells into 1 ml of MES/Sorbitol by glass pasteur to achieve the cell suspension.

Spotted 20μl of cell suspension on slide glass (S2441 micro slide glass, Matsunami glass IND., LTD) and applied 40 μl of cold and freshly-prepared PFA (4% Paraformaldehyde (SIGMA-ALDORICH), 1 M Sucrose), 80 μl of cold 1% liposol to cell suspension. Swirled the slide glass gently and observed the cell suspension by microscopy. Added 80 μl of PFA to fix cells when about 80% ~90% of nuclei have lysed. Widen the cell suspension overall slide glass with glass pasteur. Dried the glass up overnight and stocked in -20˚C. (Shinohara et al., 2015)

5.6. Immunostaining of meiotic chromatin spread

Washed the meiotic chromatin spread slide prepared from **5.5.** with 0.2 % Photo-flo 200 solution (Kodak) at room temperature for 2 min in Coplin jar. Then dried slide up for 10 min. Applied 500 μl of BSA/TBS (20 mM Tris-HCl (pH 7.5),

150 mM NaCl, 1% BSA (albumin from bovine serum, SIGMA)) to slide and incubated at room temperature for 15 min in moist chamber. Removed the BSA/TBS from slide glass. Then applied 90 μl of BSA/TBS containing primary antibody to slide and covered the slide glass with 24mm x 55 mm cover glass. The primary antibody used in the study are mentioned in Table. 1. Incubated the slide in moist chamber at 4˚C overnight. Removed the cover glass from slide by dropping slide into 200 ml of TBS solution (20mM Tris, 150 mM NaCl, pH 7.5). Washed the slide with TBS solution for 5 min 3 times in Coplin jar. Then dried the slide up for 20 min at room temperature. Applied 90 μl of BSA/TBS containing fluorescent-labeled secondary antibody to slide and covered slide with 24 mm x 55 mm cover glass. The secondary antibody used in the study are mentioned in Table. 2. Then incubated the slide at room temperature for 3 hours in moist chamber in black. Removed the cover glass from slide by dropping slide into 200 ml of TBS solution. Washed slide with TBS solution for 5 min 3 times and distilled water once in Coplin jar. Then dried the slide up for 20 min at room temperature. 13 µl of mounting medium (Vecta Shield with 1 µg ml^{-1} of DAPI) was applied to slide by three drops and covered mounting medium on slide glass with 24 mm x 50 mm cover glass. Sealed the edge of cover glass by nail polish after mounting medium spread all over the cover glass. The slide was stored in black box at 4°C and observed within one week.

5.7. Cytological analysis

The stained slide from **5.6.** was observed with an epi-fluorescence microscope (ZEISS AxioSkop2) with 100 × objective (NA1.4) and LED fluorescence light sources (X-Cite; Excelitas Technologies). Photos were captured by CCD camera (Retiga; Qimaging) and then processed by iVision

software (BioVision technologies). The cell containing over 5 foci was counted as focus positive cells. For the counting of foci number per nucleus, about 100 nuclei were analyzed at each time point.

5.8. Protein preparation

15 ml of SPM culture from **5.3.** were collected at each time point. Then harvested cells by centrifuging at 3000 rpm for 2 min at room temperature in 50 ml screw cap tube. Washed the cells with 10 ml of cold distilled water twice. Suspended cells into 1 ml of cold distilled water and transferred into 1.5 ml tube. Harvested cells by centrifuging at 3000 rpm for 2 min and suspended cells into 150 μl of 55% TCA (Trichloroacetic acid) and 500 μl of distilled water. Transferred the suspension into 2 ml bead-beating tube (Yasui Kikai Co. Ltd., Osaka, Japan) which has been added equivalent $\varnothing$ 0.5 mm low alkaline glass beads (Yasui Kikai Co. Ltd., Osaka, Japan). Disrupted the cells with multi-beads shocker (Yasui Kikai Co. Ltd., Osaka, Japan) by 90 s-on and 90 s-off repeated 5 times. Then laid the cell lysate on ice for 30min. Collected precipitation by centrifuging the cell lysate at 3000 rpm for 5 min at 4˚C in 2 ml safe-lock tube (Eppendorf). Suspended precipitation into 400 μl SDS-PAGE (Sodium Dodecyl Sulfate PolyAcrylamide Gel Electrophoresis) sample buffer (120 mM Tris-HCl (pH 6.8), 4% SDS, 10% β-mercaptoethanol, 10% glycerol, 0.04% Bromophenol Blue) and adjusted the pH of suspension to 8.8 with NaOH solution. Heated the suspension at 95˚C for 20 min and laid on ice for 10 min then centrifuging suspension at 15000 rpm for 10 min at 4 ˚C. Protein sample was harvested by collecting 300 μl of supernatant into new 1.5 ml tube and stocked in -20˚C. (Shinohara et al., 2015)

5.9. Western blotting

The protein sample of cell lysate from **5.8.** was used for SDS-PAGE electrophoresis to isolate protein. Then transformation was carried out to transfer protein from Polyacrylamide gel to 0.45 μm PVDF membrane (Immobilon-FL/Immobilon-P, MILLIORE) at 15 V for 45 min with semi-dry transfer cell (TRANS-BLOT SD, BIO-RAD). The transfer buffer contains 25 mM Tris, 0.2 M Glycine, 20% methanol. Treated PVDF membrane with blocking buffer (5% skim milk or 1% BSA in washing buffer or Blocking-one P (NacaIai Tesque)) at 10 ˚C for over 30 min to lock non-specific target sites of proteins on membrane. Incubated the membrane with primary antibody diluted in blocking buffer at 10˚C overnight. The primary antibodies used in this study are mentioned in Table. 1. Washed the membrane with washing buffer (20 mM Tris, 150 mM NaCl, 0.3% Tween-20) for 10 min 3 times. Then incubated the membrane with Alexa Fluor 680-/IR-Dye 800- conjugated secondary antibody or Alkaline Phosphatase secondary antibody diluted in blocking buffer at 10˚C for 2 hours. The secondary antibodies used in this study are mentioned in Table. 2. Washed the membrane with washing buffer for 10 min 3 time.

For Alexa Fluor 680-/IR-Dye 800- conjugated secondary antibody: washed the membrane with distilled water slight and scan the membrane with Odyssey (LiCOR). For alkaline phosphatase secondary antibody: incubated the membrane with 10 ml of AP reaction mix (100 mM Tris-HCl (pH 9.5), 100 mM NaCl, 5 mM $MgCl_2$) and 8 μl of BCIP-NBT (Nacalai tesque) at room temperature with shaker seesaw. Washed the membrane with distilled water when the bands were detected. Dried the membrane up and scanned.

5.10. Genome DNA preparation

20 ml of SPM culture from **5.3.** were collected at each time point. Then harvested cells by centrifuging at 3000 rpm for 2 min at room temperature in 50 ml screw cap tube. Suspended cell into 1 ml of 70% cold EtOH then transferred into 1.5 ml tube. Cells were harvested by centrifuging at 5000 rpm for 1 min again and suspended into 500 µl of Zymolyase buffer (10 mM Phosphate Buffer (pH 7.2), 10 mM EDTA, 0.1 M β-mercaptoethanol, 100 μg ml^{-1} Zymolyase 100T) by vortex. Then incubated suspension at 37°C for 30 min. Mixed fully the suspension with 5 µl of ProteaseK (0.1 mg ml^{-1}) and 100µl of lysing buffer (40 mM EDTA, 83 mM Tris, 0.4 % SDS). Incubated the mixture at 65°C for 1 hour and stirred mixture gently during incubation twice or 3 times. Then added 100 μl of 5 M potassium acetate into mixture and mixed them rapidly and gently. Laid the mixture on ice for 15 min. Centrifuged the mixture at 15000 rpm for 10 min at 4°C and transferred supernatant into 500 μl of 100% cold EtOH and mixed gently. Then precipitate was collected by centrifuging at 15000 rpm for 1 min at 4°C. Washed precipitate with 70% and 100% cold EtOH. Dried the precipitate up by evaporator for 10 min. 500 μl of 10:1 TE solution (10 mM Tris-HCl (pH 8.0), 1 mM EDTA, 10 μg ml^{-1} RNaseA) was applied to DNA precipitate. Laid it at room temperature for 30 min to degrade RNA. Then dissolved the DNA precipitate by rotating at 4˚C overnight.

Added 500 μl of 2-propanol to the DNA solution and mixed gently over 5 times. DNA precipitate was harvested by centrifuging at 15000 rpm for 1 min at 4˚C. Removed supernatant and washed DNA precipitate by 70% and 100% cold EtOH. Dried DNA precipitate up by evaporator for 10 min. Dissolved DNA precipitate into 100 μl of 10:1 TE solution by rotating at 4˚C overnight. Stocked the gDNA sample at 4˚C. (Shinohara et al., 2008)

5.11. Southern blotting

The restriction enzyme treatment was carried out firstly. For DSB analysis, incubated 20 μl of gDNA sample from **5.10.** with *Pst*I restriction enzyme (20 units) and 80 μl of reaction buffer (0.1 mg ml^{-1} BSA, 50 mM Tris-HCl (pH 8.0), 10 mM $MgCl_2$, 100 mM NaCl, 1 mM DTT) at 37˚C for 2 hours. For HD analysis, incubated 20 μl of gDNA sample from **5.10.** with *BamH*I (20 units), *Mlu*I (20 units), *Xho*I (10 units) and 80 μl of reaction buffer at 37˚C for 3 hours. After the retreatment of enzyme treatment, added 50 μl of 7.5 M CH_3COONH_4 solution and 100 μl of 2-propanol then mixed gently. The DNA fragments were collected by centrifuging at 15000 rpm for 10 min at 4˚C and washed with 70% and 100% cold EtOH. Dried the sample up with evaporator for 10 min. Applied 20 μl of DNA loading buffer (10 mM Tris-HCl (pH 8.0), 1 mM EDTA, Bromophenol Blue (BPB), Xylene Cyanol FF (XC), 0.1% SDS) and mixed to dissolve DNA fragment precipitation at room temperature over 1 hour.

Then Agarose electrophoresis was carried out to isolate DNA fragments. For DSB analysis, the DNA sample was isolated with 0.7 % (w/v) agarose gel (Agarose S, Nippon gene) at 50 Voltage in TAE buffer (40 mM Tris, 20 mM Acetic acid, 1 mM EDTA) until BPB ran 17 cm from well. Then gel was cut at 15 cm from wells for transformation. For HDs analysis, 20 μl of sample was isolated with 0.6 % agarose gel (Agarose HG, Nacalai tesque) at 50 Voltage until XC ran 17 cm from well. The gel was cut at 17 cm from bottom for transformation.

Then transformation was carried out. Treated the gel with 400 ml of 0.25 N HCl by horizontal shaker at room temperature for 30 min. Washed gel with distilled water twice. Then treated the gel with 500 ml of alkaline solution (0.6 M NaCl, 0.2 M NaOH) by horizontal shaker at room temperature for 20 min twice. Washed gel with distilled water twice. Treated gel with 500 ml of 25 mM

phosphate buffer (pH 6.5) by horizontal shaker at room temperature for 40 min. Transferred DNA from gel to membrane (Cilar Trans Nylon Membrane 0.45 μm; Wako) by capillary transfer at room temperature until all phosphate buffer was vaporized. Dried the membrane up then membrane is irradiated by XL-1000 UV crosslinker (SPECTROLINKER) at 1200 mJ cm^{-2} for stabilizing DNA binding on membrane.

Then Hybridization was carried out. Probe was prepared in advance. The plasmid (pNKY291 for DSB detection; pNKY155 for HD detection) was treated by *Pst*I and *EcoR*I and the products of DNA fragments were isolated by agarose electrophoresis. The DNA fragments between 1.4 kb~1.6 kb were purified by QIAGEN Gel purification kit as probe.

The membrane was incubated in hybrid bottle with 25 ml of hybrid buffer (7% SDS, 0.5 M Phosphate (pH 7.2), 0.01 M EDTA) in DNA OVEN (MI-100, KUABO) at 65˚C for at least 30 min for pre-hybridization. For one membrane of HD analysis or two membranes of DSB analysis, mixed 5 μl of primer mix (random primer 6 (NEB S1230S), 50 mM Tris-HCl (pH 8.0), 50 mM $MgCl_2$, 250 mM NaCl, 5 mM DTT) and 10 μl of probe. Heated the mixture at 95˚C for 5 min then laid on ice for 5 min. Added 10 μl of reaction mix (10 mM Tris-HCl (pH 8.0), 10 mM $MgCl_2$, 50 mM NaCl, 1 mM DTT; 0.2 mM dTTP, 0.2 mM dCTP, 0.2 mM dGTP (dNTP, Takara Bio)), 2.5 μl of α^{32}P-dATP (NEG512H, PerkinElmer), 0.25 μl of Klenow fragment (3'-5' exo-, M0210) to the mixture in turn and incubated the mixture at 37˚C for 15 min. Removed unlabeled nucleotide by centrifuging the mixture at 3000 rpm for 1 min in G-50 column. Heated the mixture at 95˚C for 5 min and laid on ice for 5 min. (Shinohara & Shinohara, 2013; Storlazzi et al., 1996)

After pre-hybridization, removed the used hybrid buffer in hybrid bottle and

added 10 ml of new hybrid buffer. Added the freshly-made probe above into hybrid bottle and continuously incubated membrane at 65˚C for overnight. Then removed the hybrid buffer in hybrid bottle and washed the membrane with washing buffer (1% SDS, 0.04 M Phosphate (pH 7.2), 0.01 M EDTA) for 5, 15 and 30 min 3 times. Dried the membrane up and contacted the membrane with IP plate overnight. Finally, scanned the membrane by IP-reader FLA-7000 and analyzed quantitatively by Image Quant TL software.

5.12. Immunoprecipitation

50 ml of SPM culture from **5.3.** at indicated time point was collected and harvested cells by centrifuging at 3000 rpm for 2 min at 4 ˚C. Washed cells with 50 ml cold distilled water twice. Then suspended cells into 1 ml of cold distilled water and transferred to 1.5 ml tube and stocked in -80 ˚C for immunoprecipitation.

The per-incubation of dynabeads protein G (Thermo Fisher Scientific, veritas) was carried out in advance. Washed dynabeads (30 μl/sample) with 1 ml of 0.5% (w/v) BSA/lysis buffer (50 mM HEPES-NaOH (pH 7.5), 0.15 M NaCl, 20% Glycerol, 1 mM Na_3VO_4, 60 mM β-Glycerophosphate) in low binding tube for 5 min twice at 4 ˚C. Then suspended dynabeads into 500 μl of 0.5% BSA/lysis buffer. Added (No. of samples) μl primary antibody and incubated at 4˚C rotating overnight.

Harvested cells by centrifuging sample from -80 ˚C at 5000 rpm for 1 min at 4 ˚C and washed cells with 1 ml of cold lysis buffer. Suspended cells in 500 μl of cold lysis buffer containing 0.1 % NP-40 and 5 μl of phosphatase inhibitor cocktail (Sigma-Aldrich, MERCK). Then transferred the suspension into 2 ml bead-beating tube (Yasui Kikai Co. Ltd., Osaka, Japan) and added equivalent ø 0.5 mm low alkaline glass beads (Yasui Kikai Co. Ltd., Osaka, Japan). Disrupted cells

with multi-beads shocker (Yasui Kikai Co. Ltd., Osaka, Japan) by 90 s-on and 90 s-off repeated 5 times. Removed low alkaline glass beads from cell lysate by centrifuging bead-beating tube held by 2 ml tube from bottom at 2000 rpm for 2 min at 4˚C. Transferred the supernatant into low binding tube after centrifuging cell lysate at 10000 rpm for 10 min 4˚C. Then Added 2.5 μl of 1 M $MgCl_2$ and 2 μl of DNase I (10 units) and incubated at 37˚C for 30 min.

Dynabeads after per-incubation were washed by 0.5% BSA/lysis buffer for 5 min twice. Suspended dynabeads into 30 *(No. of samples) μl of lysis buffer. Added 30 μl of pre-incubated dynabeads and 800 μl of lysis buffer into cell lysate after DNase I treatment. Mixed gently by rotator for 3 hours and washed dynabeads with lysis buffer for 5 min twice at 4˚C. Finally added 30 μl of SDS-PAGE sample buffer (120 mM Tris-HCl (pH 6.8), 4% SDS, 10% β-mercaptoethanol, 10% glycerol, 0.04% Bromophenol Blue) to dynabeads. Mixed dynabeads by vortex well during the incubation of mixture at 95˚C for 15 min. Removed dynabead and Stocked the supernatant sample in low binding tube at -80˚C. The samples were analyzed by western blotting.(Shinohara et al., 2008)

6. Results

6.1. Novel role of PP4 activity in promoting Hop1 and Red1 loading by directly regulating Hop1 in a Mec1/Tel1 independent manner.

6.1.1. The *pph3-H112N* and *pph3Δ* mutants were equally delayed in meiosis progress.

To determine PP4 activity in meiotic prophase I, I analyzed the phenotype of two mutations of *PPH3*, the gene encoding the catalytic subunit of PP4, during meiosis. Since PP4 binds to meiotic chromosomes (Falk et al., 2010), besides the *pph3*-null mutant (*pph3Δ*), a *pph3-H112N* mutant was analyzed to avoid the structural influence of the absence of Pph3 protein (**Figure 7A**). In Pph3-H112N, histidine 112 residue, which contributes to phosphate binding, is substituted to asparagine to generate a catalytic-dead allele of *pph3* mutant (Hustedt et al., 2015; O'Neill et al., 2007; Shi, 2009). *PSY2-13MYC* was constructed by conjugation of 13-repeat Myc epitope tag with the C-terminus of Psy2 in both the *PPH3* and *pph3-H112N* backgrounds (Bähler et al., 1998; Shinohara et al., 2015). The meiosis progress was analyzed by staining with 4′,6-diamidino-2-phenylindol (DAPI), which is defined as the percentage of cells that had already completed the first round of meiotic division (post-MI cells) at each time point during meiosis. Based on the wild type level of meiosis progress, the conjugation of Myc tag to Psy2 did not influence PP4 activity (**Figure 7B**). By immunostaining meiotic chromatin spread with MYC antibody, I localized PP4 on meiotic chromatin as a stable PP4 complex of Pph3 and Psy2. The foci of Psy2-13MYC were observed in *PPH3*, as also found previously (Falk et al., 2010), and also in the *pph3-H112N* mutant (**Figure 7C**). The finding indicated that Pph3-H112N protein is able to bind

with Psy2 and loads onto meiotic chromatin.

Then the meiosis progress by DAPI staining was analyzed in *pph3* mutants (**Figure. 7D**). In the wild type, the proportion of post-MI cells was 88.6 ± 1.4% (mean ± SEM, here and below) 8 hours after meiosis entry. The proportions in the *pph3Δ* and *pph3-H112N* mutants at the same time was 18.9 ± 2.9% and 12.1 ± 1.8%, respectively. Comparing the time in meiosis when the proportion of post-MI cells was 50% (wild type: 6 hour; *pph3Δ* and *pph3-H112N* mutants: 10 hour), a 4-hour delay in meiosis progression was observed in the *pph3-H112N* mutant confirming the previously reported result in the *pph3Δ* mutant (Falk et al., 2010). The finding indicates that PP4 catalytic activity, rather than a structural effect of Pph3 protein, is required for efficient meiosis progress.

6.1.2. Reduced spore viability in the *pph3* mutants

In addition to the delayed meiosis progress (**Figure 7D**), spore viability was also slightly reduced in the *pph3* mutants (**Figure 8**). The spore viability of 97% in the wild type (**Figure 8A**) was reduced to 88% in the *pph3Δ* mutants and to 80% in the *pph3-H112N* mutant (**Figure 8B and C**). The findings indicate that need for PP4 activity for the formation of viable spores.

The mis-segregation of chromosomes in meiosis I results in an increased percentage of asci containing even-numbered viable spores (0 #, 2 #), while the mis-segregation of chromosomes in meiosis II results in an increased percentage of asci containing odd-numbered viable spores (1 #, 3 #). The *pph3-H112N* mutant showed increased asci containing even-numbered viable spores (**Figure 8C**). The findings indicate that mis-segregation of homologous chromosomes in meiotic I increases in the *pph3-H112N* mutant. Together with the delayed meiosis progress, it was predicted that PP4 activity is required for proper segregation of

homologous chromosomes in meiotic I.

6.1.3. The *pph3* mutants showed delayed but longer observation of γH2A signal in meiosis.

γH2A was examined in the meiotic lysates of *pph3* mutants by western blotting (**Figure 9**), given the prior descriptions that the formation of meiotic DSB activates Mec1/Tel1 kinases to phosphorylate histone H2A-S129. The dephosphorylation of γH2A by PP4 as meiotic DSBs are repaired (Downs et al., 2000; Redon et al., 2003).

In wild type, γH2A bands were observed obviously from 3 hour after meiosis entry (Redon et al., 2003), and decreased continuously from 5 hour onward. In the *pph3Δ* and *pph3-H112N* mutants, γH2A bands were observed obviously beginning at 4 hour and accumulated until 10 hour, indicating delays in both the appearance and disappearance of γH2A bands. The *pph3-H112N* mutant displayed a phenotype comparable to the *pph3Δ* mutant concerning γH2A signals, confirming that the *pph3-H112N* mutation abolishes the catalytic activity of PP4 in meiosis. The accumulation of γH2A signals in both *pph3* mutants confirmed that PP4 activity is required for the dephosphorylation of γH2A in meiosis. In contrast, the delayed observation of γH2A signals in the *pph3* mutants indicated that PP4 promotes the phosphorylation of H2A-S129 in meiosis somehow, which was subsequently confirmed.

6.1.4. Wild type level of Hop1 expression with delay in both phosphorylation and dephosphorylation of Hop1-pT318 in *pph3* mutants

Given the introduction that Hop1 is a meiosis-specific chromosome

structural protein and Hop1-T318 is a meiosis-specific target of Mec1/Tel1 in meiotic recombination, I next analyzed the expression of Hop1 protein and phosphorylation of Hop1-T318 by western blotting in the *pph3* mutants (**Figure 10**). In wild type, Hop1 bands were observed beginning at 2 hour after meiosis entry. Comparable results were evident in the *pph3Δ* and *pph3-H112N* mutants. However, the *pph3Δ* and *pph3-H112N* mutants displayed similarly slight reductions in the expression of Hop1 protein at 2 hours. The latter findings may reflect a delay in pre-meiotic S-phase, as previously described in the *pph3Δ* mutant (Falk et al., 2010).

The Hop1-pT318 bands in wild type were observed from 3 to 5 hour as reported previously (Iwasaki et al., 2016). These findings indicated that meiotic DSBs began to form at 3 hour, with repair almost complete by 5 hour after meiosis entry. The *pph3-H112N* and *pph3Δ* mutants displayed delayed but longer presence of Hop1-pT318 bands, which were detected from 4 to 8 hour. The results of Hop1-pT18 were similar to the results of γH2A (**Figure 9**), suggesting delays in both phosphorylation and dephosphorylation in the *pph3* mutants. The accumulated signals of Hop1-pT318 and γH2A in the *pph3* mutants indicated a longer activated meiotic checkpoint as PP4 counteracts Mec1/Tel1 kinases, which has been previously established. Whereas, the delayed phosphorylation of Hop1-T318 and H2A-S129 in the *pph3* mutants remains to be revealed. Next, I analyzed Hop1 and the phosphorylation of Hop1-T318 in detail to determine if PP4 activity is involved in the formation of the chromosome axis.

6.1.5. Significant delay in Hop1 loading onto leptotene chromatin in the *pph3* mutants

The formation of the axis-loop structure by Hop1 loading onto chromatin is

essential for the normal formation of meiotic DSBs, while the phosphorylated Hop1-T318 (Hop1-pT318) can be used as a meiosis-specific DSB marker (Hollingsworth & Byers, 1989; Hollingsworth et al., 1990; Hollingsworth & Ponte, 1997; Niu et al., 2005; Panizza et al., 2011; Smith & Roeder, 1997). I analyzed the loading of Hop1 onto meiotic chromatin and the appearance of Hop1-pT318 foci by coimmunostaining meiotic chromatin spread with Hop1 antibody and Hop1-pT318 specific antibody in the *pph3Δ* and *pph3-H112N* mutants (**Figure 11**).

Hop1 loading on meiotic chromatin in wild type was evident morphologically as punctate foci and irregular segments, meanwhile Hop1-pT318 on nuclei were observed as punctate foci (**Figure 11A**) (Iwasaki et al., 2016; Penedos et al., 2015; Subramanian et al., 2016). There was no obvious difference in the morphologies of Hop1 and Hop1-pT318 on meiotic chromatin spread between wild type and the *pph3* mutants.

A focus positive cell displayed more than five Hop1/Hop1-pT318 foci or segments in the meiotic nucleus. The kinetics of Hop1-pT318 foci and Hop1 loading permitted determination of the percentages of focus positive cells at each time point after meiosis entry (**Figure 11B and D**). In wild type, Hop1-pT318 foci were observed in 58.3 ± 3.1% (mean ± SEM, here and subsequently) of the cells at 3 hour, with a peak of 68.7 ± 3.2% at 4 hour and subsequent decrease to 7.5 ± 1.8% at 6 hour (**Figure 11B**). The *pph3Δ* and *pph3-H112N* mutants showed delayed observation of Hop1-pT318 foci on meiotic chromatin spread. Hop1-pT318 foci were observed in only 8.7 ± 3.1% and 10.4 ± 6.8% of cells in the *pph3Δ* and *pph3-H112N* mutant at 3 hour, respectively, with increased to 64.2 ± 4.2% and 70.4 ± 5.4%, respectively, at 6 hour. The delayed observation of Hop1-pT318 foci on meiotic chromatin spread in the *pph3* mutants was consistent with

the western blotting results presented above (**Figure 10**), confirming that PP4 activity is involved in promoting the phosphorylation of Hop1-T318. However, the distribution of Hop1-pT318 foci numbers per cell indicated that the *pph3Δ* and *pph3-H112N* mutants had comparable number of Hop1-pT318 foci as wild type at 4 and 5 hours after meiosis entry (**Figure 11C**).

On the other hand, Hop1 loading on meiotic chromatin spread in wild type was observed in 50.9 ± 3.9% of cells at 2 hour, with a peak between 3 hour (75.6 ± 1.0%) and 4 hour (74.1 ± 3.5%), and a subsequent decrease (9.7 ± 2.7%) at 6 hours (**Figure 11D**). The *pph3Δ* and *pph3-H112N* mutants showed similar delays in both loading and disassembly of Hop1. Hop1 loading was observed in only 6.7 ± 3.6% and 8.6 ± 6.9% of cells at 2 hour which increased to 76.5 ± 2.2% and 83.6 ± 4.1% at 6 hour in the *pph3Δ* and *pph3-H112N* mutants, respectively. The *pph3* mutants showed significant delays in the loading of Hop1 at 2 hour comparing to wild type (**Figure 11E**). These findings indicate that PP4 activity is involved in the efficient loading of Hop1 onto meiotic chromatin. Interestingly, comparison of the percentages of Hop1 and Hop1-pT318 focus positive cells in individual strains revealed an obvious gap between the percentages of Hop1 and Hop1-pT318 focus positive cells at 2 hour in wild type (**Figure 11F**), which was not observed in the *pph3* mutants (**Figure 11G and H**). These observations indicate that the delayed Hop1 loading is caused not only by the defective pre-meiotic S-phase in the *pph3* mutants. It was possible that the delayed loading of Hop1 leads to a delayed formation of axis-loop structure which is required for the formation of meiotic DSBs.

The collective results indicate a possibility that PP4 activity promotes the efficient loading of Hop1 to form chromosome axis. Therefore, as presented next, I analyzed if PP4 activity also regulates other axial components, such as Red1

and Rec8.

6.1.6. Significant delay in loading of Red1, but not Rec8, onto leptotene chromatin in the *pph3* mutants

The architecture of the chromosome axis is established by hierarchical assemblies of multiple axial components. The Hop1-Red1 complex loads onto chromatin (Rockmill & Roeder, 1988; Smith & Roeder, 1997) determined by the Rec8 present on chromatin (Panizza et al., 2011; Sun et al., 2015). Thus, I next examined Rec8 and Red1 loadings by immunostaining of meiotic chromatin spreads with Rec8 antibody and Red1 antibody (**Figure 12**).

In wild type, Red1 mostly overlapped with Rec8 on meiotic chromatin, typically as punctate foci and segments at 3 hour after meiosis entry. The *pph3* mutants did not show obvious differences in the morphology of Red1 on meiotic chromatin spread.

A Red1 focus positive cell was defined as having a nucleus that contains more than five foci or segments. The kinetics of Red1 loading enabled the determination of the percentage of Red1 focus positive cells at each time point after meiosis entry (**Figure 12B**). The pattern of Red1 kinetics was similar to the pattern of Hop1 kinetics (**Figure 11D**). In wild type, the loading of Red1 on meiotic chromatin spread were observed in 47.0 ± 5.7% (mean ± SEM, as subsequently) of cells at 2 hour. The kinetics of Red1 loading revealed a peak at 4 hour (80.6 ± 2.5%) followed by a decline to 21.1 ± 5.7% at 6 hour. Meanwhile, the kinetics of Red1 loading in the *pph3Δ* and *pph3-H112N* mutants showed that Red1 was observed only in 19.1 ± 4.3% and 21.6 ± 8.6% of cells at 2 hour, increasing to 79.9 ± 2.8% and 82.5 ± 2.7% at 6 hour respectively. Red1 loading at 2 hour in the *pph3Δ* mutant was significantly reduced compared to that in wild type (**Figure**

12C).

In contrast, the morphology of Rec8 on meiotic chromatin was altered dramatically during meiotic prophase I. At the onset of meiotic prophase, Rec8 binding on chromatin was evident as punctate foci. Following the loading of the Hop1-Red1 complex, the axis element formed partially accompanying dotty Rec8 aggregates as a short segment. At pachytene, Rec8 linearized throughout the entire chromosomes accompanied with homolog synapsis which was evident as a complete linear structure. The change of Rec8 morphology on chromatin allowed the determination of the progression of meiotic prophase I.

Even the *pph3Δ* mutant also showed a slight delay in Rec8 loading onto leptotene chromatin at 2 hour, there was no significant difference between wild type and the *pph3* mutants (**Figure 12D**). I analyzed the Rec8 focus positive cell and divided the morphology of Rec8 on meiotic chromatin spread into 3 kinds as dotty, partial and linear. The *pph3* mutants showed an obvious delay in Rec8 linearization. The linear Rec8 fraction peaked at 4 hour in wild type (**Figure 12E**). The *pph3* mutants showed the comparable fraction of linear Rec8 at 6 hour (**Figure 12F and G**) indicating a delayed homolog synapsis.

The collective results indicated that PP4 dysfunction caused a significant delay in the loading of Hop1 and Red1 onto leptotene chromatin, not in the loading of Rec8.

6.1.7. Wild type levels of expression of Red1 and Rec8 proteins in *pph3* mutants

The expressions of Red1 and Rec8 proteins were also analyzed as a precaution, as both are meiosis-specific proteins (**Figure 13**). Rec8 bands were observed beginning at 2 hour in wild type, as also reported previously (Challa et

al., 2019). In the *pph3Δ* and *pph3-H112N* mutants, Rec8 bands were also observed beginning at 2 hour (**Figure 13A**). The expression of Red1 protein in *pph3Δ* and *pph3-H112N* mutants was similar to that in the wild type. Red1 bands were observed beginning at 2 hour in wild type and the *pph3* mutants (**Figure 13B**). Rec8 and Red1 bands showed a slight delay at 2 hour in the *pph3* mutants, similar to Hop1 protein. However, significant delay was only observed in the loading of Hop1 and Red1 onto leptotene chromatin. The delay in the loading of Hop1-Red1 essentially differed from the delay in the loading of Rec8. The latter may possibly reflect the delayed pro-meiotic S-phase in the *pph3Δ* mutant (Falk et al., 2010). The findings indicate a novel role of PP4 activity, which promotes the loading of Hop1-Red1 onto chromatin to form the chromosome axis during the onset of prophase. The next experiment analyzed if there is any physical interaction between PP4 and axial components.

6.1.8. Physical interaction of PP4 complex with Hop1 *in vivo*

To assess the involvement of PP4 activity in the formation of the chromosome axis by regulating the loading of Hop1-Red1 during meiotic prophase I, immunoprecipitation was performed using the *PSY2-13MYC* strain, since Psy2 and Pph3 formed a stable PP4 complex (**Figure 14**). Yeast meiotic lysates at 2, 4, and 6 hour after meiosis entry in *PSY2-13MYC* and *PSY2* were immunoprecipitated with anti-MYC antibody. Interaction between Hop1 and Psy2 was observed from 2 hour to 4 hour after meiosis entry, but was not detected at 6 hours. Meanwhile no physical interaction between Psy2 and Rec8 or Red1 was evident. The collective findings indicate that PP4 promotes the efficient loading of Hop1-Red1 complex to form chromosome axes by a physical interaction between PP4 and Hop1 during meiotic prophase I. Next, I analyzed if this function

of PP4 activity depends on the formation of meiotic DSBs.

6.1.9. Significantly delayed Hop1 loading caused by PP4 dysfunction even in *spo11-Y135F* mutation background

The examination of Hop1 loading in the *spo11-Y135F* background permitted the determination on whether this role of PP4 activity depends on the formation of meiotic DSBs or not (**Figure 15**). The *spo11-Y135F* mutation is a catalytic-dead allele of *SPO11* which fails to induce meiotic DSB to initiate meiotic recombination (Bergerat et al., 1997). Therefore no chiasma is produced, resulting in extremely reduced spore viability in the *spo11-Y135F* background.

No Hop1-pT318 band was detected in the *spo11-Y135F* background, confirming the absence of induced meiotic DSBs to activate Mec1, which in turn phosphorylates Hop1-T318 (**Figure 15A**). The expression of Hop1 protein in the *spo11-Y135F* and *spo11-Y135F pph3-H112N* mutants were detected beginning at 2 hour (**Figure 15A**). DAPI immunostaining revealed that *pph3-H112N* mutation introduced a delay in meiosis progress even in the *spo11-Y135F* background (**Figure 15B**).

The loading of Hop1 was analyzed. On meiotic chromatin spread, Hop1 still displayed dotty or irregular segment morphology in the *spo11-Y135F* background (**Figure 16A**). The kinetics of Hop1 loading was defined as discussed above (**Figure 16B**). The loading of Hop1 was evident in 39.3 ± 10.4% (mean ± SEM, here and subsequently) of the cells at 2 hour, with a peak at 4 hour (69.0 ± 5.3%) and subsequently decrease to 20.3 ± 11.3% at 8 hour in the *spo11-Y135F* mutant. In the *spo11-Y135F pph3-H112N* mutant the loading of Hop1 was observed in only 1.0 ± 1.0% of cells at 2 hour, which increased to 63.3 ± 8.0% at 6 hours then decreased to 40.5 ± 11.0% at 8 hours. The significantly delayed loading of Hop1

in leptotene caused by PP4 dysfunction was still observed in the *spo11-Y135F* background (**Figure 16C**). These collective results revealed the role of PP4 activity in promoting the loading of Hop1 independent of the formation of meiotic DSBs, possibly prior to meiotic recombination.

The detected physical interaction between PP4 complex and Hop1 and the observation that the catalytic-dead allele of *pph3-H112N* had a similar phenotype to the *pph3Δ* mutant supported the prediction that the dephosphorylation of Hop1 by PP4 activity is probably required for the efficient loading of Hop1-Red1 onto chromatin. However, the kinase(s) responsible remain unresolved. As PP4 is a general PPP, the involvement of Mec1 and Tel1 kinases seems to be probable options based on the known characterizations of PP4. Therefore, the next experiment was performed to assess if the promotion of Hop1-Red1 loading by PP4 activity depends on Mec1/Tel1 or not.

6.1.10. Meiosis-specific knockdown of Mec1/Tel1 kinases in the *pCLB2-MEC1 tel1Δ* background

I tried to build a background in which Mec1 activity was completely inhibited in meiosis (**Figure 17).** Checking the phosphorylation of Hop1-T318 permitted the examination of the activity of Mec1/Tel1 kinases in meiosis. *MEC1* is an essential gene for cell growth and checkpoint in budding yeast. However, the *mec1-null* mutant (*mec1Δ*) displays high lethality, which prevents analysis. For resolve this obstacle, the suppressor of Mec1 lethality gene (*SML1*) was deleted to suppress the high lethality in the *mec1Δ* mutant (Zhao et al., 1998). *SML1* is a non-essential gene whose deletion can bypass the essential role of Mec1 in growth. However, the induction of meiosis could not be synchronized stably in the *mec1Δ sml1Δ* mutant. Hop1-pT318 bands were still observed in the *mec1Δ sml1Δ*

background, indicating a deficient inhibition of activation in meiotic checkpoint (**Figure 17A**). Therefore, attempts to analyze this background were abandoned.

Next, I utilized the promotor mitotic cyclin Clb2 (*pCLB2*) to construct the *pCLB2-MEC1* allele. The *pCLB2* promotor regulates mitosis specific gene expression and the *pCLB2-MEC1* allele causes meiosis-specific shutdown of *MEC1* transcription (Lee & Amon, 2003). However, in the present study, Hop1-pT318 bands were still observed in the *pCLB2-MEC1* background (**Figure 17B**). As Tel1 kinase functions redundantly in the phosphorylation of Hop1-T318 with Mec1 kinase, *TEL1* was further deleted to construct a *pCLB2-MEC1 tel1Δ* background. Phosphorylation of Hop1-T318 was completely abolished in the *pCLB2-MEC1 tel1Δ* background (**Figure 17C**). Therefore, I analyzed the loading of Hop1-Red1 onto chromatin in the *pCLB2-MEC1 tel1Δ* background.

6.1.11. Significantly delayed Hop1-Red1 loading caused by PP4 dysfunction in the *pCLB2-MEC1 tel1Δ* background

The kinetics of Hop1-pT318 foci and Hop1 loading were analyzed by immunostaining in the *pCLB2-MEC1 tel1Δ* background (**Figure 18A**). In the *pCLB2-MEC1 tel1Δ* background, even though a few Hop1-pT318 foci were still observed, both the intensity and numbers of Hop1-pT318 foci per cell decreased dramatically (**Figure 18B and C**). The findings indicate a substantial difference of the Hop1-pT318 foci in the *pCLB2-MEC1 tel1Δ* background compared to that in wild type (**Figure 11C**).

More importantly, the *pCLB2-MEC1 tel1Δ* mutation did not produce any effect on the loading of Hop1 (**Figure 18D**). The loading of Hop1 were observed in 48.5 ± 4.1% (mean ± SEM, here and subsequently) of cells at 2 hour, with an increase to 83.5 ± 4.1% at 4 hour followed by a decrease to 43.0 ± 8.5% at 6 hour

in the *pCLB2-MEC1 tel1Δ* mutant. In the *pCLB2-MEC1 tel1Δ pph3Δ* mutant, the loading of Hop1 were observed in 14.8 ± 4.5% of cells at 2 hour, with an increased to 69.0 ± 1.7% at 5 hour and a slight decrease to 63.0 ± 6.8% at 6 hour. The significant delay in the loading of Hop1 at 2 hour caused by PP4 dysfunction was still detected in the *pCLB2-MEC1 tel1Δ* background (**Figure 18E**).

Next, the loading of Red1 was analyzed in the *pCLB2-MEC1 tel1Δ* background (**Figure 19A**). The loading of Red1 was observed in 56.3 ± 3.7% of cells at 2 hour, increased to 77.9 ± 2.0% at 3 hour, then decreased to 22.0 ± 1.9% at 6 hour in the *pCLB2-MEC1 tel1Δ* mutant (**Figure 19B**). In the *pCLB2-MEC1 tel1Δ pph3Δ* mutant, the loading of Red1 was observed in 26.9 ± 5.1% of cells at 2 hour, increased to 75.1 ± 1.9% at 4 hour then decreased to 43.7 ± 4.6% at 6 hour. The loading of Red1 at 2 hour was reduced significantly in the *pCLB2-MEC1 tel1Δ pph3Δ* mutant compared to the *pCLB2-MEC1 tel1Δ* mutant (**Figure 19C**).

PP4 dysfunction postponed the loading of Hop1-Red1, even in the *pCLB2-MEC1 tel1Δ* background. The finding indicates that PP4 activity probably promotes the timely loading of Hop1-Red1 independent of Mec1/Tel1 kinases.

6.1.12. Defective assembly of Hop1 on meiotic chromatin in the *pph3Δ pch2Δ* mutant

Axial Hop1 (the Hop1 on axial element) is very dynamically regulated by assembly and disassembly simultaneously during meiotic prophase I. The delayed loading of Hop1-Red1 onto chromatin in the *pph3* mutants indicates that PP4 activity is possibly involved in promoting the loading of Hop1-Red1 directly, or in stabilizing the binding of Hop1-Red1 on the axial element. Pch2 is a down-regulator of axial Hop1, which evicts Hop1 from the synapsed axial element (Chen et al., 2014; San-Segundo & Roeder, 1999). Therefore, the gene of *PCH2*

was deleted to block the removal of axial Hop1 from axial element (**Figure 20**). If PP4 promotes the loading of Hop1-Red1 directly, the defect in the loading of Hop1-Red1 in the *pph3Δ* mutant cannot be rescued by the deletion of *PCH2*. If PP4 stabilizes the binding of Hop1 on the axial element, the defective loading of Hop1-Red1 in the *pph3Δ* mutant will be restored in the absence of Pch2.

The expression of Pch2 protein was not observed in the *pch2Δ* mutants (**Figure 20A**). As the role of PP4 activity in the loading of Hop1 was independent of meiotic DSB formation and Mec1/Tel1 kinases, coimmunostaining of Hop1 and Zip1, (the latter is a transverse protein in the synaptonemal complex), instead of Hop1-pT318, was performed (**Figure 20B**). No colocalization of Hop1 and Zip1 was observed in wild type, which displayed a few segmental Hop1 signals and linear Zip1 signals on meiotic chromatin spread. As meiosis I was initiated at 6 hour in wild type (**Figure 7D**), Hop1 and Zip1 signals were not observed. Hop1 and Zip1 signals accumulated on meiotic chromosomes until 6 hours in the *pph3Δ* mutant, but only a little segmental Hop1 and few colocalizations of Hop1 and Zip1 were observed. In the *pch2Δ* mutant, the Hop1 signal on meiotic chromatin spread was obviously more intense and displayed a linear morphology in both unsynapsed and synapsed axial regions at 4 hour. Homolog synapsis was completed at 6 hour when Hop1 overlapped with linear Zip1 throughout entire chromosomes. The *pph3 pch2* double mutant showed an obvious defect in Hop1 assembly on meiotic chromatin spread. Segmental and dotty Hop1 signals were observed without linear Zip1 signals on meiotic chromatin at 4 hour. Although the linear Hop1 signals colocalized with linear Zip1 signals in some regions at 6 hour, faint dotty Hop1 signals remained detectable in the unsynapsed regions. Compared to the assembly of Hop1 on the unsynapsed regions in the *pch2Δ* mutant at 4 hour, the *pph3Δ pch2Δ* mutant showed a defect in the assembly of

Hop1 on the unsynapsed regions, indicating a defective assembly of Hop1 on meiotic chromatin. Although the *pch2Δ* and *pph3Δ pch2Δ* mutants showed comparable kinetics of Hop1 loading (**Figure 20C**), I analyzed the numbers of linear Hop1 signals per cell at 6 hour. The numbers of linear Hop1 signals per nucleus was reduced significantly in the *pph3Δ pch2Δ* mutant (median: 9 linear Hop1) compared with the *pch2Δ* mutant (median: 12 linear Hop1) (**Figure 20D**). No difference was defected in the lengths of linear Hop1 signals between the *pph3Δ pch2Δ* and *pch2Δ* mutants (**Figure 20E**).

The deletion of *PPH3* introduced a defect in the assembly of Hop1 on meiotic chromatin in the *pch2Δ* background, which suggested that PP4 directly promotes the loading of Hop1, rather than stabilizing Hop1 binding on the axial element. Moreover, in the *pph3Δ pch2Δ* double mutant, the defect in Hop1 assembly caused a significant reduction in Zip1 polymerization, indicating an incomplete homolog synapsis and the risk of mis-segregation of homologous chromosomes in meiosis I.

6.1.13. Obvious Red1-related reduction in Rec8 linearization in the *pph3Δ pch2Δ* mutant

To reveal if the defective Hop1 assembly in the *pph3Δ pch2Δ* double mutant resulted from upstream influence, the loading of Rec8 and Red1 was also analyzed in the *pch2Δ* background (**Figure 21**). Red1 signals overlapped with Rec8 signals on meiotic chromatin spread in both unsynapsed and synapsed regions at 4 hour in the *pch2Δ* mutant. As homolog synapsis was completed at 6 hour, the linear signals of Red1 overlapped with Rec8 signals throughout entire chromosomes. Moreover, the *pph3Δ pch2Δ* double mutant showed an obvious defect, similar to Hop1, in the assembly of Red1 on meiotic chromatin. In the

pph3Δ pch2Δ mutant at both 4 and 6 hour, Rec8 binding regions remained where no Red1 signal was observed. The fractions of Rec8 morphology on meiotic chromatin were analyzed in the same way in the *pch2Δ* background. The *pph3Δ pch2Δ* mutant showed an obvious reduction in Rec8 linearization from the *pch2Δ* mutant **(Figure 21B)**. The fraction of linear Rec8 decreased robustly even at 6 hour in the *pph3Δ pch2Δ* mutant **(Figure 21C).**

These results in the *pch2Δ* background suggest that the Rec8 binding regions without Hop1-Red1 loading failed to perform homolog synapsis, while most Hop1-Red1 loading regions performed normal homolog synapsis. These findings indicate that PP4 activity promotes the loading of Hop-Red1 onto meiotic chromatin, which is required for the homolog synapsis of entire chromosomes.

6.1.14. A genetic interaction between *PPH3* and *HOP1*

A KIS motif (a.a. 593~595) is highly conserved in the closure motif of Hop1 protein, which plays an important role in Hop1 function (Friedman et al., 1994; Niu et al., 2005). The mutation in the KIS motif (*hop1-S595N*) markedly reduces the formation of meiotic DSBs (Hollingsworth & Johnson, 1993). Moreover, unpublished results from our laboratory indicate that Hop1-S595 is phosphorylated. I constructed a unphosphorylable allele *hop1-S595L*, which is not phosphorylated at serine 595, to determine if there is any correlation between the phosphorylation of Hop1-S595 and the role of PP4 in promoting the loading of Hop1 onto chromatin.

The *hop1-S595L* mutant showed hypomorphic defects in the Hop1 function, meanwhile the *hop1-S595L* and *pph3-H112N* mutations showed synergistic defect, such as the delayed meiosis progress **(Figure 22A)** and decreased spore viability **(Figure 22B and C).** The distribution of viable spores in the *hop1-S595L*

pph3-H112N mutant suggests mis-segregation of homologous chromosomes, indicating defective meiotic prophase I. Therefore, the loading of Hop1 and the phosphorylation of Hop1-T318 was analyzed in the *hop1-S595L* background **(Figure 22D)**. The *hop1-S595L* mutant showed a normal loading of Hop1 onto meiotic chromatin **(Figure 22E)**, while the *hop1-S595L pph3-H112N* mutant still showed a significant delay in the loading of Hop1 onto leptotene chromatin **(Figure 22F)**. The findings indicated that the loading of Hop1 by PP4 is independent of the phosphorylation of Hop1-S595. Interestingly, a slight reduced expression of Hop1 protein was restored by PP4 dysfunction in the *hop1-S595L* background **(Figure. 22G)**, indicating a genetic interaction between *PPH3* and *HOP1*.

As a short summary, the preceding results define a novel role of PP4 activity in promoting the loading of Hop1-Red1 onto chromatin to form the chromosome axis through a physical interaction with Hop1. This role of PP4 activity is not independent of meiotic DSB formation and Mec1/Tel1 kinases. In the next experiments, I assessed if the defective formation of chromosome axis caused by PP4 dysfunction could produce any substantive effect on meiotic recombination.

6.2. PP4 dysfunction causes ZMM protein-related decrease in crossover formation.

6.2.1. Synergistic defect in meiotic prophase I in the *pph3Δ pch2Δ* mutants

The spore viability was 91% in the *pch2Δ* mutant with a wild type level of distribution of viable spores (**Figure 23A**). Spore viability was dramatically reduced to 25% in the *pph3Δ pch2Δ* double mutant with the increased ratio of asci containing 0# or 2# viable spores (**Figure 23B**). This distribution of viable spores indicated frequent mis-segregation of homologous chromosomes in meiosis I in the *pph3Δ pch2Δ* mutant, supporting my supposition of mis-segregation in meiosis I **(see Results 6.1.12.**).

The *pph3Δ pch2Δ* mutant showed a longer delay in meiosis progress compared to the *pph3Δ* and *pch2Δ* single mutants (**Figure 23C**). This finding indicated that the deletion of *PCH2* failed to restore delayed meiosis progress in the *pph3* mutants. Deletion of *PCH2* can restore the delayed meiosis progress in *zip1* mutant as Pch2 mirrors the defect in homolog synapsis to arrest meiosis I (Börner et al., 2008; San-Segundo & Roeder, 1999). Therefore, the defect occurring in the *pph3Δ* mutant is likely more than homolog synapsis (Zip1 polymerization). The possibility of any defect in crossover formation in the *pph3* mutants was assessed.

6.2.2. The *pph3* mutants showed a Mec1/Tel1-independent delay in the formation of meiotic DSBs.

The formation of meiotic DSB in the *pph3* mutants was assessed by utilizing the well-known hotspot *HIS4-LEU2* on chromosome III by southern blotting (**Figure 24**) (Schwacha & Kleckner, 1994). There are two DSB sites present in

the *HIS4-LEU2* hotspot (**Figure 24A**). In addition to parental signals, signals of DSBs were observed as two smeared bands from 3 to 4 hour in wild type, while the signals of DSBs were observed from 3 to 8 hour in the *pph3* mutants (**Figure 24B**).

The kinetics of meiotic DSB I signals were analyzed quantitatively (**Figure 24C**). In wild type, 20.1% ± 1.8% and 22.7 ± 3.5% of total DNA harbored meiotic DSB at DSB I site at 3 and 4 hour respectively. The DSB signals decreased to 4.3% ± 1.0% at 8 hour. In the *pph3Δ* and *pph3-H112N* mutants, the detection rates of DSB signals were 10.5 ± 2.5% and 7.6 ± 3.1% at 3 hour, with an increase to 23.2 ± 2.5% and 23.6 ± 2.0%, respectively, at 5 hour followed by a gradual decrease. However, 10.1 ± 1.7% and 13.8 ± 1.1% of the DSB signals remained at 8 hour in the *pph3Δ* and *pph3-H112N* mutants, respectively.

Quantitative analysis of meiotic DSB formation revealed no significant difference in the peaks of DSB signals between wild type and the *pph3* mutants. However, the *pph3* mutants showed a delay in the formation of meiotic DSB. The signals of meiotic DSB at 3 hour in the *pph3Δ* and *pph3-H112N* mutants were reduced significantly to half of that in wild type (**Figure 24D**). The findings indicated an inefficient induction of meiotic DSB, which confirmed the delayed formation of chromosome axis in the *pph3* mutants.

The induction of meiotic DSB at *HIS4-LEU2* hotspot in the *pCLB2-MEC1 tel1Δ* background was also examined (**Figure 25)**. Quantitative analysis of the DNA blot image in the *pCLB2-MEC1 tel1Δ* mutant (**Figure 25A**) showed DSB signals beginning at 3 hour (7.1 ± 2.4%), with a peak at 4 hour (7.7 ± 3.9%) followed by a decreased to 2.3 ± 0.4% at 8 hour. The *pCLB2-MEC1 tel1Δ pph3Δ* mutant displayed decreased formation of DSB, with 2.1 ± 1.8% at 3 hour, 5.3 ± 1.0% at 4 hour and 2.1 ± 1.3% at 8 hour (**Figure 25B**). The findings indicated that

the deletion of *PPH3* caused a decrease in the formation of meiotic DSB even in the *pCLB2-MEC1 tel1Δ* background. The findings are consistent with the role of PP4 activity in promoting the formation of chromosome axis independent of Mec1/Tel1 kinases.

6.2.3. Delayed assembly of Rad51 onto meiotic chromatin in the *pph3* mutants

Next, I analyzed the kinetics of the assembly Rad51 on chromatin in the *pph3* mutants (**Figure 26**). The Rad51 recombinase is recruited to ssDNA overhands of meiotic DSB ends to drive homolog search with Dmc1. Then Rad51 dissociates from DSB sites accompanying meiotic recombination proceeds. Therefore, Rad51 assembly on meiotic nuclei can be a predictive marker of DSB formation and repair in meiotic recombination. (Schwacha & Kleckner, 1997; Shinohara et al., 2000; Shinohara & Shinohara, 2013)

Meiotic chromatin spreads at each meiotic time point were immunostained with anti Rad51 antibody. The signals of Rad51 on chromatin were observed as punctate foci (Shinohara et al., 2000) (**Figure 26A**). There was no difference in the morphology of Rad51 foci between wild type and the *pph3* mutants. A Rad51 focus positive cell was defined as having a nucleus with more than five Rad51 foci. The kinetics of Rad51 assembly allowed the determination of the percentage of Rad51 focus positive cells at each time point (**Figure 26B**). In wild type, 66.4 ± 4.0% (mean ± SEM, here and subsequently) of Rad51 focus positive cells were observed at 3 hour, with an increase to 72.8 ± 2.9% at 4 hour, then a marked decrease to 6.8 ± 1.7% at 6 hour. The *pph3Δ* and *pph3-H112N* mutants showed poorly efficient Rad51 assembly. Only 18.1 ± 5.2% and 23.3 ± 12.4% of Rad51 focus positive cells were observed at 3 hour in the *pph3Δ* and *pph3-H112N*

mutants, respectively. At 6 hours after meiosis entry, the respective values were 73.4 ± 4.2% and 70.5 ± 4.9%. The distributions of the number of Rad51 foci per individual cell were also analyzed at 3, 4, and 5 hour (**Figure 26C**). In wild type, a median of 64 Rad51 foci were observed per cell at 3 hour, which decreased to a median of 42 foci per cell at 5 hour. In the *pph3Δ* mutant, the median numbers of Rad51 foci per cell were 56 at 3 hour, 49 at 4 hour and 50 at 5 hour. The median numbers of Rad51 foci per cell in the *pph3-H112N* mutant were 48.5 at 3 hour, 51 at 4 hour, and 50 at 5 hour. The distributions of Rad51 foci numbers per individual cell in the *pph3* mutants were slightly reduced at 3 hour, but were still comparable at their peaks with the numbers of Rad51 foci in wild type.

The results of Rad51 assembly were consistent with the southern blot analysis of meiotic DSB formation at *HIS4-LEU2* hotspot (**Figure 24**), indicating a delay in the formation of meiotic DSB during meiotic prophase I in the *pph3* mutants. The findings support the delayed formation of chromosome axis in the *pph3* mutants, which is required for the formation of meiotic DSBs.

6.2.4. The comparable numbers of Rad51 foci per cell in the *pph3Δ pch2Δ* mutant and *pch2Δ* mutant

The kinetics of Rad51 assembly were also analyzed in the *pch2Δ* background (**Figure 27**)**.** Morphologically, Rad51 foci on meiotic chromatin spread were still observed as punctate foci in the *pch2Δ* background (**Figure 27A**). The median number of Rad51 foci per cell was 48 at 3 hour and decreased to 30 at 6 hour in the *pch2Δ* mutant. The respective median number at 3 and 6 hour in the *pph3Δ pch2Δ* mutant were 53 at 3 hour and 42 at 6 hour (**Figure 27B**). The median number in the *pph3Δ pch2Δ* mutant were comparable with the numbers in the *pch2Δ* mutant at peak, which indicated the quantity of meiotic

DSBs at 3 hour was not influenced by the deletion of *PPH3* gene in the *pch2Δ* background.

The localizations of Hop1-pT318 and Hop1 on meiotic chromatin spread were analyzed in the *pch2Δ* background (**Figure 27C**). The signals of Hop1-pT318 foci were distributed along the linear Hop1 signals on meiotic chromosomes in the *pch2Δ* mutant. Interestingly, in the *pph3Δ pch2Δ* mutant, Hop1-pT318 foci were observed in both regions displaying linear and faint dotty Hop1 signals. These findings indicated that the faint dotty Hop1 loading on chromatin could recruit RMM proteins to induce DSB in the *pph3Δ pch2Δ* mutant, but failed to proceed with homolog synapsis. The next experiment was performed to analyze the assembly of Zip3 on the meiotic chromatin, which is required for crossover formation and homolog synapsis.

6.2.5. Pch2-independent decrease in assembly of Zip3 on chromatin in *pph3* mutants

The Zip3 component of ZMM proteins (San-Segundo & Roeder, 1999) is required for the recruitment of other ZMM proteins at sites of DSBs to promote crossover recombination and homolog synapsis (**Figure 3 and 4**). Therefore, Zip3 is usually analyzed as a marker of meiotic crossover formation. As only crossover recombination can initiate homolog synapsis and produce chiasma structure, which are essential for the proper segregation of homologous chromosomes in meiosis I, the proper assembly of Zip3 is significant for meiosis I.

The signals of Zip3 on meiotic chromatin were observed as punctate foci (**Figure 28A**). The peak distribution of Zip3 foci numbers per cell was analyzed. Deletion of the *PPH3* gene resulted in decreased numbers of Zip3 foci per cell in

both wild type and *pch2Δ* background (**Figure 28B and C**). The median peak number of Zip3 foci per cell was 75 in wild type. The median peak number of 47 in the *pph3Δ* mutant represented a significant decrease (**Figure 28B**). In the *pch2Δ* background, the deletion of *PPH3* significantly reduced the median number of Zip3 foci per cell from 70 to 40 (**Figure 28C**). The findings suggest a defective Zip3 assembly caused by PP4 dysfunction and independent of Pch2.

In the *pch2Δ* mutant, Zip3 foci were distributed along the signals of linear Hop1 on meiotic chromosomes, except for the ribosomal DNA region. In the *pph3Δ pch2Δ* mutant, in addition to decreased Zip3 assembly, Zip3 foci were observed only in the regions exhibiting the signals of linear Hop1, which was different from Hop1-pT318 foci (**Figure 28D**). These findings together with the data of the distribution of Rad51 foci numbers (**Figure 27B**) and localization of Hop1-pT318 foci (**Figure 27C**) indicate that DSBs induced in regions displaying faint dotty Hop1 signals may fail to recruit Zip3, leading to an incomplete homolog synapsis in the *pph3Δ pch2Δ* mutant.

6.2.6. Decreased crossover formation and increased noncrossover formation in meiotic recombination in the *pph3* mutants

It has been demonstrated that the *pph3Δ* mutant shows a *zmm* mutant-like phenotype in meiotic recombination, with decreased crossover formation and increased noncrossover formation (Falk et al., 2010). To clarify if this phenotype is caused by the absence of PP4 catalysis, the products of meiotic recombination were analyzed at the *HIS4-LEU2* hotspot in the *pph3-H112N* mutant (**Figure 29**). The heteroduplexes (HDs) of recombination intermediator at the *HIS4-LEU2* hotspot were detected as previously reported (Storlazzi et al., 1996). HDs formed through both crossover recombination (HD2 and 3) and noncrossover

recombination (HD1 and 4) (**Figure 29A**). In wild type, the HD signals were detected as smeared bands beginning at 4 hour after meiosis entry. The *pph3Δ* and *pph-H112N* mutants showed a similar delay in the observation of HDs signals (**Figure 29B**).

The kinetics analysis of the total HDs production (**Figure 29C**) revealed that in wild type 1.1 ± 1.0% of total DNA was repaired to produce HDs at 4 hours after meiosis entry, which increased to 4.1 ± 0.4% at 6 hours. In the *pph3Δ* and *pph3-H112N* mutants, the total products of HDs were detected as only 0.2 ± 0.4% of total DNA at 4 hour which increased to 4.1 ± 0.2% and 3.9 ± 1.4% at 8 hour respectively. Interestingly, the ratio of crossover-HD products (HD 2 and HD 3) to noncrossover-HD products (HD 1 and HD 4) revealed similar phenotype of the *pph3-H112N* and *pph3Δ* mutants (**Figure 29D**). The ratio in wild type (0.9 ± 0.1; mean ± SEM) indicated a relatively equal formation of crossover and noncrossover products. However, the ratios in the *pph3Δ* and *pph3-H112N* mutants were significantly reduced to 0.4 ± 0.1 and 0.46 ± 0.0, respectively, indicating PP4 dysfunction results in a remarkable decreased crossover formation and an increased noncrossover formation. Moreover, in the *pph3* mutants, the formation of crossover was reduced to two-thirds that of wild type, which was consistent with the decreased Zip3 assembly (**Figure 28B**). The findings suggest that the catalytic activity of PP4 is required for sufficient ZMM-dependent crossover formation.

As a short summary, these results suggest that there is a delay in the initiation of meiotic recombination, which supports the delayed formation of chromosome axis in the *pph3* mutants. Moreover, the defective homolog synapsis was supported by the decreased Zip3 assembly caused by PP4

dysfunction. This was correlated to the defective localization of Hop1-Red1 on meiotic chromatin in the *pch2Δ* mutant.

7. Discussion

The proteinaceous architecture of meiotic chromosome axes provides fundament for both meiotic recombination and homolog synapsis. The axial Hop1 is a prerequisite for the recruitment of Spo11 accessory proteins to induce meiotic DSB (Keeney et al., 1997; Klapholz et al., 1985; Panizza et al., 2011). Hop1 proximity to a DSB site is phosphorylated at T318 by Mec1/Tel1 kinase, which promotes inter-homologous recombination (Carballo et al., 2008). Moreover, axial Hop1 also coordinates crossover recombination and homolog synapsis. Therefore, the proper assembly and disassembly of Hop1 are significant for meiosis I. Recently, it is reported that the loading of Hop1 onto chromatin displays a chromosome size-dependent characterization, preferentially binding on the three shortest chromosomes (Chr I, III, VI) prior to other chromosomes (Murakami et al., 2020). However, this regulatory mechanism of Hop1 loading to form chromosome axis is still unclear.

The catalytic-dead Pph3-H112N protein was able to bind on chromosomes (**Figure 7C**), which introduced a delay in meiosis progress in both wild type (4 hours) and *spo11-Y135F* background (2 hours) (**Figure 7D and 15B)**. These findings indicate that PP4 activity is required for meiosis progress from at least two perspectives: independent from and dependent on the formation of meiotic DSBs. The meiotic DSBs-dependent mechanism concerns PP4 counteracts Mec1/Tel1 kinases in meiotic recombination (Falk et al., 2010). The findings of the present study defines the independent mechanism as a novel role of PP4 activity in promoting the formation of the chromosome axis through Hop1 assembly. Moreover, the defective formation of the chromosome axis in the *pph3* mutants seems to be related to a decreased ZMM proteins-dependent crossover

formation.

7.1. Novel role of PP4 activity in the formation of chromosome axis: promoting the loading of Hop1-Red1 complex onto chromatin by direct regulating Hop1

The *pph3Δ* and *pph3-H112N* mutants showed significantly delayed loadings of Hop1 and Red1, but normal Rec8 binding on chromatin (**Figure 11E, 12B and C**) accompanied with the wild type level of proteins expression (**Figure 10 and 13**). Physical interaction with Rec8 or Red1 was not detected in meiotic prophase I, but a physical interaction of PP4 complex with only Hop1 was evident even when Hop1-T318 was not yet phosphorylated (**Figure 10 and 14**). Moreover, the delayed loading of Hop1 caused by PP4 dysfunction in the meiotic DSB deficient background (*spo11-Y135F*) indicates that this role of PP4 activity is independent of meiotic DSBs formation and might occur prior to meiotic recombination (**Figure 16C**). In addition, the deletion of *PPH3* also introduced a significant delay in the loading of Hop1 and Red1 in a Mec1/Tel1 meiosis-specific knockdown background (*pCLB2-MEC1 tel1Δ*) (**Figure 18E and 19C**). The findings indicate that this role of PP4 activity is probably independent of Mec1 and Tel1 kinases.

Deletion of *PPH3* still introduced an obvious defect in the loading of Hop1 and Red1 in the *pch2Δ* background, even though Pch2 is a down-regulator of axial Hop1 that removes Hop1 from synapsed axial regions (**Figure 20B**). The findings indicate that PP4 activity promotes the loading of Hop1-Red1 onto meiotic chromatin directly, rather than stabilizing the binding of Hop1-Red1 on the axial element.

The collective results defined a novel role of PP4 activity that promotes the loading of Hop1 and Red1 to form the chromosome axis through a physical

interaction with Hop1. The *pph3Δ* and *pph3-H112N* mutants displayed a comparable phenotype in the cytological analyses, indicating the significance of PP4 catalytic activity in this novel role.

Interestingly, Hop1 is able to bind on DNA substrate *in vitro* (Chen et al., 2014). However, Hop1 fails to load on chromatin without the presence of Red1 *in vivo* and the formation of Hop1-Red1 complex via the strong interaction between the HORMA domain of Hop1 and the closure motif of Red1 is essential for the loading of Hop1 (Blat et al., 2002; Hollingsworth & Ponte, 1997; Rockmill & Roeder, 1988; Woltering et al., 2000). The localization of the Hop1-Red1 complex is correlated to Rec8 on chromatin through an interaction between Rec8 and Red1. However, the complex still can bind on chromatin through Hop1 at a reduced level in a *rec8* mutant (Panizza et al., 2011).

The present model explains the novel role of PP4 activity in promoting the loading of Hop1-Red1 (**Figure. 30A**). Just after translation, the Hop1 protein is phosphorylated to suppress the random and improper loading onto chromatin. PP4 physically interacts and dephosphorylates Hop1 to promote the formation of the Hop1-Red1 complex. This complex Hop1-Red1 is recruited to the Rec8 binding region to form chromosome axes and generate the stable axis-loop structure. In the absence of PP4 catalytic activity, the Hop1-Red1 complex loads onto chromatin inefficiently. Moreover Red1 can load onto chromatin itself through the interaction with Rec8 (Panizza et al., 2011). Therefore the delay in Red1 loading was relatively milder than Hop1 in the *pph3* mutants.

Another possibility is that the formation of Hop1-Red1 complex might disengage the C-terminus of Hop1, which exhibits a structure-specific DNA binding activity (Khan et al., 2013). The sequence homologous closure motif is conserved in the C-terminus of Hop1, which interacts modestly with HORMA

domain to promote self-assembly of Hop1. These interactions give rise to a topological change of HORMA domain, which is possibly regulated by the post-translational modification of Hop1 (West et al., 2018).

Deletion of C-terminus of Hop1 introduces a *hop1*-null mutant comparable defect. Thus, it is also possible that the stable localization of the Hop1-Red1 complex on chromatin requires both the interaction between Red1 and Rec8, and the binding of C-terminus of Hop1 on chromatin. PP4 activity may be involved in the latter. However, the target site of dephosphorylation in Hop1 by PP4 activity that promotes Hop1 assembly is still unclear. Our previous phospho-proteomics analysis in extracts of yeast cells arrested in meiotic prophase I demonstrated the phosphorylation at Hop1-S595 in the closure motif of Hop1, which was possibly due to Mek1/Mre4 kinase (Shinohara M., unpublished result). The *hop1-S595L* mutation (unphosphorylatable allele) did not results in a phenotype compared with wild type including the formation of meiotic chromosome axis, meiosis progress and spore viability. More severe defects in meiotic prophase I were observed upon PP4 dysfunction in the *hop1-S595L* mutant, supporting the possible genetic correlation for PP4 activity and closure motif of Hop1.

7.2. Influences of defective Hop1-Red1 loading on meiotic recombination in the *pph3* mutants

Based on the present results, the defective Hop1-Red1 loading on meiotic chromatin in the *pph3* mutants influences meiotic recombination in two ways. First, the inefficient loading of Hop1-Red1 in the *pph3* mutants indicates that delayed formation of the axis-loop structure postpones the formation of meiotic DSBs. This was confirmed by the delays in the phosphorylation of Hop1-T318 and H2A-S129 (**Figure 9 and 10**), by observation of Hop1-pT318 foci (**Figure**

11B), by the finding of DSB formation at the *HIS4-LEU2* hotspot (**Figure 24D**), and by Rad51 assembly (**Figure 26B**)**.** Especially, the cytological results of Hop1 and Hop1-pT318 on meiotic chromatin spread showed that approximately half of wild type cells exhibited Hop1 loading, but few Hop1-pT318 foci were detected at 2 hour after meiosis entry (**Figure 11F**). These findings suggest that the formation of meiotic DSBs is synchronized until Hop1 loads on chromatin to a certain extent, like a threshold formation of DSBs. The *pph3* mutants showed delayed observation of Hop1-pT318 foci accompanied by inefficient Hop1 loading (**Figure 11G and H**). The findings indicate that the inefficient formation of DSBs may be governed by the loose Hop1 loading in the *pph3* mutants. This idea is supported by the observation that assembly of Hop1 is involved in determining the rate of meiotic DSBs formation (Panizza et al., 2011). This threshold of DSB formation is abolished in the *pph3* mutants.

Decreased crossover formation and increased noncrossover formation was observed in the *pph3* mutants (**Figure 29**). The delayed linearization of Rec8 (**Figure 12E~G**) indicates defective homolog synapsis in the *pph3* mutants, which can be explained by obviously decreased Zip3 assembly (**Figure 28B**). As the assembly of Zip3 at the recombination site to recruit other ZMM proteins is required for the normal crossover formation and homolog synapsis. In the *pch2Δ* background, besides the decreased numbers of Zip3 foci per cell, it was clearly evident that Zip3 foci localized only in regions exhibiting linear Hop1 signals. This suggests that Zip3 fails to assemble on defective axial regions exhibiting faint dotty Hop1. This suggests that the distribution of the axial element may be involved in the recruitment of ZMM proteins.

7.3. Requirement of PP4 activity for efficient meiotic recombination

depending on Mec1/Tel1 kinases

Besides this novel primary role of PP4 in promoting the loading of Hop1-Red1, PP4 activity is also required for the efficient meiotic recombination, which is dependent on Mec1/Tel1 kinases. In addition to the delayed initiation of meiotic DSBs formation, the *pph3* mutants also showed a longer progress of meiotic recombination with the accumulations of meiotic DSB signals (**Figure 24**) and of Rad51 foci on chromatin (**Figure 26**). The delay in the disappearance of DSB signals at *HIS4-LEU2* hotspot in the *pph3-H112N* mutant confirmed the positive role of PP4 catalytic activity in promoting efficient meiotic recombination (18.3% reduction in DSB signals from 4 to 6 hour in wild type and 9.8% from 5 to 8 hour in the *pph3-H112N* mutant in **Figure 24C**). These results were previously revealed in the *pph3Δ* mutant (13.1% from 5 to 8 hour in the *pph3Δ* mutant; (Falk et al., 2010). It is also supported by the reduced numbers of Rad51 foci per cell from 3 to 5 hour in wild type, which showed slowdowns in the *pph3* mutants (22 foci in wild type, 6 foci in the *pph3Δ* mutant, -1.5 foci in the *pph3-H112N* mutant in **Figure 26C**). Moreover, the delayed disappearance of DSB signals in the *pph3Δ* mutant was rescued in the *pCLB2-MEC1 tel1Δ* background (**Figure 25**). The accumulated Hop1 and Red1 on chromatin in the *pph3* mutants during late meiotic prophase I were restored in the *spo11-Y135F* and *pCLB2-MEC1 tel1Δ* backgrounds. These results confirm a Mec1/Tel1 dependent role in promoting efficient meiotic recombination, which is supported by the prior demonstration that the loss of PP4 activity alleviates activation of Mec1 kinase (Hustedt et al., 2015).

The primary role of PP4 activity is completely separated from the second role in the *spo11-Y135F* and *pCLB2-MEC1 tel1Δ* backgrounds. This confirmed the novel primary role that PP4 activity that occurs irrespective of meiotic

recombination or Mec1/Tel1 kinases. The second role in meiotic prophase requires Mec1/Tel1 kinases. Therefore, PP4 dysfunction postpones meiosis progress in two aspects. One is the delayed formation of meiotic chromosome axis independent of Mec1/Tel1 kinases. The other is the inefficient and longer meiotic recombination that depends on Mec1/Tel1 kinases. This suggests the significant and multiple functions of PP4 activity throughout meiotic prophase I.

7.4. Defect and checkpoint activity in meiotic prophase I in the *pph3Δ pch2Δ* mutant

During homolog synapsis, the loading of Hop1-Red1 onto chromatin is antagonized by the eviction of Hop1 by Pch2. Therefore, Hop1 displays a relatively dynamic distribution on the axial element. Accumulated Hop1 on the axial element was observed in the *pph3Δ* and *pph3-H112N* mutants and deletion of *PCH2* failed to restore the loading of Hop1 in the *pph3Δ* mutant (**Figure 20B and D**). These findings are strong evidence that PP4 activity directly promotes the loading of Hop1, rather than stabilizing Hop1 binding on the axial element. However, the linear Hop1 was still observed on some axial elements in the *pph3Δ pch2Δ* mutant, suggesting that Hop1 loading is probably regulated by multiple pathways to form chromosome axis in addition to PP4 activity. The loading of Hop1 chromosome size characterization, preferential binding on the three shortest chromosomes (Murakami et al., 2020). This prompts the question of whether this characteristic of Hop1 loading is correlated with PP4 activity. However, there was no significant difference in lengths of linear Hop1 between the *pch2Δ* and *pph3Δ pch2Δ* mutants (**Figure 20E**), which suggests PP4 activity randomly promotes Hop1 loading.

As Hop1 may self-assemble by the interaction HORMA domain with closure

motif of Hop1 itself, Hop1 may prefer to be recruited to the axial regions enriched with Hop1. Therefore the self-assembly of Hop1 proceeds inefficiently in axial regions poorly exhibiting Hop1. This raises the possibility of collapsed axial Hop1 distribution, in which some axial regions over-aggregate with Hop1, whereas other regions present with little Hop1. The defective Hop1 loading in the *pph3* mutants became much more serious with the deletion of Pch2. This finding suggests that the removed Hop1 can reload on other unsynapsed regions to initiate the formation of meiotic DSBs. The dramatically collapsed distribution of axial Hop1 observed in the *pph3Δ pch2Δ* mutant (**Figure 20B**) indicates that the suppression of regional over-aggregation is possibly abolished.

The distribution of viable spores in the *pph3 pch2Δ* mutant indicated frequent mis-segregation of chromosomes in meiosis I, in turn suggesting a crucially defective meiotic prophase I. The absence of Pch2 can silence meiotic checkpoint activation by defective chromosome synapsis in *zip1* mutant (San-Segundo & Roeder, 1999). In the present study, the delayed meiosis progress in the *pph3* mutant was not rescued by the deletion of *PCH2* as the *pph3Δ pch2Δ* mutant showed a longer meiotic prophase compared to the two single mutants (**Figure 23C**). The finding indicated that the defects in the *pph3Δ pch2Δ* mutant involved a stage before homolog synapsis.

Comparable numbers of Rad51 foci per cell between the *pch2Δ* and *pph3Δ pch2Δ* mutants (**Figure 27B**) and the localization of Hop1-pT318 foci on regions exhibiting both linear and faint dotty Hop1 (**Figure 27C**) were detected in the *pph3Δ pch2Δ* mutants. These findings indicate no obvious defect in the formation of meiotic DSBs in axial elements exhibiting both linear and faint dotty Hop1. In contrast, the deletion of *PPH3* introduced a Pch2-independent decrease in Zip3 assembly (**Figure 28B and C**). This decreased Zip3 assembly was correlated to

reduced crossover formation (**Figure 29D**), as has been reported (Agarwal & Roeder, 2000; Shinohara et al., 2015). Importantly, the Zip3 foci showed a dramatically collapsed distribution in the *pph3Δ pch2Δ* mutant only in regions exhibiting linear Hop1 (**Figure 28D**), where Zip1 normally polymerizes to promote homolog synapsis (**Figure 20B**). As the formation of the chromosome axis is not influenced in *zip3* mutants (Zhu et al., 2021). These results indicate that the DSBs induced in defective axial regions exhibiting faint dotty Hop1 possibly undergo noncrossover recombination without Zip3 assembly in where fails to proceed polymerization of Zip1. Therefore, both chiasma formation and homolog synapsis are frustrated in defective axial regions, which may continuously activate the meiotic checkpoint.

We have previously demonstrated that the DNA damage responder 9-1-1 clamp (Mec3-Ddc1-Rad17) is essential for Zip3 assembly (Shinohara et al., 2015). The C-terminal domain of Red1 strongly interacted with two subunits (Mec3 and Ddc1) of the 9-1-1 clamp (Eichinger & Jentsch, 2010). It is possible that the distribution of Red1 on axial element influences the recruitment of Zip3 through the interaction between the 9-1-1 clamp and Red1. The severe defects in the *pph3Δ pch2Δ* mutant might be involved in the decreased Zip3 assembly caused by the defective Red1 loading on chromatin. This is supported by the absence of Pch2 fails to restore delayed meiosis progress in *zip3* mutant (Wu & Burgess, 2006).

The model that was constructed (**Figure 30B**) can explain the defects correlating with defective Hop1-Red1 assembly in the *pph3Δ pch2Δ* mutant. The axial regions exhibiting faint dotty Hop1 is able to recruit RMM proteins to induce meiotic DSB, in where the insufficient defective loading of Red1 fails to interact with the 9-1-1 clamp to recruit Zip3 to the DSB site, which probably undergoes

noncrossover recombination without chiasma formation and homolog synapsis. There is a possible relationship between the distributions of axial components and the recruitment of ZMM proteins, which may be involved in the regulation of crossover assurance.

8. Acknowledgements

Firstly, my sincere gratitude for Prof. Miki Shinohara and Prof. Akira Shinohara Thank you so much for giving me so many precious suggestions during this research. Your careful guidance helped me through many difficulties. Then, I would also like to appreciate all of members in Shinohara Lab.in Kindai. University and Osaka University, especially Dr. Matsuzaki for helpful advises. Finally, I would like to thank my mother and my dear friends Vicky&Sherry, for caring encouragement.

9. Tables

Table 1. Primary antibody list

Antigen	Primary antibody(dilution)	Reference
Rad51	Guinea pig anti Rad51 antibody (1: 500 in cytology)	(Sasanuma et al., 2013; Shinohara et al., 2003; Storlazzi et al., 1996)
Zip1	Rabbit anti Zip1 antibody (1: 500 in cytology)	(Zhu et al., 2008)
Hop1	Guinea pig anti Hop1 antibody (1: 500 in cytology; 1:3000 in WB)	(Iwasaki et al., 2016)
Hop1-pT318	Rabbit anti Hop1-pT318 antibody (1: 500 in cytology; 1:5000 in WB)	(Iwasaki et al., 2016)
Red1	Chick anti Red1 antibody (1: 500 in cytology; 1:3000 in WB)	(Shinohara et al., 2008)
Rec8	Rabbit anti Rec8 antibody (1: 1000 in cytology; 1:5000 in WB)	(Zhu et al., 2010)
λH2A	Rabbit anti gammaH2Ax.S139 antibody, AF2288 (1: 1000 in cytology; 1:5000 in WB)	
α-Tubulin	Santa cruz, Rat Anti-α-Tubulin antibody, YL1/2 (1: 3000 in WB)	
Myc	Nacalai tesque, Mouse Anti-Myc, MC045 (1: 500 in cytology)	
Zip3	Rabbit anti Zip3 antibody (1: 500 in cytology)	(Shinohara et al., 2015)

Table 2. Secondary antibody list

Antibody(dilution)	Reference
Invitrogen, Goat anti- Rabbit IgG (H+L), Alexa Fluor® 488 (1:1000)	in cytology
Invitrogen, Goat anti- mouse IgG (H+L), Alexa Fluor® 488 (1:1000)	in cytology
Invitrogen, Goat anti- Guinea pig IgG (H+L), Alexa Fluor® 488 (1:1000)	in cytology
Invitrogen, Goat anti- Guinea pig IgG (H+L), Alexa Fluor® 568 (1:1000)	in cytology
Invitrogen, Goat anti- Chick g IgG (H+L), Alexa Fluor® 568 (1:1000)	in cytology
Invitrogen, Goat anti- Rat IgG (H+L), Alexa Fluor® 488 (1:1000)	in cytology
Abcam, Goat anti- Rabbit IgG (H+L), Alexa Fluor® 680 (1: 5000)	in WB
Abcam, Goat anti- Mouse IgG (H+L), Alexa Fluor® 680 (1: 5000)	in WB
LI-COR, IRDye® 800CW Donkey anti- Guinea pig (1: 5000)	in WB
LI-COR, IRDye® 800CW Donkey anti- Chicken (1: 5000)	in WB
LI-COR, IRDye® 800CW Donkey anti- Rat (1: 5000)	in WB
SIGMA goat Anti-Rat IgG conjugated alkaline phosphatase (1: 3000)	in WB

Table 3. Strain list

Strain	Genotype	Reference
NKY1303	*MAT*a, *ho::LYS2, lys2, ura3, leu2::hisG, his4B-LEU2(Mlu*I*), arg4-bgl*	(Storlazzi et al., 1996)
NKY1543	*MAT*α, *ho::LYS2, lys2, ura3, leu2::hisG, his4X-LEU2 (Bam*HI*)-URA3, arg4-nsp*	(Storlazzi et al., 1996)
MSY5632	NKY1303 with *pph3::Hyg^R*	Provided form M, Shinohara
MSY5634	NKY1543 with *pph3::Hyg^R*	Provided form M, Shinohara
MSY6219	NKY1303 with *pph3-H112N::MluI*	Provided form M, Shinohara
MSY6220	NKY1543 with *pph3-H112N::MluI*	Provided form M, Shinohara
MSY6198	NKY1303 with *PSY2-13MYC::TRP1*	Provided form M, Shinohara
MSY6190	NKY1543 with *PSY2-13MYC::TRP1*	Provided form M, Shinohara
MSY6242	NKY1303 with *PSY2-13MYC::TRP1, pph3-H112N::MluI*	Provided form M, Shinohara
MSY6244	NKY1543 with *PSY2-13MYC::TRP1, pph3-H112N::MluI*	Provided form M, Shinohara
MSY5544	NKY1303 with *pCLB2-MEC1, tel1::TRP1*	Provided form M, Shinohara
MSY5546	NKY1543 with *pCLB2-MEC1, tel1::TRP1*	Provided form M, Shinohara
MSY5760	NKY1303 with *pCLB2-MEC1, tel1::TRP1, pph3::Hyg^R*	Provided form M, Shinohara
MSY5762	NKY1543 with *pCLB2-MEC1, tel1::TRP1, pph3::Hyg^R*	Provided form M, Shinohara
MSY6446	NKY1303 with *pch2::TRP1*	Provided form M, Shinohara
MSY6448	NKY1543 with *pch2::TRP1*	Provided form M, Shinohara
MSY6417	NKY1303 with *pph3::Hyg^R, pch2::TRP1*	Provided form M, Shinohara
MSY6419	NKY1543 with *pph3::Hyg^R, pch2::TRP1*	Provided form M, Shinohara
MSY831	*MAT*α, *ho::LYS2, lys2, ura3, leu2::hisG, trp1::hisG*	Provided form M, Shinohara
MSY833	*MAT*a, *ho::LYS2, lys2, ura3, leu2::hisG, trp1::hisG*	Provided form M, Shinohara
MSY3643	MSY831 with *mec1::LEU2, sml1::KANMX6*	Provided form M, Shinohara

MSY3644	MSY833 with *mec1::LEU2, sml1::KANMX6*	Provided form M, Shinohara
MSY6560	MSY831 with *mec1::LEU2, sml1::KANMX6, pph3-H112N::MluI*	Provided form M, Shinohara
MSY6565	MSY833 with *mec1::LEU2, sml1::KANMX6, pph3-H112N::MluI*	Provided form M, Shinohara
MSY6346	MSY831 with *spo11-Y135F-HA::Gen*	Provided form M, Shinohara
MSY6345	MSY833 with *spo11-Y135F-HA::Gen*	Provided form M, Shinohara
MSY6568	MSY831 with *spo11-Y135F-HA::Gen, pph3-H112N::MluI*	Provided form M, Shinohara
MSY6570	MSY833 with *spo11-Y135F-HA::Gen, pph3-H112N::MluI*	Provided form M, Shinohara
MSY6551	NKY1303 with *pCLB2-MEC1*	Provided form M, Shinohara
MSY6552	NKY1543 with *pCLB2-MEC1*	Provided form M, Shinohara
MSY6574	NKY1303 with *pCLB2-MEC1, pph3-H112N::MluI*	Provided form M, Shinohara
MSY6576	NKY1543 with *pCLB2-MEC1, pph3-H112N::MluI*	Provided form M, Shinohara
MSY6314	NKY1303 with *hop1-S595L::SpeI*	Provided form M, Shinohara
MSY6319	NKY1543 with *hop1-S595L::SpeI*	Provided form M, Shinohara
MSY6541	NKY1303 with *hop1-S595L::SpeI, pph3-H112N::MluI*	Provided form M, Shinohara
MSY6543	NKY1543 with *hop1-S595L::SpeI, pph3-H112N::MluI*	Provided form M, Shinohara

10. References

Abdullah, M. F., Hoffmann, E. R., Cotton, V. E., & Borts, R. H. (2004). A role for the MutL homologue MLH2 in controlling heteroduplex formation and in regulating between two different crossover pathways in budding yeast. *Cytogenet Genome Res*, *107*(3-4), 180-190. https://doi.org/10.1159/000080596

Agarwal, S., & Roeder, G. S. (2000). Zip3 provides a link between recombination enzymes and synaptonemal complex proteins. *Cell*, *102*(2), 245-255. https://doi.org/10.1016/s0092-8674(00)00029-5

Aravind, L., & Koonin, E. V. (1998). The HORMA domain: a common structural denominator in mitotic checkpoints, chromosome synapsis and DNA repair. *Trends Biochem Sci*, *23*(8), 284-286. https://doi.org/10.1016/s0968-0004(98)01257-2

Bergerat, A., de Massy, B., Gadelle, D., Varoutas, P. C., Nicolas, A., & Forterre, P. (1997). An atypical topoisomerase II from Archaea with implications for meiotic recombination. *Nature*, *386*(6623), 414-417. https://doi.org/10.1038/386414a0

Blat, Y., Protacio, R. U., Hunter, N., & Kleckner, N. (2002). Physical and functional interactions among basic chromosome organizational features govern early steps of meiotic chiasma formation. *Cell*, *111*(6), 791-802. https://doi.org/10.1016/s0092-8674(02)01167-4

Bonetti, D., Clerici, M., Manfrini, N., Lucchini, G., & Longhese, M. P. (2010). The MRX complex plays multiple functions in resection of Yku- and Rif2-protected DNA ends. *PLoS One*, *5*(11), e14142. https://doi.org/10.1371/journal.pone.0014142

Borde, V., Robine, N., Lin, W., Bonfils, S., Géli, V., & Nicolas, A. (2009). Histone H3 lysine 4 trimethylation marks meiotic recombination initiation sites. *EMBO J*, *28*(2), 99-111. https://doi.org/10.1038/emboj.2008.257

Borner, G. V., Barot, A., & Kleckner, N. (2008). Yeast Pch2 promotes domainal axis organization, timely recombination progression, and arrest of defective recombinosomes during meiosis. *Proc Natl Acad Sci U S A*, *105*(9), 3327-3332. https://doi.org/10.1073/pnas.0711864105

Branzei, D., & Foiani, M. (2006). The Rad53 signal transduction pathway: Replication fork stabilization, DNA repair, and adaptation. *Exp Cell Res*, *312*(14), 2654-2659. https://doi.org/10.1016/j.yexcr.2006.06.012

Busygina, V., Sehorn, M. G., Shi, I. Y., Tsubouchi, H., Roeder, G. S., & Sung, P. (2008). Hed1 regulates Rad51-mediated recombination via a novel mechanism. *Genes Dev*, *22*(6), 786-795. https://doi.org/10.1101/gad.1638708

Bähler, J., Wu, J. Q., Longtine, M. S., Shah, N. G., McKenzie, A., Steever, A. B., . . . Pringle, J. R. (1998). Heterologous modules for efficient and versatile PCR-based gene targeting in Schizosaccharomyces pombe. *Yeast*, *14*(10), 943-951. https://doi.org/10.1002/(SICI)1097-0061(199807)14:10<943::AID-YEA292>3.0.CO;2-Y

Börner, G. V., Barot, A., & Kleckner, N. (2008). Yeast Pch2 promotes domainal axis organization, timely recombination progression, and arrest of defective recombinosomes during meiosis. *Proc Natl Acad Sci U S A*, *105*(9), 3327-3332. https://doi.org/10.1073/pnas.0711864105

Callender, T. L., Laureau, R., Wan, L., Chen, X., Sandhu, R., Laljee, S., . . . Hollingsworth, N. M. (2016). Mek1 Down Regulates Rad51 Activity during Yeast Meiosis by Phosphorylation of Hed1. *PLoS Genet*, *12*(8), e1006226.

https://doi.org/10.1371/journal.pgen.1006226

Carballo, J. A., Johnson, A. L., Sedgwick, S. G., & Cha, R. S. (2008). Phosphorylation of the axial element protein Hop1 by Mec1/Tel1 ensures meiotic interhomolog recombination. *Cell*, *132*(5), 758-770. https://doi.org/10.1016/j.cell.2008.01.035

Challa, K., Fajish V, G., Shinohara, M., Klein, F., Gasser, S. M., & Shinohara, A. (2019). Meiosis-specific prophase-like pathway controls cleavage-independent release of cohesin by Wapl phosphorylation. *PLoS Genet*, *15*(1), e1007851. https://doi.org/10.1371/journal.pgen.1007851

Chen, C., Jomaa, A., Ortega, J., & Alani, E. E. (2014). Pch2 is a hexameric ring ATPase that remodels the chromosome axis protein Hop1. *Proc Natl Acad Sci U S A*, *111*(1), E44-53. https://doi.org/10.1073/pnas.1310755111

Cheng, Y. H., Chuang, C. N., Shen, H. J., Lin, F. M., & Wang, T. F. (2013). Three distinct modes of Mec1/ATR and Tel1/ATM activation illustrate differential checkpoint targeting during budding yeast early meiosis. *Mol Cell Biol*, *33*(16), 3365-3376. https://doi.org/10.1128/MCB.00438-13

Chowdhury, D., Xu, X., Zhong, X., Ahmed, F., Zhong, J., Liao, J., . . . Lieberman, J. (2008). A PP4-phosphatase complex dephosphorylates gamma-H2AX generated during DNA replication. *Mol Cell*, *31*(1), 33-46. https://doi.org/10.1016/j.molcel.2008.05.016

Chua, P. R., & Roeder, G. S. (1998). Zip2, a meiosis-specific protein required for the initiation of chromosome synapsis. *Cell*, *93*(3), 349-359. https://doi.org/10.1016/s0092-8674(00)81164-2

Chuang, C. N., Cheng, Y. H., & Wang, T. F. (2012). Mek1 stabilizes Hop1-Thr318 phosphorylation to promote interhomolog recombination and checkpoint responses during yeast meiosis. *Nucleic Acids Res*, *40*(22), 11416-11427.

https://doi.org/10.1093/nar/gks920

Downs, J. A., Lowndes, N. F., & Jackson, S. P. (2000). A role for Saccharomyces cerevisiae histone H2A in DNA repair. *Nature*, *408*(6815), 1001-1004. https://doi.org/10.1038/35050000

Durocher, D., & Jackson, S. P. (2001). DNA-PK, ATM and ATR as sensors of DNA damage: variations on a theme? *Curr Opin Cell Biol*, *13*(2), 225-231. https://doi.org/10.1016/s0955-0674(00)00201-5

Eichinger, C. S., & Jentsch, S. (2010). Synaptonemal complex formation and meiotic checkpoint signaling are linked to the lateral element protein Red1. *Proc Natl Acad Sci U S A*, *107*(25), 11370-11375. https://doi.org/10.1073/pnas.1004248107

Eytan, E., Wang, K., Miniowitz-Shemtov, S., Sitry-Shevah, D., Kaisari, S., Yen, T. J., . . . Hershko, A. (2014). Disassembly of mitotic checkpoint complexes by the joint action of the AAA-ATPase TRIP13 and p31(comet). *Proc Natl Acad Sci U S A*, *111*(33), 12019-12024. https://doi.org/10.1073/pnas.1412901111

Falk, J. E., Chan, A. C., Hoffmann, E., & Hochwagen, A. (2010). A Mec1- and PP4-dependent checkpoint couples centromere pairing to meiotic recombination. *Dev Cell*, *19*(4), 599-611. https://doi.org/10.1016/j.devcel.2010.09.006

Ferrari, S. R., Grubb, J., & Bishop, D. K. (2009). The Mei5-Sae3 protein complex mediates Dmc1 activity in Saccharomyces cerevisiae. *J Biol Chem*, *284*(18), 11766-11770. https://doi.org/10.1074/jbc.C900023200

Freeman, A. K., & Monteiro, A. N. (2010). Phosphatases in the cellular response to DNA damage. *Cell Commun Signal*, *8*, 27. https://doi.org/10.1186/1478-811X-8-27

Friedman, D. B., Hollingsworth, N. M., & Byers, B. (1994). Insertional mutations in the yeast HOP1 gene: evidence for multimeric assembly in meiosis. *Genetics*, *136*(2), 449-464.

Gobbini, E., Cassani, C., Villa, M., Bonetti, D., & Longhese, M. P. (2016). Functions and regulation of the MRX complex at DNA double-strand breaks. *Microb Cell*, *3*(8), 329-337. https://doi.org/10.15698/mic2016.08.517

Grushcow, J. M., Holzen, T. M., Park, K. J., Weinert, T., Lichten, M., & Bishop, D. K. (1999). Saccharomyces cerevisiae checkpoint genes MEC1, RAD17 and RAD24 are required for normal meiotic recombination partner choice. *Genetics*, *153*(2), 607-620. https://doi.org/10.1093/genetics/153.2.607

Hayase, A., Takagi, M., Miyazaki, T., Oshiumi, H., Shinohara, M., & Shinohara, A. (2004). A protein complex containing Mei5 and Sae3 promotes the assembly of the meiosis-specific RecA homolog Dmc1. *Cell*, *119*(7), 927-940. https://doi.org/10.1016/j.cell.2004.10.031

Herruzo, E., Ontoso, D., González-Arranz, S., Cavero, S., Lechuga, A., & San-Segundo, P. A. (2016). The Pch2 AAA+ ATPase promotes phosphorylation of the Hop1 meiotic checkpoint adaptor in response to synaptonemal complex defects. *Nucleic Acids Res*, *44*(16), 7722-7741. https://doi.org/10.1093/nar/gkw506

Hoffmann, R., Jung, S., Ehrmann, M., & Hofer, H. W. (1994). The Saccharomyces cerevisiae gene PPH3 encodes a protein phosphatase with properties different from PPX, PP1 and PP2A. *Yeast*, *10*(5), 567-578. https://doi.org/10.1002/yea.320100502

Hollingsworth, N. M., & Byers, B. (1989). HOP1: a yeast meiotic pairing gene. *Genetics*, *121*(3), 445-462.

Hollingsworth, N. M., Goetsch, L., & Byers, B. (1990). The HOP1 gene encodes a meiosis-specific component of yeast chromosomes. *Cell*, *61*(1), 73-84. https://doi.org/10.1016/0092-8674(90)90216-2

Hollingsworth, N. M., & Johnson, A. D. (1993). A conditional allele of the Saccharomyces cerevisiae HOP1 gene is suppressed by overexpression of two other meiosis-specific genes: RED1 and REC104. *Genetics*, *133*(4), 785-797. https://doi.org/10.1093/genetics/133.4.785

Hollingsworth, N. M., & Ponte, L. (1997). Genetic interactions between HOP1, RED1 and MEK1 suggest that MEK1 regulates assembly of axial element components during meiosis in the yeast Saccharomyces cerevisiae. *Genetics*, *147*(1), 33-42.

Hollingsworth, N. M., Ponte, L., & Halsey, C. (1995). MSH5, a novel MutS homolog, facilitates meiotic reciprocal recombination between homologs in Saccharomyces cerevisiae but not mismatch repair. *Genes Dev*, *9*(14), 1728-1739. https://doi.org/10.1101/gad.9.14.1728

Holm, P. B., Rasmussen, S. W., & von Wettstein, D. (1979). The possible contribution of electron microscopy to the understanding of the mechanism of non-disjunction in man. *Mutat Res*, *61*(1), 115-119. https://doi.org/10.1016/0027-5107(79)90012-5

Hong, E. J., & Roeder, G. S. (2002). A role for Ddc1 in signaling meiotic double-strand breaks at the pachytene checkpoint. *Genes Dev*, *16*(3), 363-376. https://doi.org/10.1101/gad.938102

Hunter, N., & Kleckner, N. (2001). The single-end invasion: an asymmetric intermediate at the double-strand break to double-holliday junction transition of meiotic recombination. *Cell*, *106*(1), 59-70. https://doi.org/10.1016/s0092-8674(01)00430-5

Hustedt, N., Seeber, A., Sack, R., Tsai-Pflugfelder, M., Bhullar, B., Vlaming, H., . . . Gasser, S. M. (2015). Yeast PP4 interacts with ATR homolog Ddc2-Mec1 and regulates checkpoint signaling. *Mol Cell*, *57*(2), 273-289. https://doi.org/10.1016/j.molcel.2014.11.016

Iwasaki, D., Hayashihara, K., Shima, H., Higashide, M., Terasawa, M., Gasser, S. M., & Shinohara, M. (2016). The MRX Complex Ensures NHEJ Fidelity through Multiple Pathways Including Xrs2-FHA-Dependent Tel1 Activation. *PLoS Genet*, *12*(3), e1005942. https://doi.org/10.1371/journal.pgen.1005942

Jessop, L., Rockmill, B., Roeder, G. S., & Lichten, M. (2006). Meiotic chromosome synapsis-promoting proteins antagonize the anti-crossover activity of sgs1. *PLoS Genet*, *2*(9), e155. https://doi.org/10.1371/journal.pgen.0020155

Karányi, Z., Halász, L., Acquaviva, L., Jónás, D., Hetey, S., Boros-Oláh, B., . . . Székvölgyi, L. (2018). Nuclear dynamics of the Set1C subunit Spp1 prepares meiotic recombination sites for break formation. *J Cell Biol*, *217*(10), 3398-3415. https://doi.org/10.1083/jcb.201712122

Keeney, S., Giroux, C. N., & Kleckner, N. (1997). Meiosis-specific DNA double-strand breaks are catalyzed by Spo11, a member of a widely conserved protein family. *Cell*, *88*(3), 375-384. https://doi.org/10.1016/s0092-8674(00)81876-0

Keogh, M. C., Kim, J. A., Downey, M., Fillingham, J., Chowdhury, D., Harrison, J. C., . . . Krogan, N. J. (2006). A phosphatase complex that dephosphorylates gammaH2AX regulates DNA damage checkpoint recovery. *Nature*, *439*(7075), 497-501. https://doi.org/10.1038/nature04384

Khan, K., Madhavan, T. P., Kshirsagar, R., Boosi, K. N., Sadhale, P., & Muniyappa, K. (2013). N-terminal disordered domain of Saccharomyces cerevisiae Hop1 protein is dispensable for DNA binding, bridging, and synapsis of double-stranded DNA molecules but is necessary for spore formation. *Biochemistry*, *52*(31), 5265-5279. https://doi.org/10.1021/bi4005528

Klapholz, S., Waddell, C. S., & Esposito, R. E. (1985). The role of the SPO11 gene in meiotic recombination in yeast. *Genetics*, *110*(2), 187-216.

Klein, F., Mahr, P., Galova, M., Buonomo, S. B., Michaelis, C., Nairz, K., & Nasmyth, K. (1999). A central role for cohesins in sister chromatid cohesion, formation of axial elements, and recombination during yeast meiosis. *Cell*, *98*(1), 91-103. https://doi.org/10.1016/S0092-8674(00)80609-1

Kugou, K., & Ohta, K. (2009). Genome-wide high-resolution chromatin immunoprecipitation of meiotic chromosomal proteins in Saccharomyces cerevisiae. *Methods Mol Biol*, *557*, 285-304. https://doi.org/10.1007/978-1-59745-527-5_18

Lai, Y. J., Lin, F. M., Chuang, M. J., Shen, H. J., & Wang, T. F. (2011). Genetic requirements and meiotic function of phosphorylation of the yeast axial element protein Red1. *Mol Cell Biol*, *31*(5), 912-923. https://doi.org/10.1128/MCB.00895-10

Lee, B. H., & Amon, A. (2003). Polo kinase--meiotic cell cycle coordinator. *Cell Cycle*, *2*(5), 400-402.

Leem, S. H., & Ogawa, H. (1992). The MRE4 gene encodes a novel protein kinase homologue required for meiotic recombination in Saccharomyces cerevisiae. *Nucleic Acids Res*, *20*(3), 449-457. https://doi.org/10.1093/nar/20.3.449

Li, J., Hooker, G. W., & Roeder, G. S. (2006). Saccharomyces cerevisiae Mer2, Mei4 and Rec114 form a complex required for meiotic double-strand break formation. *Genetics*, *173*(4), 1969-1981. https://doi.org/10.1534/genetics.106.058768

Liu, Y., Gaines, W. A., Callender, T., Busygina, V., Oke, A., Sung, P., . . . Hollingsworth, N. M. (2014). Down-regulation of Rad51 activity during meiosis in yeast prevents competition with Dmc1 for repair of double-strand breaks. *PLoS Genet*, *10*(1), e1004005. https://doi.org/10.1371/journal.pgen.1004005

Lo, Y. H., Chuang, C. N., & Wang, T. F. (2014). Pch2 prevents Mec1/Tel1-mediated Hop1 phosphorylation occurring independently of Red1 in budding yeast meiosis. *PLoS One*, *9*(1), e85687. https://doi.org/10.1371/journal.pone.0085687

Luger, K., Mäder, A. W., Richmond, R. K., Sargent, D. F., & Richmond, T. J. (1997). Crystal structure of the nucleosome core particle at 2.8 A resolution. *Nature*, *389*(6648), 251-260. https://doi.org/10.1038/38444

Manfrini, N., Guerini, I., Citterio, A., Lucchini, G., & Longhese, M. P. (2010). Processing of meiotic DNA double strand breaks requires cyclin-dependent kinase and multiple nucleases. *J Biol Chem*, *285*(15), 11628-11637. https://doi.org/10.1074/jbc.M110.104083

Mantiero, D., Clerici, M., Lucchini, G., & Longhese, M. P. (2007). Dual role for Saccharomyces cerevisiae Tel1 in the checkpoint response to double-strand breaks. *EMBO Rep*, *8*(4), 380-387. https://doi.org/10.1038/sj.embor.7400911

Mao-Draayer, Y., Galbraith, A. M., Pittman, D. L., Cool, M., & Malone, R. E. (1996). Analysis of meiotic recombination pathways in the yeast Saccharomyces

cerevisiae. *Genetics*, *144*(1), 71-86.

McMahill, M. S., Sham, C. W., & Bishop, D. K. (2007). Synthesis-dependent strand annealing in meiosis. *PLoS Biol*, *5*(11), e299. https://doi.org/10.1371/journal.pbio.0050299

Mimitou, E. P., & Symington, L. S. (2009). DNA end resection: many nucleases make light work. *DNA Repair (Amst)*, *8*(9), 983-995. https://doi.org/10.1016/j.dnarep.2009.04.017

Muller, H., Scolari, V. F., Agier, N., Piazza, A., Thierry, A., Mercy, G., . . . Koszul, R. (2018). Characterizing meiotic chromosomes' structure and pairing using a designer sequence optimized for Hi-C. *Mol Syst Biol*, *14*(7), e8293. https://doi.org/10.15252/msb.20188293

Murakami, H., Lam, I., Huang, P. C., Song, J., van Overbeek, M., & Keeney, S. (2020). Multilayered mechanisms ensure that short chromosomes recombine in meiosis. *Nature*, *582*(7810), 124-128. https://doi.org/10.1038/s41586-020-2248-2

Nakada, S., Chen, G. I., Gingras, A. C., & Durocher, D. (2008). PP4 is a gamma H2AX phosphatase required for recovery from the DNA damage checkpoint. *EMBO Rep*, *9*(10), 1019-1026. https://doi.org/10.1038/embor.2008.162

Nakagawa, T., & Kolodner, R. D. (2002). Saccharomyces cerevisiae Mer3 is a DNA helicase involved in meiotic crossing over. *Mol Cell Biol*, *22*(10), 3281-3291. https://doi.org/10.1128/MCB.22.10.3281-3291.2002

Nakagawa, T., & Ogawa, H. (1999). The Saccharomyces cerevisiae MER3 gene, encoding a novel helicase-like protein, is required for crossover control in meiosis. *EMBO J*, *18*(20), 5714-5723. https://doi.org/10.1093/emboj/18.20.5714

Niu, H., Wan, L., Baumgartner, B., Schaefer, D., Loidl, J., & Hollingsworth, N. M. (2005). Partner choice during meiosis is regulated by Hop1-promoted dimerization of Mek1. *Mol Biol Cell*, *16*(12), 5804-5818. https://doi.org/10.1091/mbc.e05-05-0465

Novak, J. E., Ross-Macdonald, P. B., & Roeder, G. S. (2001). The budding yeast Msh4 protein functions in chromosome synapsis and the regulation of crossover distribution. *Genetics*, *158*(3), 1013-1025.

O'Neill, B. M., Szyjka, S. J., Lis, E. T., Bailey, A. O., Yates, J. R., Aparicio, O. M., & Romesberg, F. E. (2007). Pph3-Psy2 is a phosphatase complex required for Rad53 dephosphorylation and replication fork restart during recovery from DNA damage. *Proc Natl Acad Sci U S A*, *104*(22), 9290-9295. https://doi.org/10.1073/pnas.0703252104

Panizza, S., Mendoza, M. A., Berlinger, M., Huang, L., Nicolas, A., Shirahige, K., & Klein, F. (2011). Spo11-accessory proteins link double-strand break sites to the chromosome axis in early meiotic recombination. *Cell*, *146*(3), 372-383. https://doi.org/10.1016/j.cell.2011.07.003

Paques, F., & Haber, J. E. (1999). Multiple pathways of recombination induced by double-strand breaks in Saccharomyces cerevisiae. *Microbiol Mol Biol Rev*, *63*(2), 349-404. https://doi.org/10.1128/MMBR.63.2.349-404.1999

Penedos, A., Johnson, A. L., Strong, E., Goldman, A. S., Carballo, J. A., & Cha, R. S. (2015). Essential and Checkpoint Functions of Budding Yeast ATM and ATR during Meiotic Prophase Are Facilitated by Differential Phosphorylation of a Meiotic Adaptor Protein, Hop1. *PLoS One*, *10*(7), e0134297. https://doi.org/10.1371/journal.pone.0134297

Petukhova, G., Sung, P., & Klein, H. (2000). Promotion of Rad51-dependent D-loop formation by yeast recombination factor Rdh54/Tid1. *Genes Dev*,

14(17), 2206-2215. https://doi.org/10.1101/gad.826100

Prieler, S., Penkner, A., Borde, V., & Klein, F. (2005). The control of Spo11's interaction with meiotic recombination hotspots. *Genes Dev*, *19*(2), 255-269. https://doi.org/10.1101/gad.321105

Raina, V. B., & Vader, G. (2020). Homeostatic Control of Meiotic Prophase Checkpoint Function by Pch2 and Hop1. *Curr Biol*, *30*(22), 4413-4424.e4415. https://doi.org/10.1016/j.cub.2020.08.064

Redon, C., Pilch, D. R., Rogakou, E. P., Orr, A. H., Lowndes, N. F., & Bonner, W. M. (2003). Yeast histone 2A serine 129 is essential for the efficient repair of checkpoint-blind DNA damage. *EMBO Rep*, *4*(7), 678-684. https://doi.org/10.1038/sj.embor.embor871

Rockmill, B., & Roeder, G. S. (1988). RED1: a yeast gene required for the segregation of chromosomes during the reductional division of meiosis. *Proc Natl Acad Sci U S A*, *85*(16), 6057-6061. https://doi.org/10.1073/pnas.85.16.6057

Rockmill, B., & Roeder, G. S. (1991). A meiosis-specific protein kinase homolog required for chromosome synapsis and recombination. *Genes Dev*, *5*(12B), 2392-2404. https://doi.org/10.1101/gad.5.12b.2392

Roeder, G. S. (1990). Chromosome synapsis and genetic recombination: their roles in meiotic chromosome segregation. *Trends Genet*, *6*(12), 385-389. https://doi.org/10.1016/0168-9525(90)90297-j

Ross-Macdonald, P., & Roeder, G. S. (1994). Mutation of a meiosis-specific MutS homolog decreases crossing over but not mismatch correction. *Cell*, *79*(6), 1069-1080. https://doi.org/10.1016/0092-8674(94)90037-x

San-Segundo, P. A., & Roeder, G. S. (1999). Pch2 links chromatin silencing to meiotic checkpoint control. *Cell*, *97*(3), 313-324.

https://doi.org/10.1016/s0092-8674(00)80741-2

Sasanuma, H., Furihata, Y., Shinohara, M., & Shinohara, A. (2013). Remodeling of the Rad51 DNA strand-exchange protein by the Srs2 helicase. *Genetics*, *194*(4), 859-872. https://doi.org/10.1534/genetics.113.150615

Sasanuma, H., Murakami, H., Fukuda, T., Shibata, T., Nicolas, A., & Ohta, K. (2007). Meiotic association between Spo11 regulated by Rec102, Rec104 and Rec114. *Nucleic Acids Res*, *35*(4), 1119-1133. https://doi.org/10.1093/nar/gkl1162

Schalbetter, S. A., Fudenberg, G., Baxter, J., Pollard, K. S., & Neale, M. J. (2019). Principles of meiotic chromosome assembly revealed in S. cerevisiae. *Nat Commun*, *10*(1), 4795. https://doi.org/10.1038/s41467-019-12629-0

Schwacha, A., & Kleckner, N. (1994). Identification of joint molecules that form frequently between homologs but rarely between sister chromatids during yeast meiosis. *Cell*, *76*(1), 51-63. https://doi.org/10.1016/0092-8674(94)90172-4

Schwacha, A., & Kleckner, N. (1997). Interhomolog bias during meiotic recombination: meiotic functions promote a highly differentiated interhomolog-only pathway. *Cell*, *90*(6), 1123-1135. https://doi.org/10.1016/s0092-8674(00)80378-5

Shi, Y. (2009). Serine/threonine phosphatases: mechanism through structure. *Cell*, *139*(3), 468-484. https://doi.org/10.1016/j.cell.2009.10.006

Shinohara, M., Bishop, D. K., & Shinohara, A. (2019). Distinct Functions in Regulation of Meiotic Crossovers for DNA Damage Response Clamp Loader Rad24(Rad17) and Mec1(ATR) Kinase. *Genetics*, *213*(4), 1255-1269. https://doi.org/10.1534/genetics.119.302427

Shinohara, M., Gasior, S. L., Bishop, D. K., & Shinohara, A. (2000). Tid1/Rdh54

promotes colocalization of rad51 and dmc1 during meiotic recombination. *Proc Natl Acad Sci U S A*, *97*(20), 10814-10819. https://doi.org/10.1073/pnas.97.20.10814

Shinohara, M., Hayashihara, K., Grubb, J. T., Bishop, D. K., & Shinohara, A. (2015). DNA damage response clamp 9-1-1 promotes assembly of ZMM proteins for formation of crossovers and synaptonemal complex. *J Cell Sci*, *128*(8), 1494-1506. https://doi.org/10.1242/jcs.161554

Shinohara, M., Oh, S. D., Hunter, N., & Shinohara, A. (2008). Crossover assurance and crossover interference are distinctly regulated by the ZMM proteins during yeast meiosis. *Nat Genet*, *40*(3), 299-309. https://doi.org/10.1038/ng.83

Shinohara, M., Sakai, K., Ogawa, T., & Shinohara, A. (2003). The mitotic DNA damage checkpoint proteins Rad17 and Rad24 are required for repair of double-strand breaks during meiosis in yeast. *Genetics*, *164*(3), 855-865.

Shinohara, M., & Shinohara, A. (2013). Multiple pathways suppress non-allelic homologous recombination during meiosis in Saccharomyces cerevisiae. *PLoS One*, *8*(4), e63144. https://doi.org/10.1371/journal.pone.0063144

Smith, A. V., & Roeder, G. S. (1997). The yeast Red1 protein localizes to the cores of meiotic chromosomes. *J Cell Biol*, *136*(5), 957-967. https://doi.org/10.1083/jcb.136.5.957

Sollier, J., Lin, W., Soustelle, C., Suhre, K., Nicolas, A., Géli, V., & de La Roche Saint-André, C. (2004). Set1 is required for meiotic S-phase onset, double-strand break formation and middle gene expression. *EMBO J*, *23*(9), 1957-1967. https://doi.org/10.1038/sj.emboj.7600204

Sommermeyer, V., Béneut, C., Chaplais, E., Serrentino, M. E., & Borde, V. (2013). Spp1, a member of the Set1 Complex, promotes meiotic DSB formation in

promoters by tethering histone H3K4 methylation sites to chromosome axes. *Mol Cell*, *49*(1), 43-54. https://doi.org/10.1016/j.molcel.2012.11.008

Storlazzi, A., Xu, L., Schwacha, A., & Kleckner, N. (1996). Synaptonemal complex (SC) component Zip1 plays a role in meiotic recombination independent of SC polymerization along the chromosomes. *Proc Natl Acad Sci U S A*, *93*(17), 9043-9048. https://doi.org/10.1073/pnas.93.17.9043

Subramanian, V. V., MacQueen, A. J., Vader, G., Shinohara, M., Sanchez, A., Borde, V., . . . Hochwagen, A. (2016). Chromosome Synapsis Alleviates Mek1-Dependent Suppression of Meiotic DNA Repair. *PLoS Biol*, *14*(2), e1002369. https://doi.org/10.1371/journal.pbio.1002369

Sun, X., Huang, L., Markowitz, T. E., Blitzblau, H. G., Chen, D., Klein, F., & Hochwagen, A. (2015). Transcription dynamically patterns the meiotic chromosome-axis interface. *Elife*, *4*. https://doi.org/10.7554/eLife.07424

Sym, M., Engebrecht, J. A., & Roeder, G. S. (1993). ZIP1 is a synaptonemal complex protein required for meiotic chromosome synapsis. *Cell*, *72*(3), 365-378. https://doi.org/10.1016/0092-8674(93)90114-6

Traven, A., & Heierhorst, J. (2005). SQ/TQ cluster domains: concentrated ATM/ATR kinase phosphorylation site regions in DNA-damage-response proteins. *Bioessays*, *27*(4), 397-407. https://doi.org/10.1002/bies.20204

Tsubouchi, H., & Roeder, G. S. (2006). Budding yeast Hed1 down-regulates the mitotic recombination machinery when meiotic recombination is impaired. *Genes Dev*, *20*(13), 1766-1775. https://doi.org/10.1101/gad.1422506

Tsubouchi, T., Zhao, H., & Roeder, G. S. (2006). The meiosis-specific zip4 protein regulates crossover distribution by promoting synaptonemal complex formation together with zip2. *Dev Cell*, *10*(6), 809-819.

https://doi.org/10.1016/j.devcel.2006.04.003

Usui, T., Ogawa, H., & Petrini, J. H. (2001). A DNA damage response pathway controlled by Tel1 and the Mre11 complex. *Mol Cell*, *7*(6), 1255-1266. https://doi.org/10.1016/s1097-2765(01)00270-2

van den Berg, J., G Manjón, A., Kielbassa, K., Feringa, F. M., Freire, R., & Medema, R. H. (2018). A limited number of double-strand DNA breaks is sufficient to delay cell cycle progression. *Nucleic Acids Res*, *46*(19), 10132-10144. https://doi.org/10.1093/nar/gky786

Watanabe, Y., & Nurse, P. (1999). Cohesin Rec8 is required for reductional chromosome segregation at meiosis. *Nature*, *400*(6743), 461-464. https://doi.org/10.1038/22774

West, A. M. V., Komives, E. A., & Corbett, K. D. (2018). Conformational dynamics of the Hop1 HORMA domain reveal a common mechanism with the spindle checkpoint protein Mad2. *Nucleic Acids Res*, *46*(1), 279-292. https://doi.org/10.1093/nar/gkx1196

Wojtasz, L., Daniel, K., Roig, I., Bolcun-Filas, E., Xu, H., Boonsanay, V., . . . Toth, A. (2009). Mouse HORMAD1 and HORMAD2, two conserved meiotic chromosomal proteins, are depleted from synapsed chromosome axes with the help of TRIP13 AAA-ATPase. *PLoS Genet*, *5*(10), e1000702. https://doi.org/10.1371/journal.pgen.1000702

Woltering, D., Baumgartner, B., Bagchi, S., Larkin, B., Loidl, J., de los Santos, T., & Hollingsworth, N. M. (2000). Meiotic segregation, synapsis, and recombination checkpoint functions require physical interaction between the chromosomal proteins Red1p and Hop1p. *Mol Cell Biol*, *20*(18), 6646-6658. https://doi.org/10.1128/MCB.20.18.6646-6658.2000

Wu, H. Y., & Burgess, S. M. (2006). Two distinct surveillance mechanisms monitor

meiotic chromosome metabolism in budding yeast. *Curr Biol*, *16*(24), 2473-2479. https://doi.org/10.1016/j.cub.2006.10.069

Yadav, V. K., & Claeys Bouuaert, C. (2021). Mechanism and Control of Meiotic DNA Double-Strand Break Formation in. *Front Cell Dev Biol*, *9*, 642737. https://doi.org/10.3389/fcell.2021.642737

Zhang, Y., Suzuki, T., Li, K., Gothwal, S. K., Shinohara, M., & Shinohara, A. (2020). Genetic Interactions of Histone Modification Machinery Set1 and PAF1C with the Recombination Complex Rec114-Mer2-Mei4 in the Formation of Meiotic DNA Double-Strand Breaks. *Int J Mol Sci*, *21*(8). https://doi.org/10.3390/ijms21082679

Zhao, X., Muller, E. G., & Rothstein, R. (1998). A suppressor of two essential checkpoint genes identifies a novel protein that negatively affects dNTP pools. *Mol Cell*, *2*(3), 329-340. https://doi.org/10.1016/s1097-2765(00)80277-4

Zhu, Z., Bani Ismail, M., Shinohara, M., & Shinohara, A. (2021). SCF. *Life Sci Alliance*, *4*(2). https://doi.org/10.26508/lsa.202000933

Zhu, Z., Chung, W. H., Shim, E. Y., Lee, S. E., & Ira, G. (2008). Sgs1 helicase and two nucleases Dna2 and Exo1 resect DNA double-strand break ends. *Cell*, *134*(6), 981-994. https://doi.org/10.1016/j.cell.2008.08.037

Zhu, Z., Mori, S., Oshiumi, H., Matsuzaki, K., Shinohara, M., & Shinohara, A. (2010). Cyclin-dependent kinase promotes formation of the synaptonemal complex in yeast meiosis. *Genes Cells*, *15*(10), 1036-1050. https://doi.org/10.1111/j.1365-2443.2010.01440.x

11. Figures and legends

Figure 1

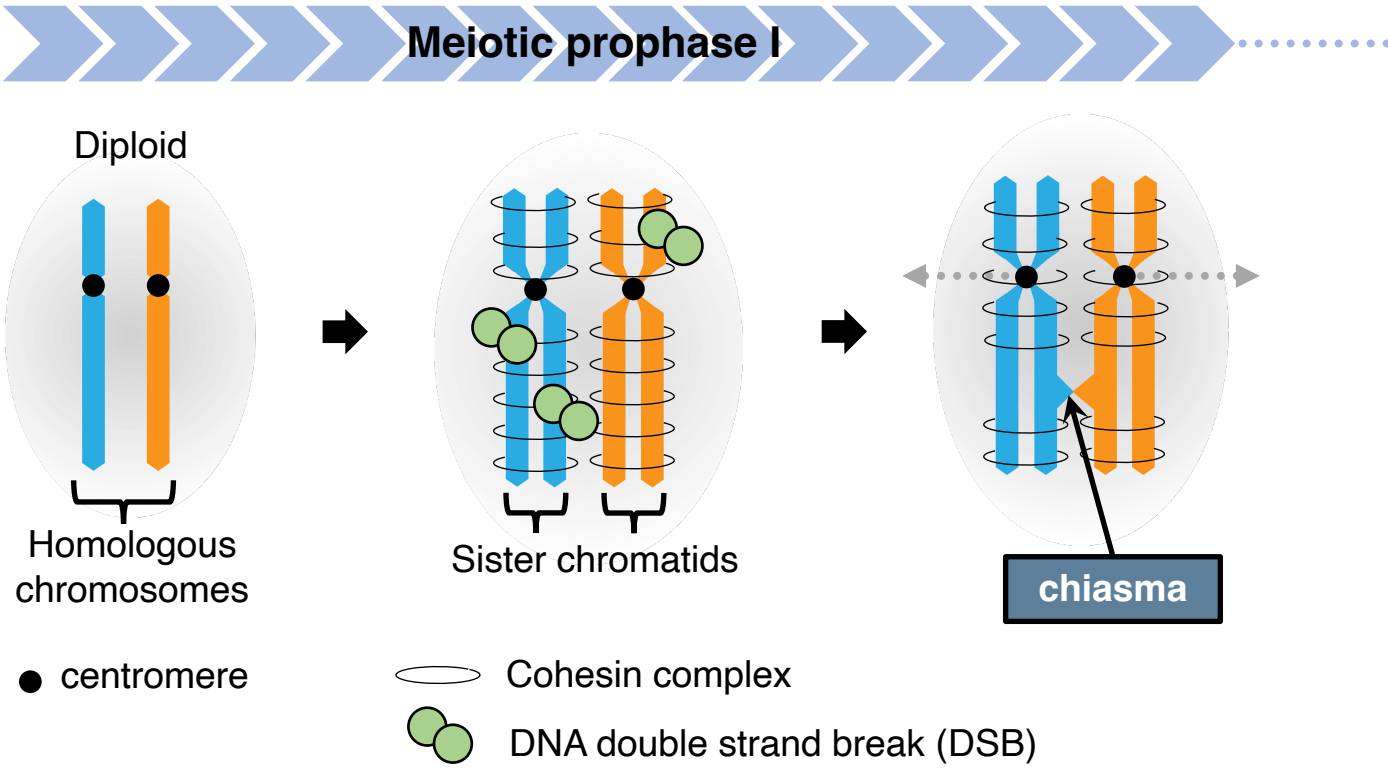

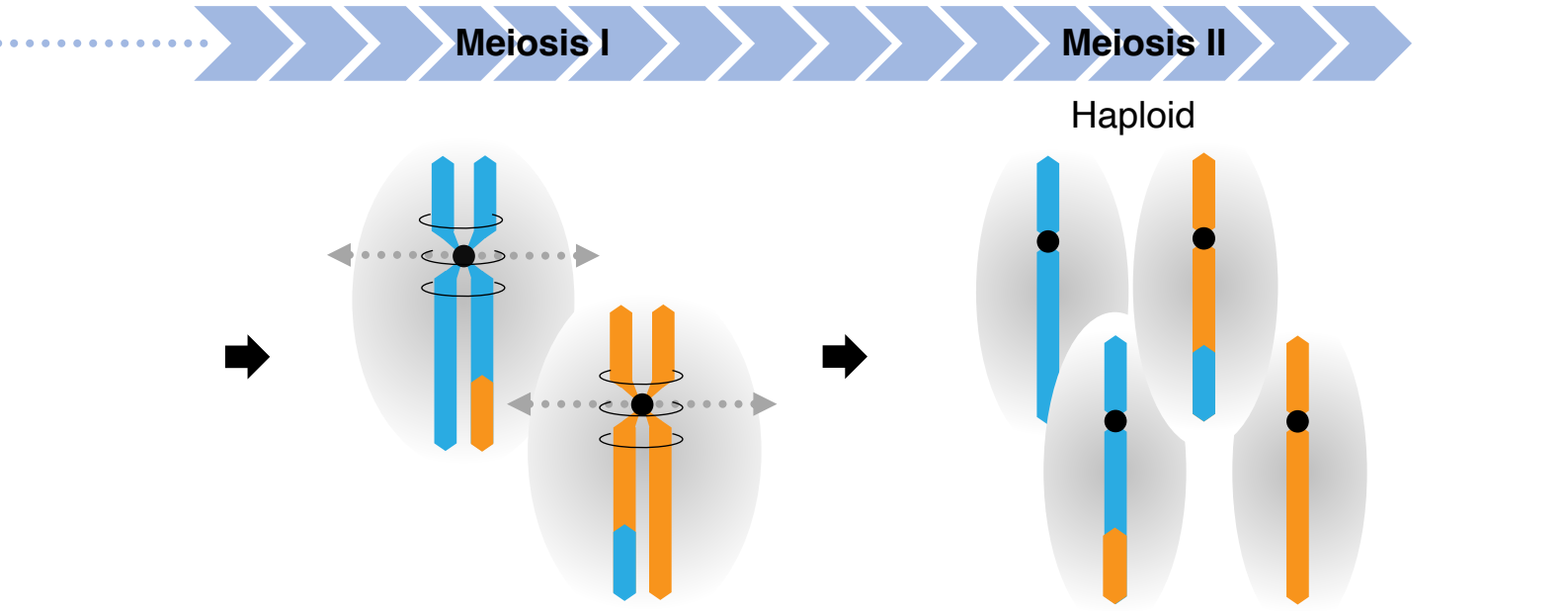

Figure 1. Meiosis progress.
In eukaryote, one diploidy cell produces four haploidy gametes through meiosis which consists of one round of DNA replication followed by two round of chromosome segregation. During meiotic prophase I, Meiotic programmed DSB induced by Topoisomerase-like protein Spo11 initiates meiotic recombination, which produces chiasma structure through inter-homologous crossover. The chiasma and cohesin complexes in armed regions of chromosome ensure the segregation of homologous chromosomes into opposite poles (meiosis I). Sister chromatids are divided into opposite poles in meiosis II, which is similar to mitotic cell division.

Figure 2

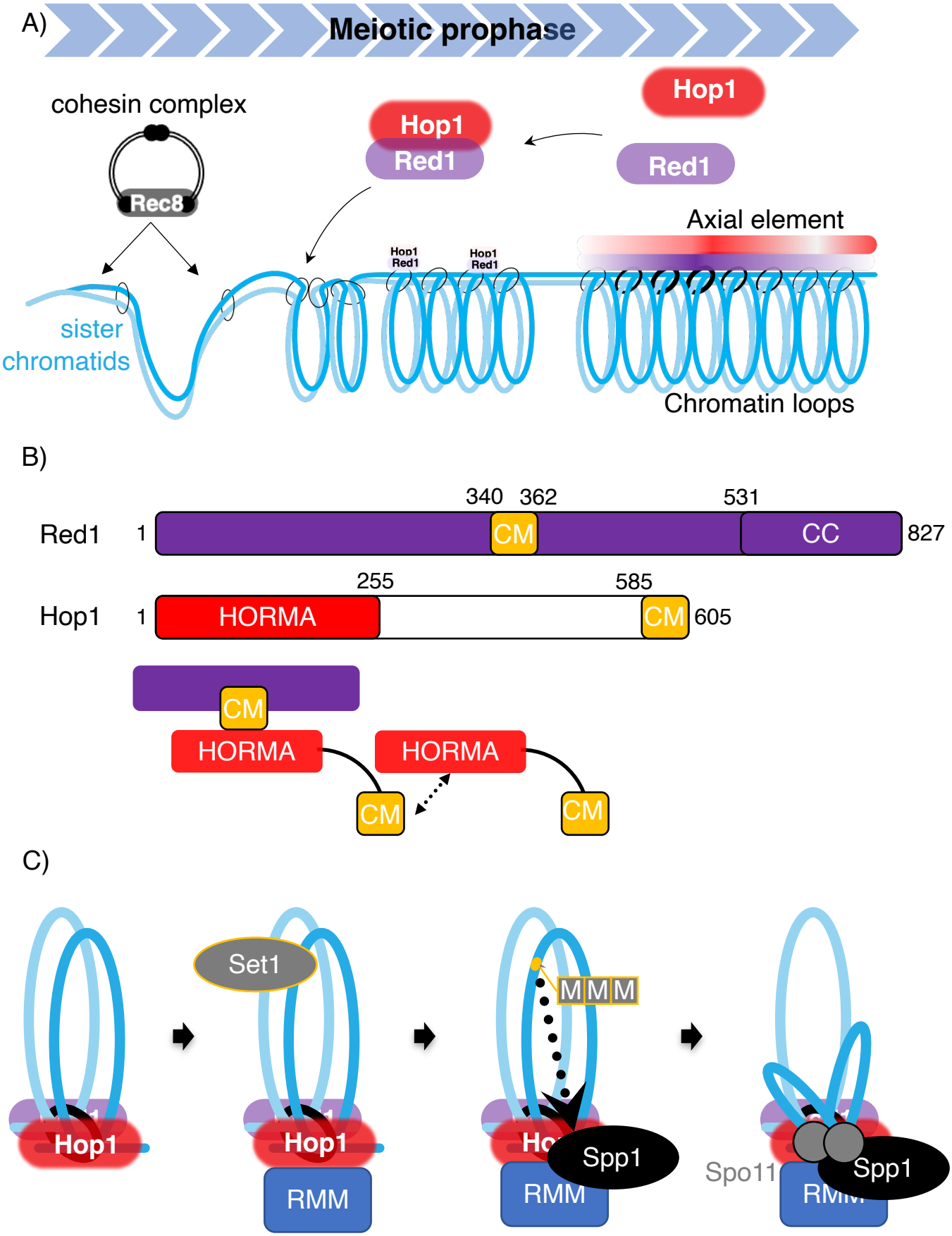
A)
Meiotic prophase
cohesin complex
Rec8
Hop1
Red1
Hop1
Red1
Axial element
Hop1 Red1
Hop1 Red1
sister chromatids
Chromatin loops
B)
Red1
1
340
362
531
CM
CC
827
Hop1
1
255
585
HORMA
CM
605
CM
HORMA
HORMA
CM
CM
C)
Hop1
Set1
Hop1
RMM
M M M
Spp1
RMM
Spo11
Spp1

Figure 2. The axis-loop structure in meiotic prophase.

A) At the onset of meiotic prophase, DNA replication accomplishes in accompany with cohesion of sister chromatids. Axial components such as Red1 and Hop1 are recruited to duplicated chromatin region to form axis-loop structure, which is required for the formation of meiotic DSBs by Spo11.

B) Schematic presentation of Red1 and Hop1 proteins. Coiled coil domain and closure motif are shown as CC and CM, respectively. HORMA domain interacts with closure motif.

C) Spo11-accessory proteins-RMM complex localizes on chromosome axial region enriched with Hop1. RMM complex recruits Spo11 and Spp1 to axis. Spp1 tethers the H3K4me3 region in loop sequences to axis, where is cleaved by Spo11.

Figure 3

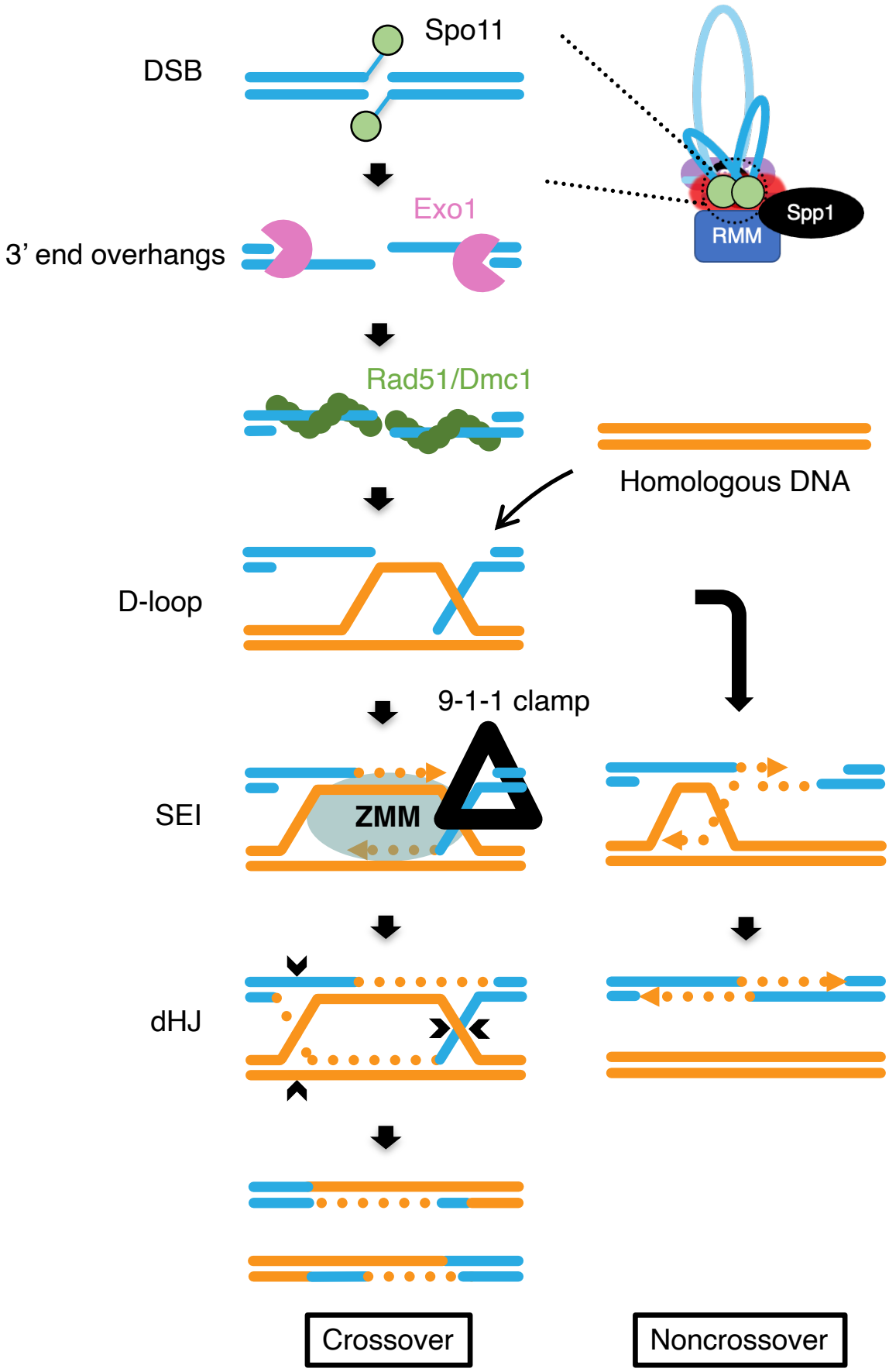
DSB
Spo11
Exo1
3' end overhangs
Spp1
RMM
Rad51/Dmc1
Homologous DNA
D-loop
9-1-1 clamp
SEI
ZMM
dHJ
Crossover
Noncrossover

Figure 3. Meiotic recombination pathway.
Meiotic DSB induction by Topoisomerase-like protein Spo11 initiates meiotic recombination. Spo11-oligonucleotides is removed from DSB ends then DNA resection start to generate 3' overhang single strand DNA by nuclease Exo1. The recombinases Rad51 and Dmc1 form filaments on ssDNA overhand and drive recombination template search between homologous chromosome. The 3`end ssDNA overhand invades into intact homologous chromosome to form D-loop structure initiating DNA synthesis. The ZMM proteins are recruited to stabilize D-loop structure and the 2nd end capture processes, SEI structure is established to promote the formation of dHJ structure. The dHJ structure is resolved by endonucleases to generate crossover product. Whereas the newly synthesized DNA disgorges back when D-loop is unstable without the assembly of ZMM proteins. The DSB is possible to be repaired by SDSA (synthesis dependent strand annealing) pathway which generates noncrossover product. Both crossover recombination and noncrossover recombination are collectively termed as meiotic recombination.

Figure 4

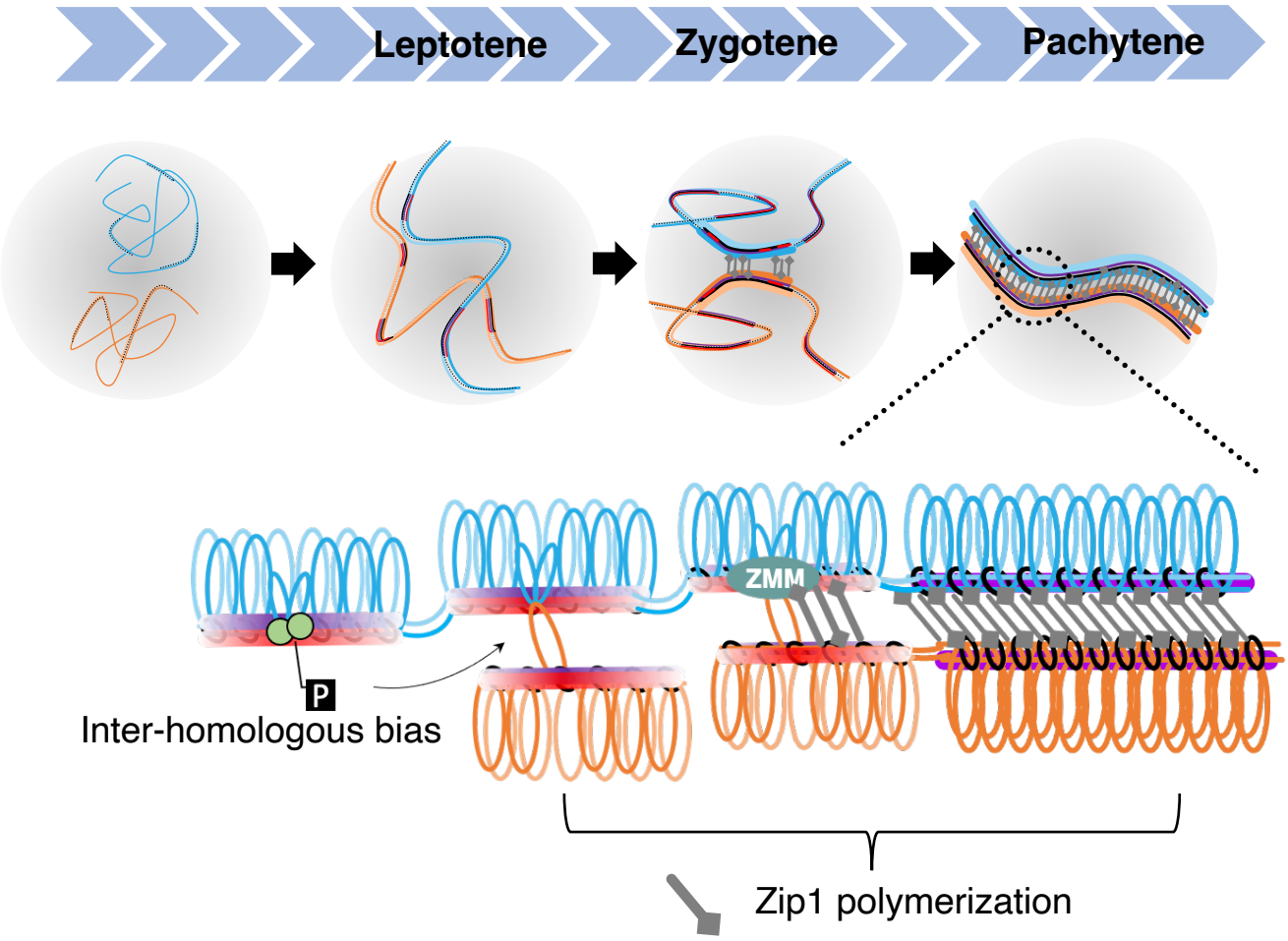

Figure 4. Homolog synapsis.
According to homolog synapsis, meiotic prophase I is divided into 4 substages, from leptotene, zygotene, pachytene to diplotene. Here shows the model from leptotene to pachytene. In leptotene, proteinaceous axial structure forms partially in where meiotic DSB is formed to initiate meiotic recombination. Since zygotene, homologous chromosomes are initiated to be synapsed by the polymerization of transverse filament Zip1 in a zipper-like fashion from recombination sites, which is initiated by ZMM proteins assembly. All autosomal chromosomes have been synapsed in pachytene.

Figure 5

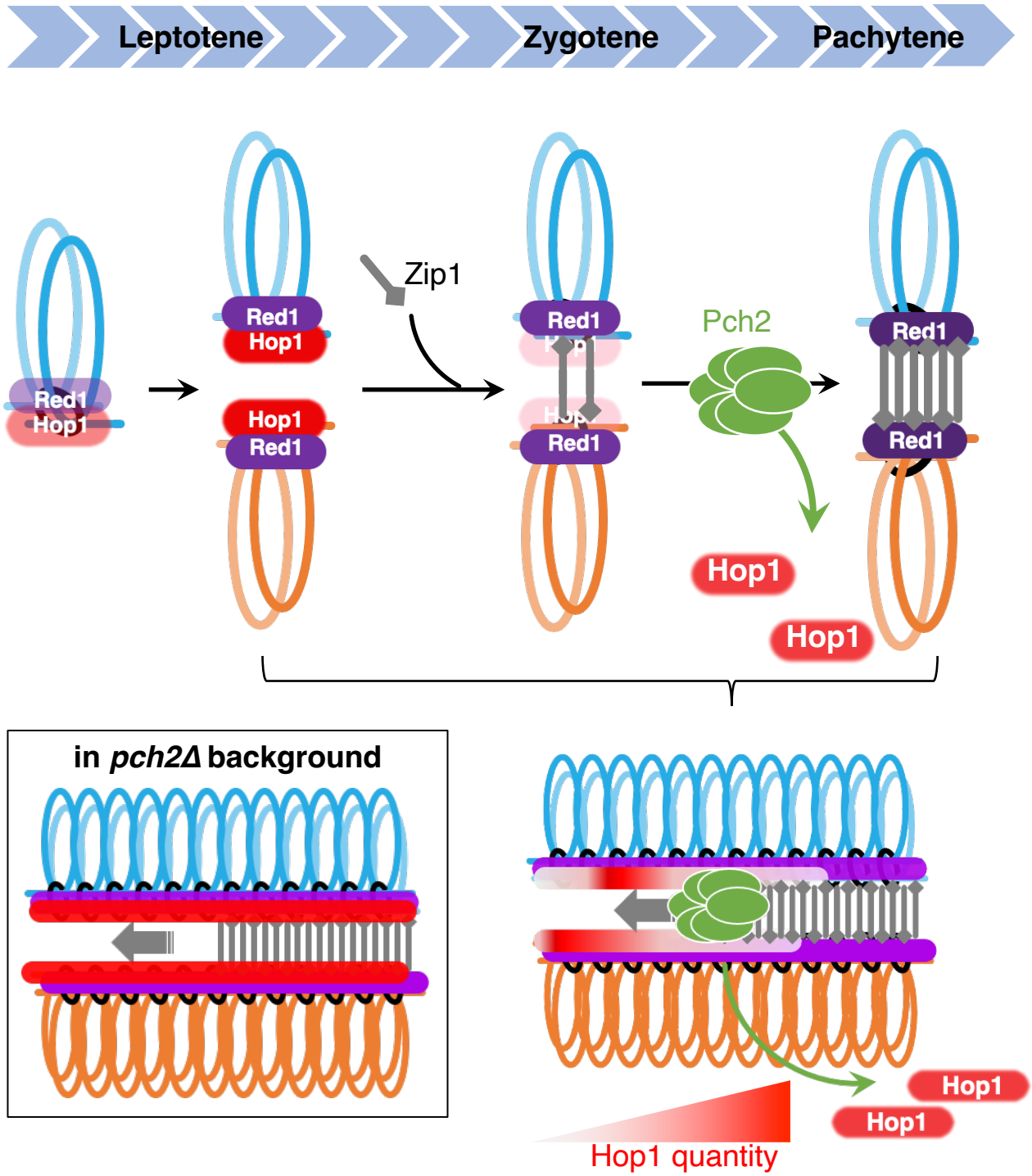

Figure 5. Dynamic loading of Hop1 on chromatin during meiotic prophase I. The distribution of axial Hop1 is dynamic. The regulations of Hop1 assembly and disassembly antagonize through prophase. In early prophase, the regulation of Hop1 assembly is intense. In accompany with meiotic prophase proceeds, the regulation of Hop1 disassembly is enhanced so that Hop1 is completely removed by Pch2 from synapsed axis until pachytene.

Figure 6

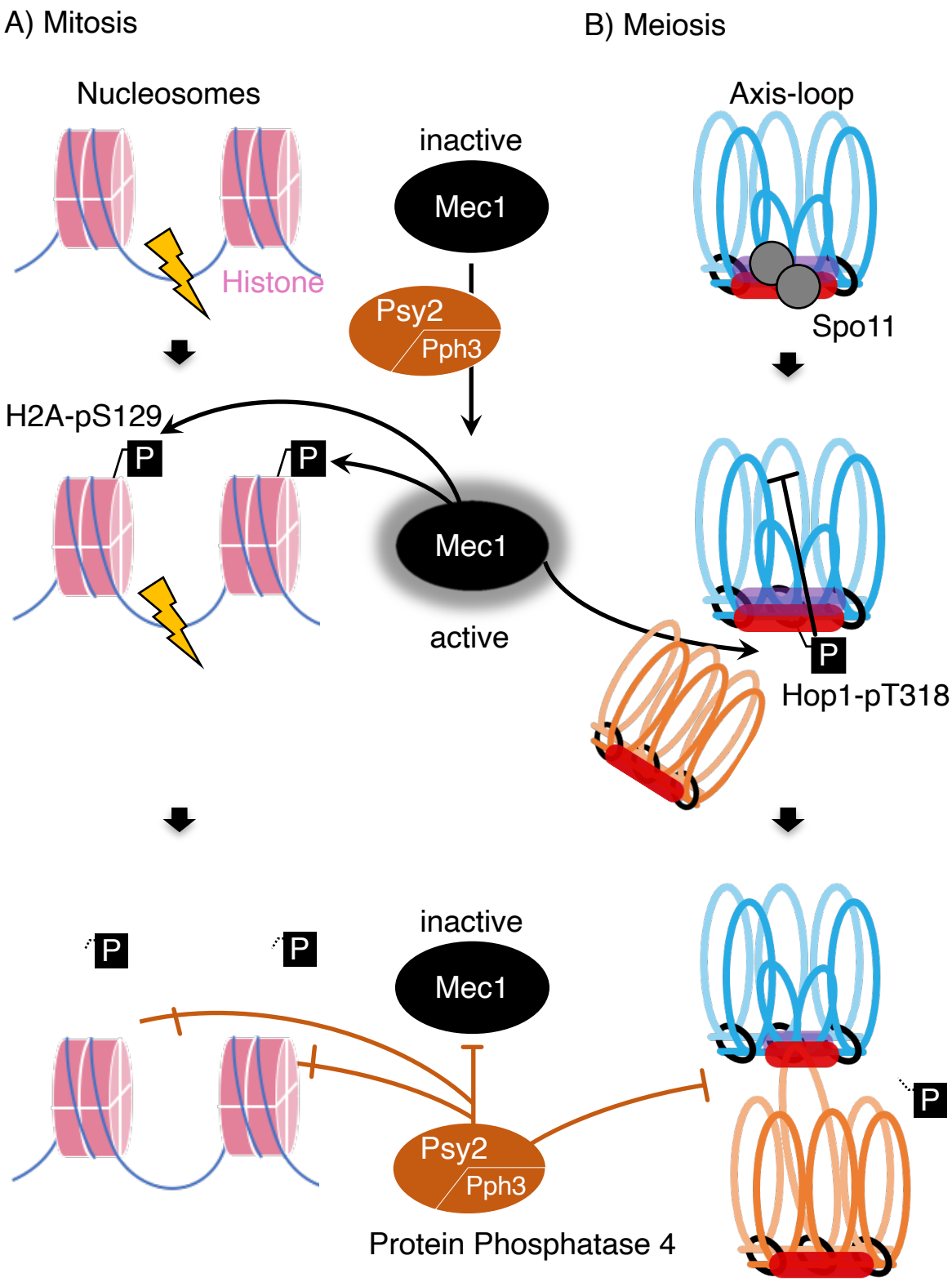
A) Mitosis
B) Meiosis
Nucleosomes
Histone
inactive
Mec1
Psy2
Pph3
Axis-loop
Spo11
H2A-pS129
P
P
Mec1
active
P
Hop1-pT318
P
P
inactive
Mec1
Psy2
Pph3
Protein Phosphatase 4
P

Figure 6. The cooperation of PP4 and Mec1^{ATR}/Tel1^{ATM} kinases in DNA damage response.

A) In mitosis, Mec1/Tel1 kinases are activated by DNA and phosphorylates multiple targets including histone H2A-S139 adjacent to DNA damage to promote DNA damage repair. After DNA damage repair finishes, PP4 counteracts Mec1/Tel1 kinases by dephosphorylating targets of Mec1/Tel1 kinases.

B) In meiotic recombination, Mec1/Tel1 kinases are activated by programmed DSB induction and phosphorylates multiple targets including Hop1-T318 in axial region adjacent to formed DSB site. In accompany with meiotic recombination proceed, PP4 dephosphorylates Hop1-pT318 to counteracts Mec1/Tel1 kinases since meiotic DSB is repaired.

Figure 7

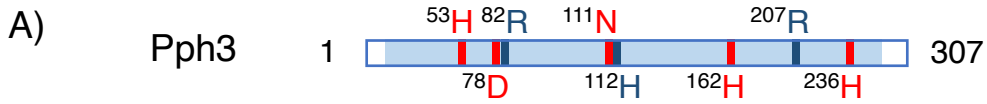
A)
Pph3
1
307
53H
82R
111N
207R
78D
112H
162H
236H

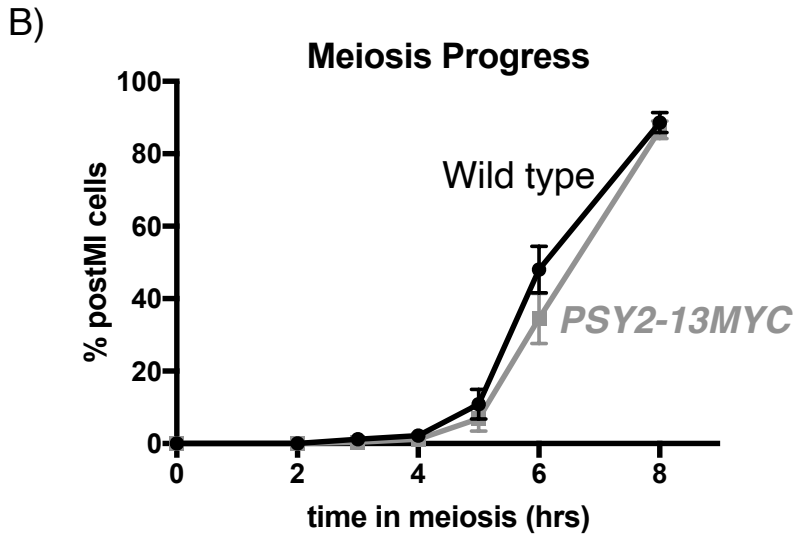
B)
Meiosis Progress
% postMI cells
100
80
60
40
20
0
0
2
4
6
8
time in meiosis (hrs)
Wild type
PSY2-13MYC

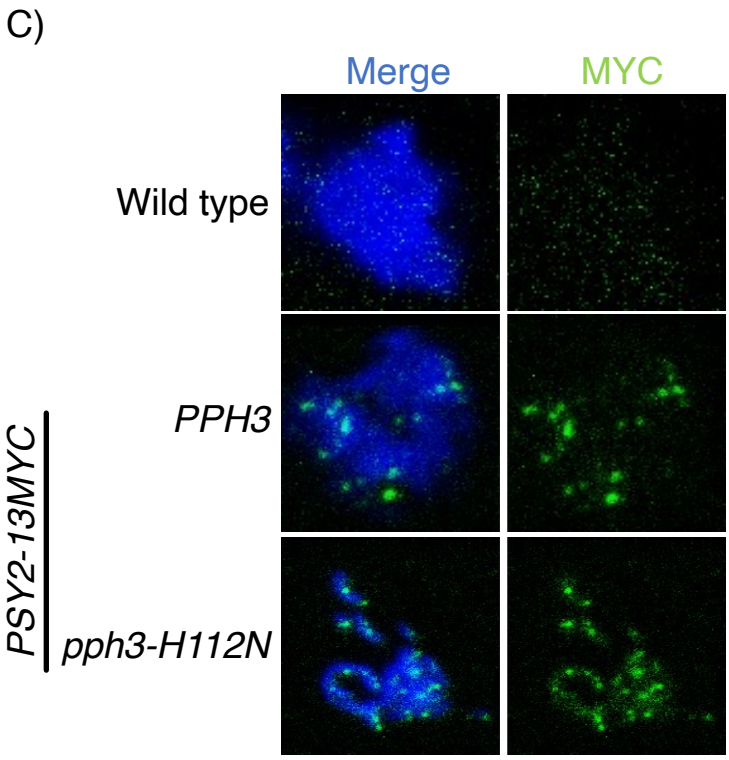
C)
Merge
MYC
Wild type
PPH3
PSY2-13MYC
pph3-H112N

D)

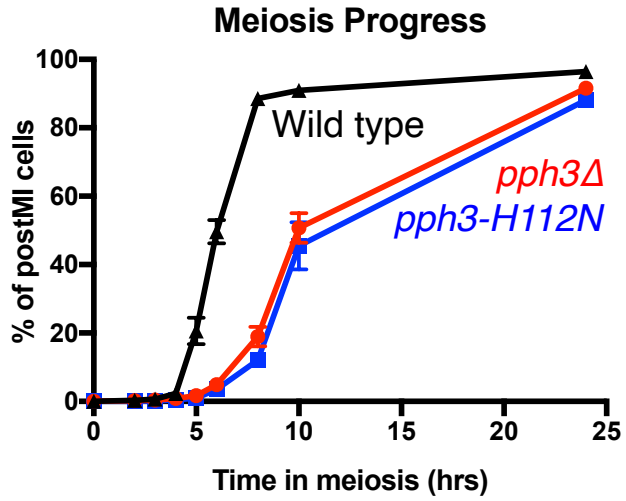

Figure 7. The *pph3-H112N* mutant showed an equivalent delay with *pph3Δ* mutant in meiosis progress.

A) Schematic presentation of amino acid sequence Pph3 protein. Residues contributing phosphate binding and metal coordination are shown in dark blue and red, respectively.

B) Meiosis progress was defined by frequency of post-meiosis I cell with more than 2 DAPI-stained bodies in wild type (black, NKY1303/1543), *PSY2-13MYC* (gray, MSY6198/6190) mutants. At least 100 cells were counted at the indicated time point. Error bars show the mean ± S.E.M (standard error of the mean) from over 3 times independent trials.

C) Localization of Psy2-13MYC on meiotic nuclei spread was analyzed by mouse anti-Myc antibody in wild type (NKY1303/1543), *PSY2-13MYC* (MSY6198/6190), and *pph3-H112N PSY2-13MYC* (MSY6242/6244) stains. The representative cytological immunostaining images of Psy2-13MYC (green) overlaid with DAPI (blue) are shown at 6 hour after meiosis entry.

D) Meiosis progress was defined by frequency of post-meiosis I cell with more than 2 DAPI-stained bodies) in wild type (black, NKY1303/1543), *pph3Δ* (red, MSY5632/5634) and *pph3-H112N* (blue, MSY6219/6220) mutants. At least 100 cells were counted at the indicated time point. Error bars show the mean ± S.E.M (standard error of the mean) from over 3 times independent trials.

Figure 8

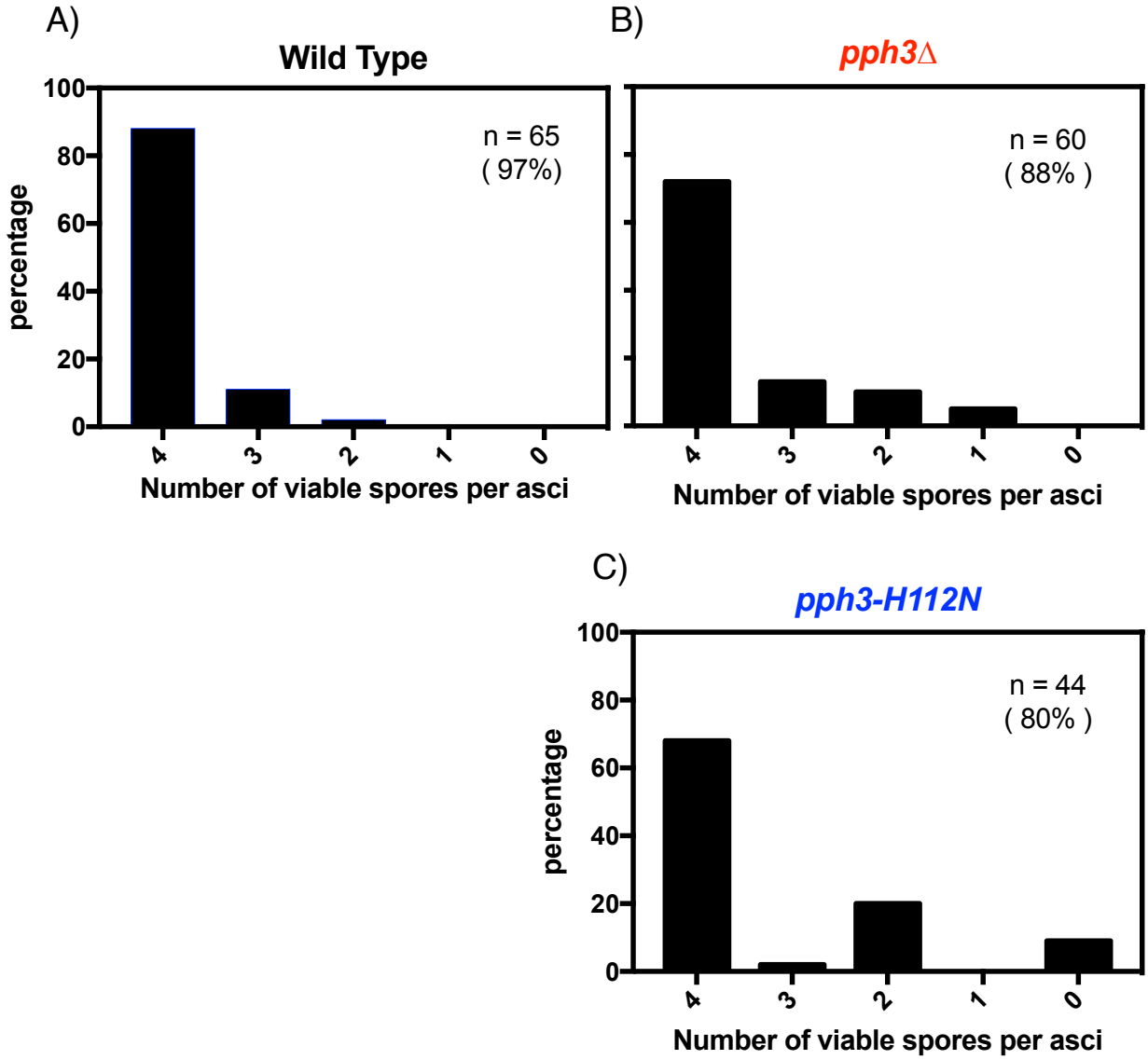

Figure 8. The *pph3* mutants showed reduced spore viability.

A) Tetrad analysis of spore viability in wild type (black, NKY1303/1543). The graph shows the respective fraction of 0#, 2#, 3#, 4# viable spore from one asci. n: the number of analyzed asci and the overall spore viability are shown.

B) Tetrad analysis of spore viability in *pph3Δ* (red, MSY5632/5634) mutant. The graph shows the respective fraction of 0#, 2#, 3#, 4# viable spore from one asci. n: the number of analyzed asci and the overall spore viability are shown.

C) Tetrad analysis of spore viability in *pph3-H112N* (blue, MSY6219/6220) mutant. The graph shows the respective fraction of 0#, 2#, 3#, 4# viable spore from one asci. n: the number of analyzed asci and the overall spore viability are shown.

Figure 9

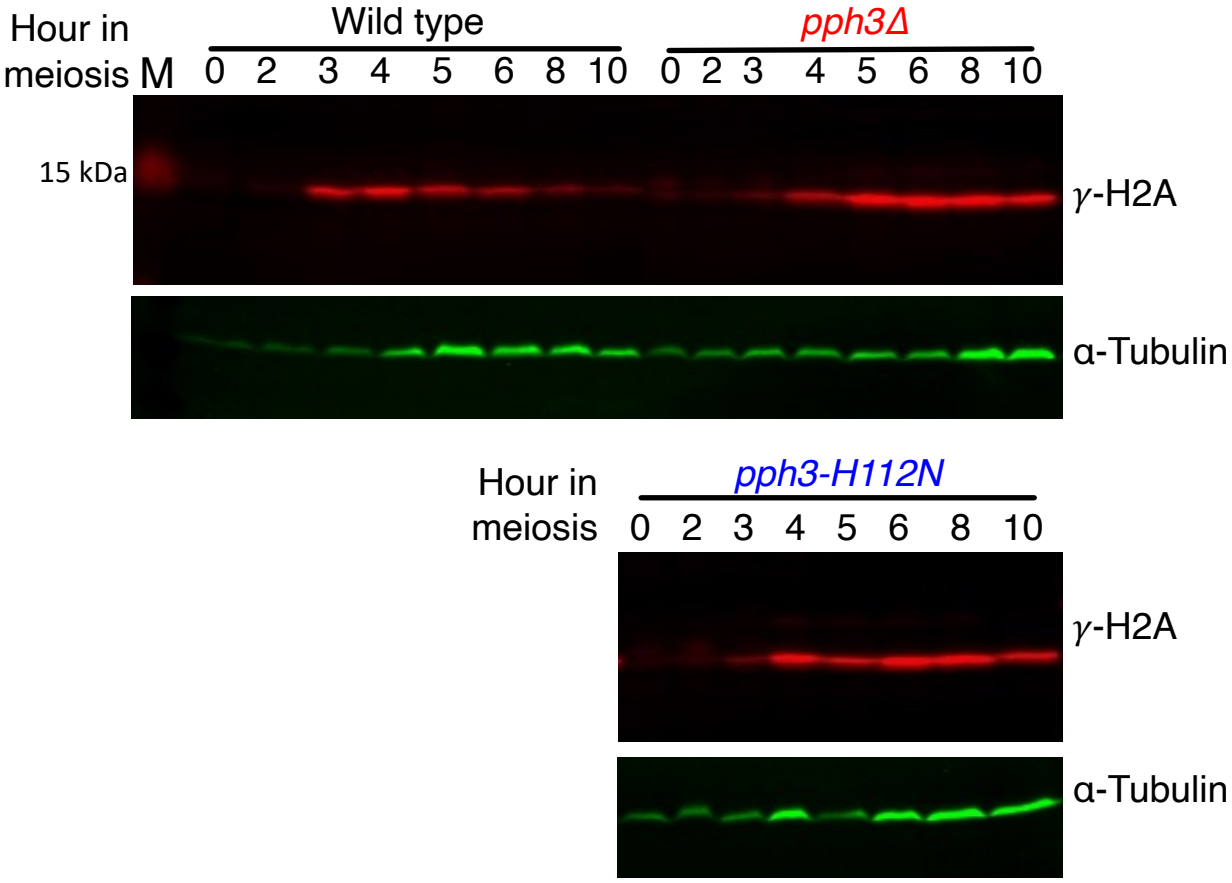

Figure 9. The *pph3* mutants showed delayed but longer observation of γH2A signal in meiosis.
Representative western blot images of phosphorylated H2A-S129 (γ-H2A) in wild type (black, NKY1303/1543), *pph3Δ* (red, MSY5632/5634), *pph3-H112N* (blue, MSY6219/6220) mutants at the indicated time point during meiosis. The meiotic yeast lysates were subjected to western blotting with rabbit anti-γH2A antibody (upper, red) and rat-α-Tubulin (bottom, green) as loading control. M denotes molecular weight marker.

Figure 10

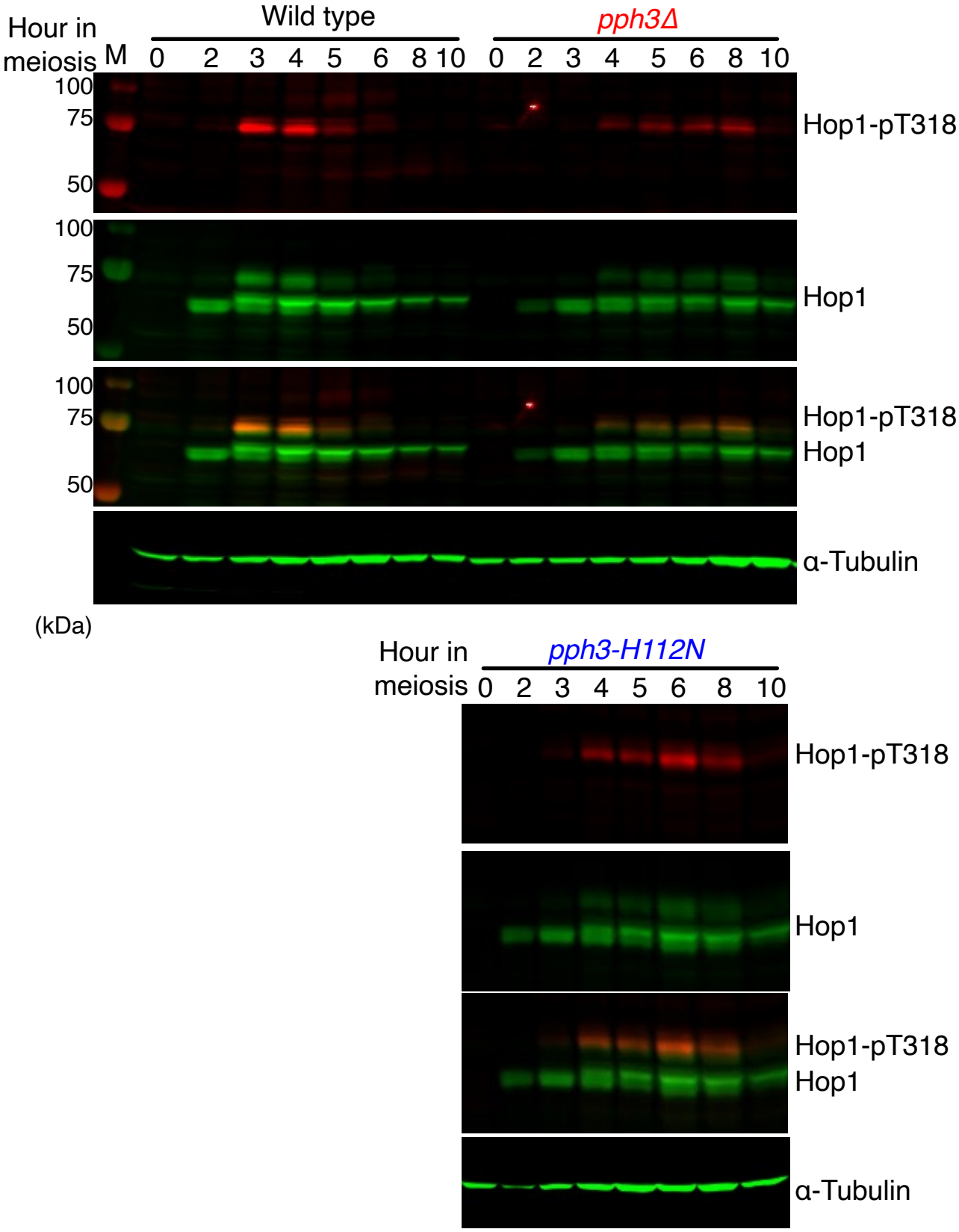
Hour in meiosis
Wild type
pph3Δ
M 0 2 3 4 5 6 8 10 0 2 3 4 5 6 8 10
100
75
50
Hop1-pT318
Hop1
Hop1-pT318
Hop1
α-Tubulin
(kDa)
Hour in meiosis
pph3-H112N
0 2 3 4 5 6 8 10
Hop1-pT318
Hop1
Hop1-pT318
Hop1
α-Tubulin

Figure 10. The *pph3* mutants showed wild type level of Hop1 expression with delay in both phosphorylation and dephosphorylation of Hop1-T318. Representative western blot images of phosphorylated Hop1-T318 (Hop1-pT318), Hop1 and merge Hop1p-T318 (red) and Hop1 (green) in wild type (black, NKY1303/1543), *pph3Δ* (red, MSY5632/5634), *pph3-H112N* (blue, MSY6219/6220) mutants at the indicated time point during meiosis. The meiotic yeast lysates were subjected to western blotting with rabbit anti-Hop1-pT318 antibody and guinea pig anti-Hop1 antibody. α-Tubulin (green) is also showed bottom as loading control. M denotes molecular weight markers.

Figure 11

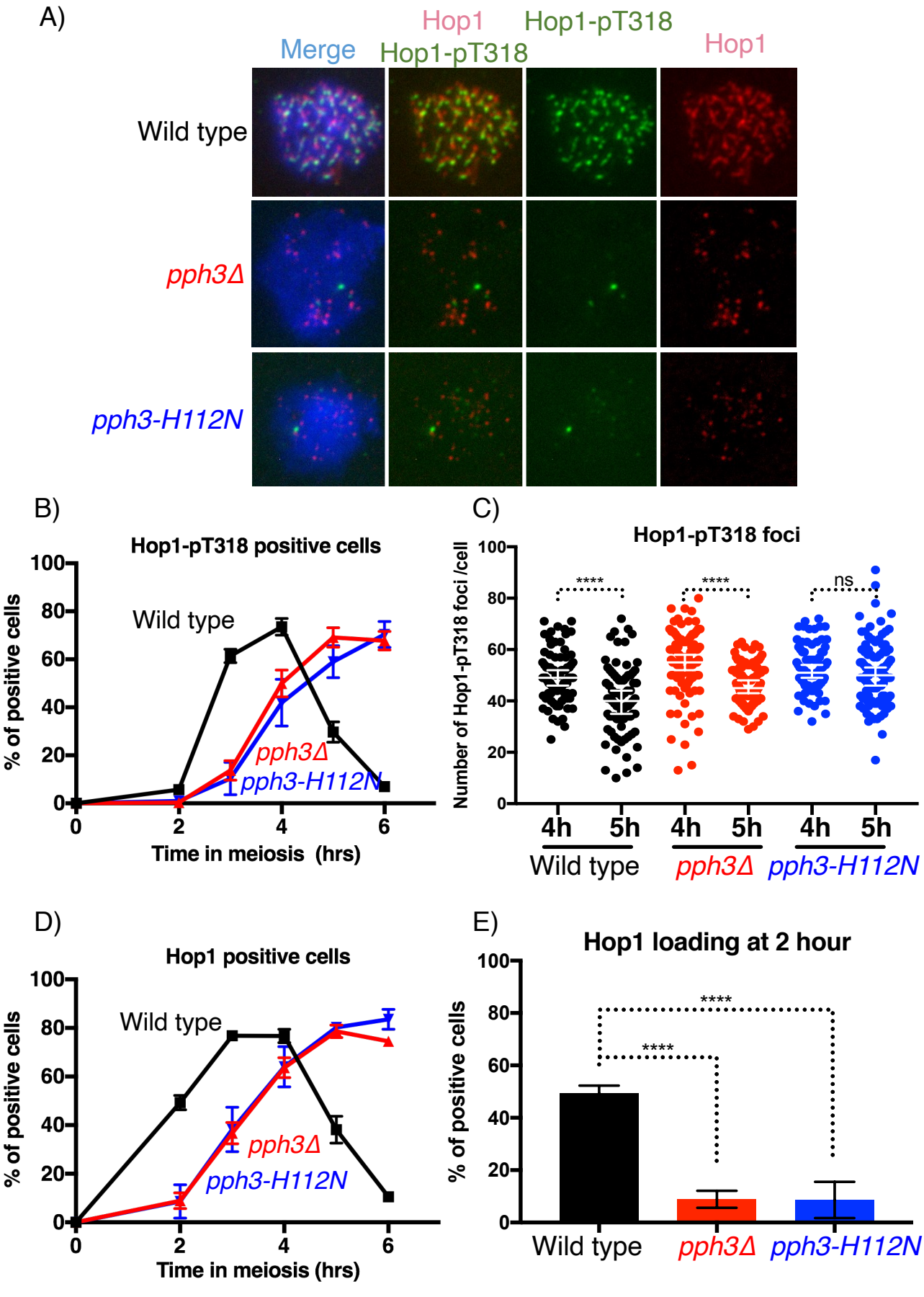
A)
Merge
Hop1
Hop1-pT318
Hop1-pT318
Hop1
Wild type
pph3Δ
pph3-H112N
B)
Hop1-pT318 positive cells
% of positive cells
Wild type
pph3Δ
pph3-H112N
Time in meiosis (hrs)
C)
Hop1-pT318 foci
Number of Hop1-pT318 foci /cell
****
****
ns
4h
5h
4h
5h
4h
5h
Wild type
pph3Δ
pph3-H112N
D)
Hop1 positive cells
% of positive cells
Wild type
pph3Δ
pph3-H112N
Time in meiosis (hrs)
E)
Hop1 loading at 2 hour
% of positive cells
****
****
Wild type
pph3Δ
pph3-H112N

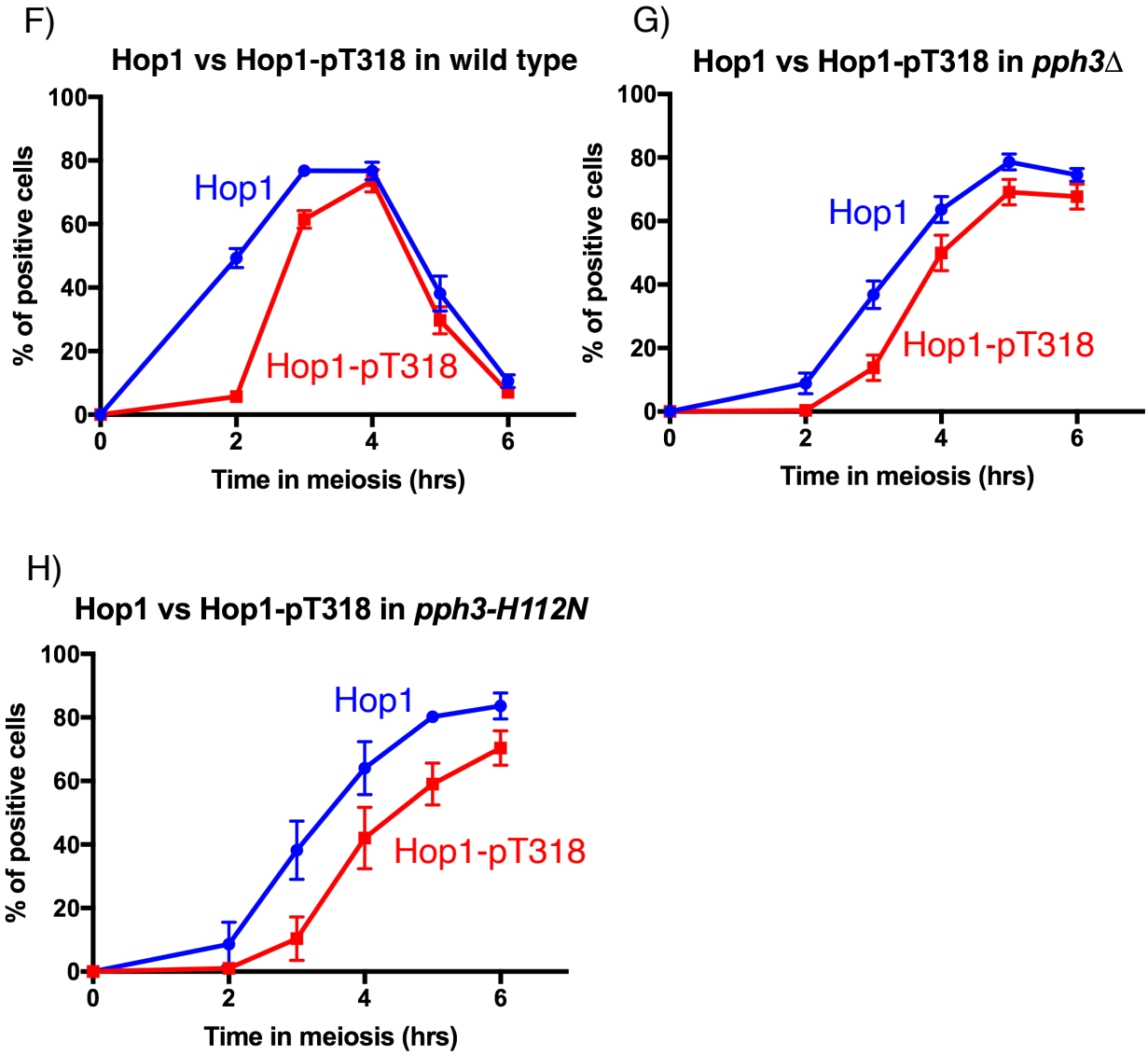

Figure 11. The *pph3* mutants showed significantly delay in the loading of Hop1 onto leptotene chromatin.

A) Immunostaining analysis of Hop1-pT318 and Hop1 with rabbit anti-Hop1-pT318 antibody, guinea pig anti-Hop1 antibody on meiotic nuclear spreads was carried out in wild type (black, NKY1303/1543), *pph3Δ* (red, MSY5632/5634), *pph3-H112N* (blue, MSY6219/6220) mutants. The representative images overlaid with DAPI (blue), Hop1-pT318 (green) and Hop1 (red) at 3 hour after meiosis entry are showed.

B) Kinetics of Hop1-pT318 focus positive cells (cell with more than 5 Hop1-pT318 foci) in wild type (black, NKY1303/1543), *pph3Δ* (red, MSY5632/5634), *pph3-H112N* (blue, MSY6219/6220) mutants. Graph shows the percentage of Hop1-pT318 focus positive cells in association with meiosis progress. Error bars indicate the mean ± S.E.M (standard error of the mean) from over 3 times independent trials.

C) Distributions of Hop1-pT318 foci number per Hop1-pT318 focus positive cell in wild type (black, NKY1303/1543), *pph3Δ* (red, MSY5632/5634), *pph3-H112N* (blue, MSY6219/6220) mutants at 4 hour and 5 hour after meiosis entry. Over 70 nuclei were analyzed in each strain. Error bars indicate the median ± 95% C.I. (Confidence Interval). Statistically significant differences were determined by Mann-Whitney's U-test using Prism9 software.(****: p value < 0.0001; ns: not significant)

D) Kinetics of Hop1 focus positive cells (cell with more than 5 Hop1 foci) in wild type (black, NKY1303/1543), *pph3Δ* (red, MSY5632/5634), *pph3-H112N* (blue, MSY6219/6220) mutants. Graph shows the percentage of Hop1 focus positive cells in association with meiosis progress. Error bars indicate the mean ± S.E.M (standard error of the mean) from over 3 times independent trials.

E) Graph re-presents the percentage of Hop1 focus positive cells in wild type (black, NKY1303/1543), *pph3Δ* (red, MSY5632/5634), *pph3-H112N* (blue, MSY6219/6220) mutants at 2 hour after meiosis entry. Error bars indicate the mean ± S.E.M (standard error of the mean) from over 3 times independent trials. Statistically significant differences were determined by paired t-test using Prism9 software.(****: p value < 0.0001)

F) Kinetics of Hop1 (blue) and Hop1-pT318 (red) focus positive cells in wild type (NKY1303/1543). Graph shows the percentage of Hop1 and Hop1-pT318 focus positive cells in association with meiosis progress. Error bars indicate the mean ± S.E.M (standard error of the mean) from over 3 times independent trials.

G) Kinetics Hop1 (blue) and Hop1-pT318 (red) focus positive cells in *pph3Δ* (MSY5632/5634) mutant. Graph shows the percentage of Hop1 and Hop1-pT318 focus positive cells in association with meiosis progress. Error bars indicate the mean ± S.E.M (standard error of the mean) from over 3 times independent trials.

H) Kinetics of Hop1 (blue) and Hop1-pT318 (red) focus positive cells in *pph3-H112N* (MSY6219/6220) mutant. Graph shows the percentage of Hop1 and Hop1-pT318 focus positive cells in association with meiosis progress. Error bars indicate the mean ± S.E.M (standard error of the mean) from over 3 times independent trials.

Figure 12

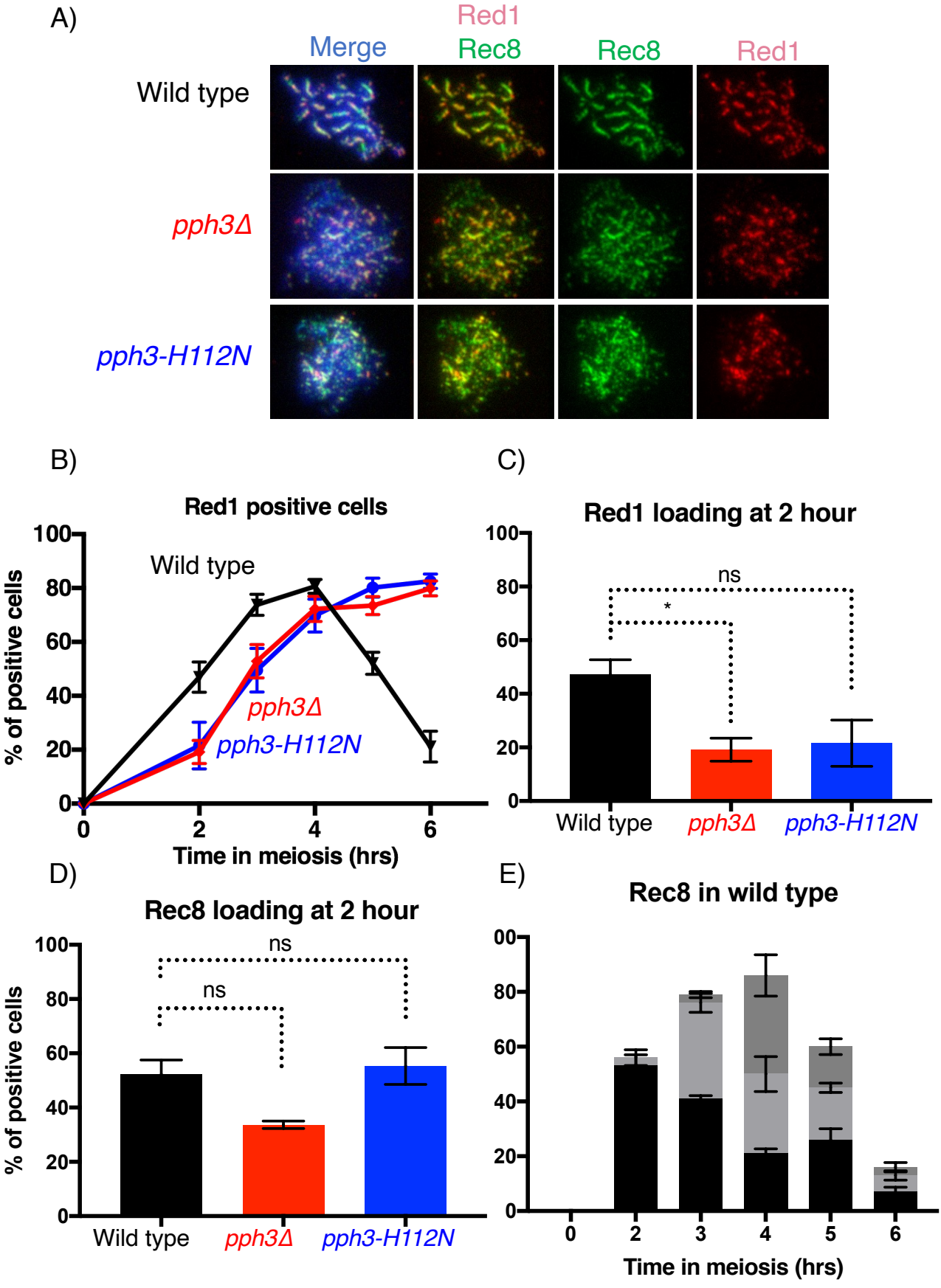
A)
Merge
Red1
Rec8
Rec8
Red1
Wild type
pph3Δ
pph3-H112N
B)
Red1 positive cells
Wild type
pph3Δ
pph3-H112N
% of positive cells
Time in meiosis (hrs)
C)
Red1 loading at 2 hour
ns
*
Wild type
pph3Δ
pph3-H112N
D)
Rec8 loading at 2 hour
ns
ns
% of positive cells
Wild type
pph3Δ
pph3-H112N
E)
Rec8 in wild type
Time in meiosis (hrs)

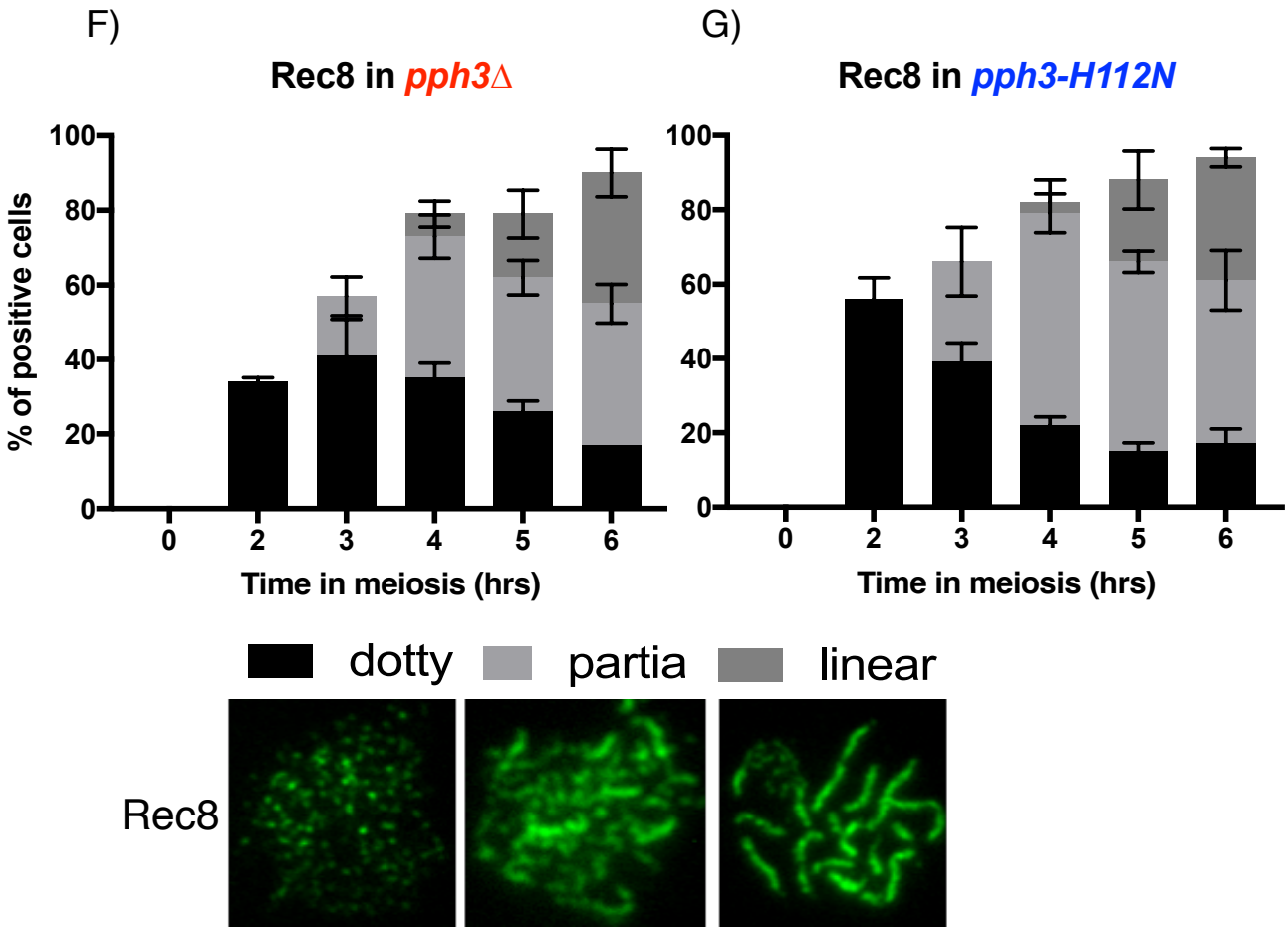
F)
Rec8 in pph3Δ
% of positive cells
100
80
60
40
20
0
0
2
3
4
5
6
Time in meiosis (hrs)
G)
Rec8 in pph3-H112N
100
80
60
40
20
0
0
2
3
4
5
6
Time in meiosis (hrs)
dotty
partia
linear
Rec8

Figure 12. The *pph3* mutants showed significant delay in the loading of Red1 onto leptotene chromatin, but not in the loading of Rec8.

A) Immunostaining analysis of Rec8 and Red1 with rabbit anti-Rec8 antibody and chick anti-Red1 antibody in meiotic nuclear spread was carried out in wild type (black, NKY1303/1543), *pph3Δ* (red, MSY5632/5634), *pph3-H112N* (blue, MSY6219/6220) mutants. The representative images overlaid with DAPI (blue), Rec8 (green) and Red1 (red) at 3 hour after meiosis entry are shown.

B) Kinetics of Red1 focus positive cells (cell with more than 5 Red1 foci) in wild type (black, NKY1303/1543), *pph3Δ* (red, MSY5632/5634), *pph3-H112N* (blue, MSY6219/6220) mutants. Graph shows the percentage of Red1 focus positive cells in association with meiosis progress. Error bars indicate the mean ± S.E.M (standard error of the mean) from over 3 times independent trials.

C) Graph re-presents the percentage of Red1 focus positive cells in wild type (black, NKY1303/1543), *pph3Δ* (red, MSY5632/5634), *pph3-H112N* (blue, MSY6219/6220) mutants at 2 hour after meiosis entry. Error bars indicate the mean ± S.E.M (standard error of the mean) from over 3 times independent trials. Statistically significant differences were determined by paired t-test using Prism9 software. (*: p value < 0.05; ns: not significant)

D) Graph shows the percentage of Rec8 focus positive cells in wild type (black, NKY1303/1543), *pph3Δ* (red, MSY5632/5634), *pph3-H112N* (blue, MSY6219/6220) mutants at 2 hour after meiosis entry. Error bars indicate the mean ± S.E.M (standard error of the mean) from over 3 times independent trials. Statistically significant differences were determined by paired t-test using Prism9 software. (ns: not significant)

E) Kinetics of Rec8 morphology on meiotic nuclei spread in wild type (black, NKY1303/1543), which was analyzed by classifying into linear (dark gray), partial (light gray) and dotty (black). A minimum 100 cells were counted at the indicated time point. Error bars indicate the mean ± S.E.M (standard error of the mean) from over 3 times independent trials.

F) Kinetics of Rec8 morphology on meiotic nuclei spread in *pph3Δ* (red, MSY5632/5634) mutant, which was analyzed by classifying into linear (dark gray), partial (light gray) and dotty (black). A minimum 100 cells were counted at the indicated time point. Error bars indicate the mean ± S.E.M (standard error of the mean) from over 3 times independent trials.

G) Kinetics of Rec8 morphology on meiotic nuclei spread in *pph3-H112N* (blue, MSY6219/6220) mutant, which was analyzed by classifying into linear (dark gray), partial (light gray) and dotty (black). A minimum 100 cells were counted at the indicated time point. Error bars indicate the mean ± S.E.M (standard error of the mean) from over 3 times independent trials.

Figure 13

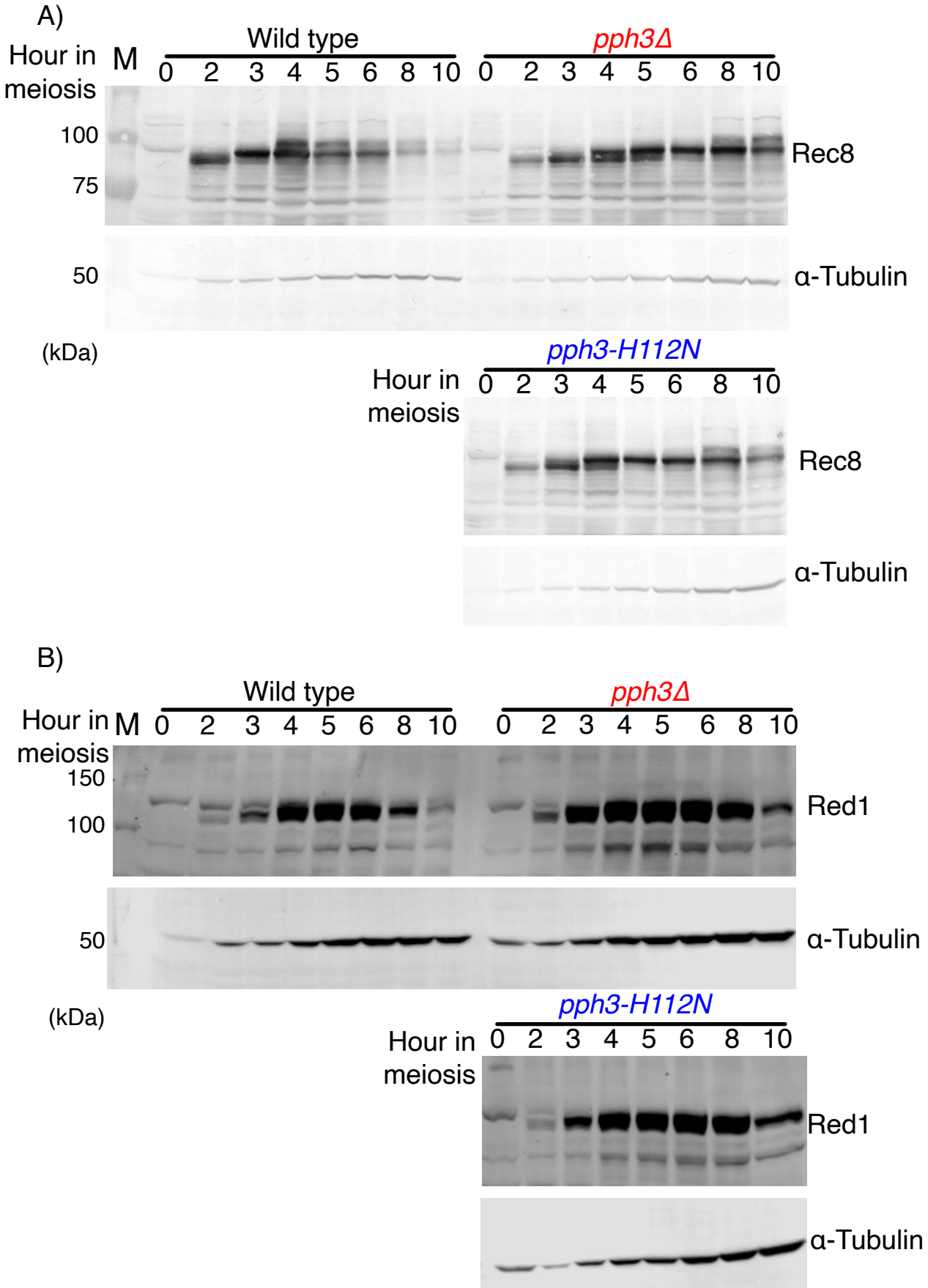
A)
Hour in meiosis
M
Wild type
0 2 3 4 5 6 8 10
pph3Δ
0 2 3 4 5 6 8 10
100
75
Rec8
50
α-Tubulin
(kDa)
pph3-H112N
Hour in meiosis
0 2 3 4 5 6 8 10
Rec8
α-Tubulin
B)
Hour in meiosis
M
Wild type
0 2 3 4 5 6 8 10
pph3Δ
0 2 3 4 5 6 8 10
150
100
Red1
50
α-Tubulin
(kDa)
pph3-H112N
Hour in meiosis
0 2 3 4 5 6 8 10
Red1
α-Tubulin

Figure 13. The *pph3* mutants showed wild type level of the expression of Red1 protein and Rec8 protein.

A) Representative western blot images of expression of Rec8 protein in wild type wild type (black, NKY1303/1543), *pph3Δ* (red, MSY5632/5634), *pph3-H112N* (blue, MSY6219/6220) mutants at the indicated time point during meiosis. The meiotic yeast lysates were subjected to western blotting with rabbit anti-Rec8 antibody. α-Tubulin is also showed bottom as loading control. M denotes molecular weight markers.

B) Representative western blot images of expression of Red1 protein in wild type (black, NKY1303/1543), *pph3Δ* (red, MSY5632/5634), *pph3-H112N* (blue, MSY6219/6220) mutants at the indicated time point during meiosis. The meiotic yeast lysates were subjected to western blotting with chick anti-Red1 antibody. α-Tubulin is also showed bottom as loading control. M denotes molecular weight markers.

Figure 14

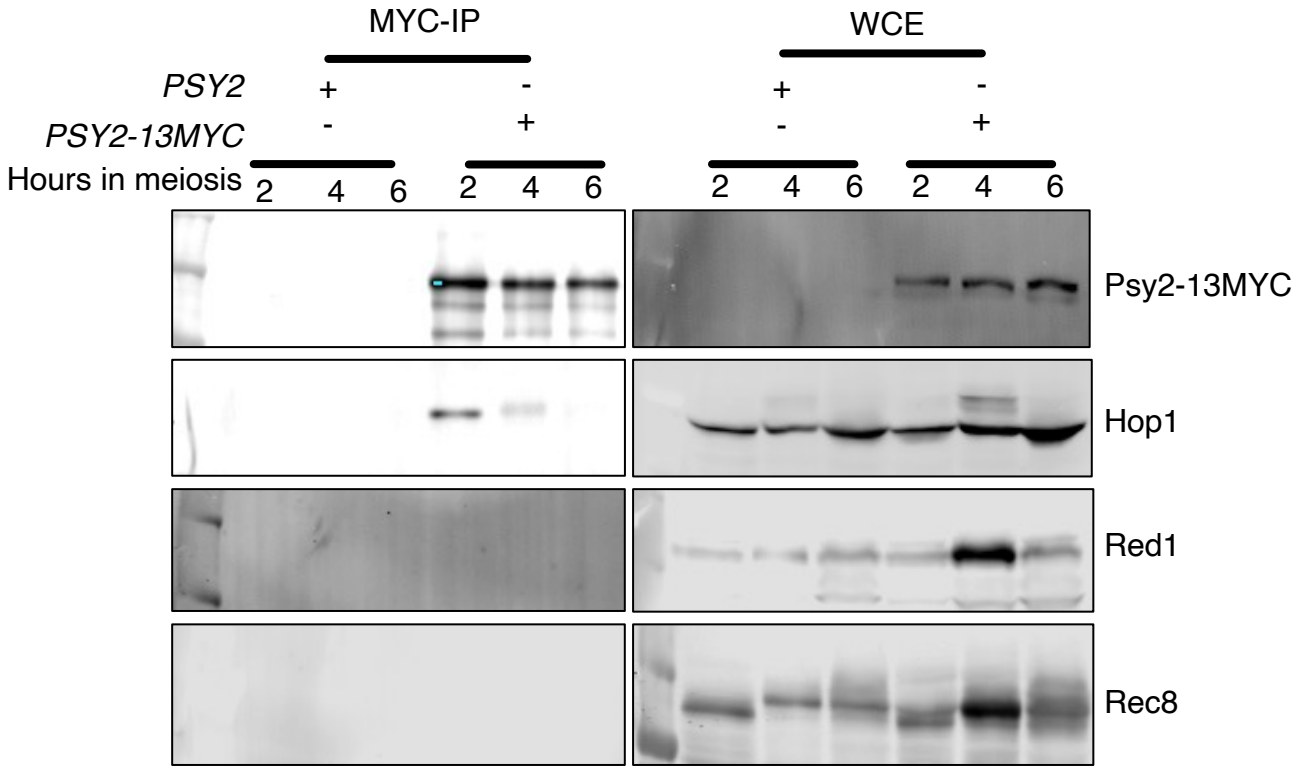

Figure 14. PP4 complex showed a physical interaction with Hop1 *in vivo*, neither Rec8 nor Red1.

Immunoprecipitation analysis of Psy2-13Myc from *PSY2* (non-tag, NKY1303/1543) and *PSY2-13MYC* (MSY6188/6190) was carried out with mouse anti-MYC antibody at the indicated time point. The immunoprecipitation products (MYC-IP) and whole cell extracts (WCEs) were subjected to western blotting by mouse anti-Myc antibody, guinea pig anti-Hop1 antibody, chick anti-Red1antibody, rabbit anti-Rec8 antibody.

Figure 15

A)

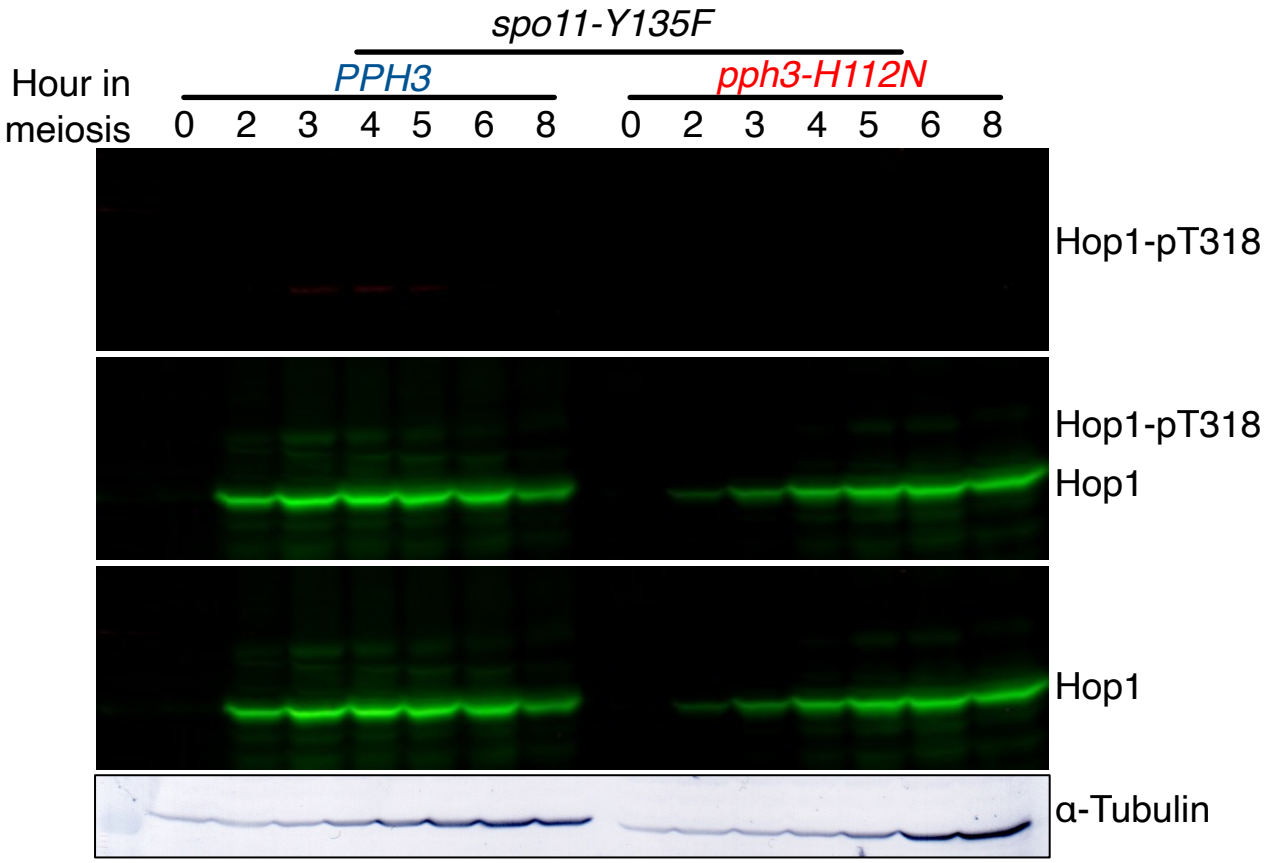
spo11-Y135F
Hour in meiosis
PPH3
pph3-H112N
0 2 3 4 5 6 8
0 2 3 4 5 6 8
Hop1-pT318
Hop1-pT318
Hop1
Hop1
α-Tubulin

B)

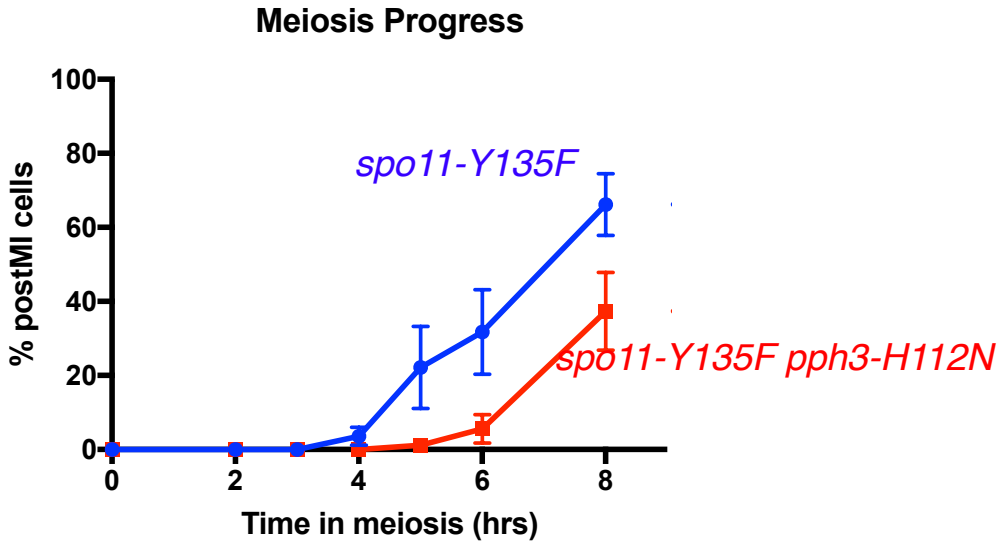
Meiosis Progress
% postMI cells
100
80
60
40
20
0
0
2
4
6
8
Time in meiosis (hrs)
spo11-Y135F
spo11-Y135F pph3-H112N

Figure 15. The *pph3* mutant showed a delay in meiosis progress even in the *spo11-Y135F* background.

A) Representative western blot images of phosphorylated Hop1-T318 (Hop1-pT318), Hop1 and merge Hop1p-T318 (red) and Hop1 (green) in *spo11-Y135F* (blue, MSY6345/6346) and *spo11-Y135F pph3-H112N* (red, MSY6568/6570) mutants at the indicated time point during meiosis. The meiotic yeast lysates were subjected to western blotting with rabbit anti-Hop1-pT318 antibody and guinea pig anti-Hop1 antibody. α-Tubulin (green) is also showed bottom as loading control.

B) Meiosis progress was defined by frequency of post-meiosis I cell with more than 2 DAPI-stained bodies in *spo11-Y135F* (blue, MSY6345/6346) and *spo11-Y135F pph3-H112N* (red, MSY6568/6570) mutants. At least 100 cells were counted at the indicated time point. Error bars show the mean ± S.E.M (standard error of the mean) from over 3 times independent trials.

Figure 16

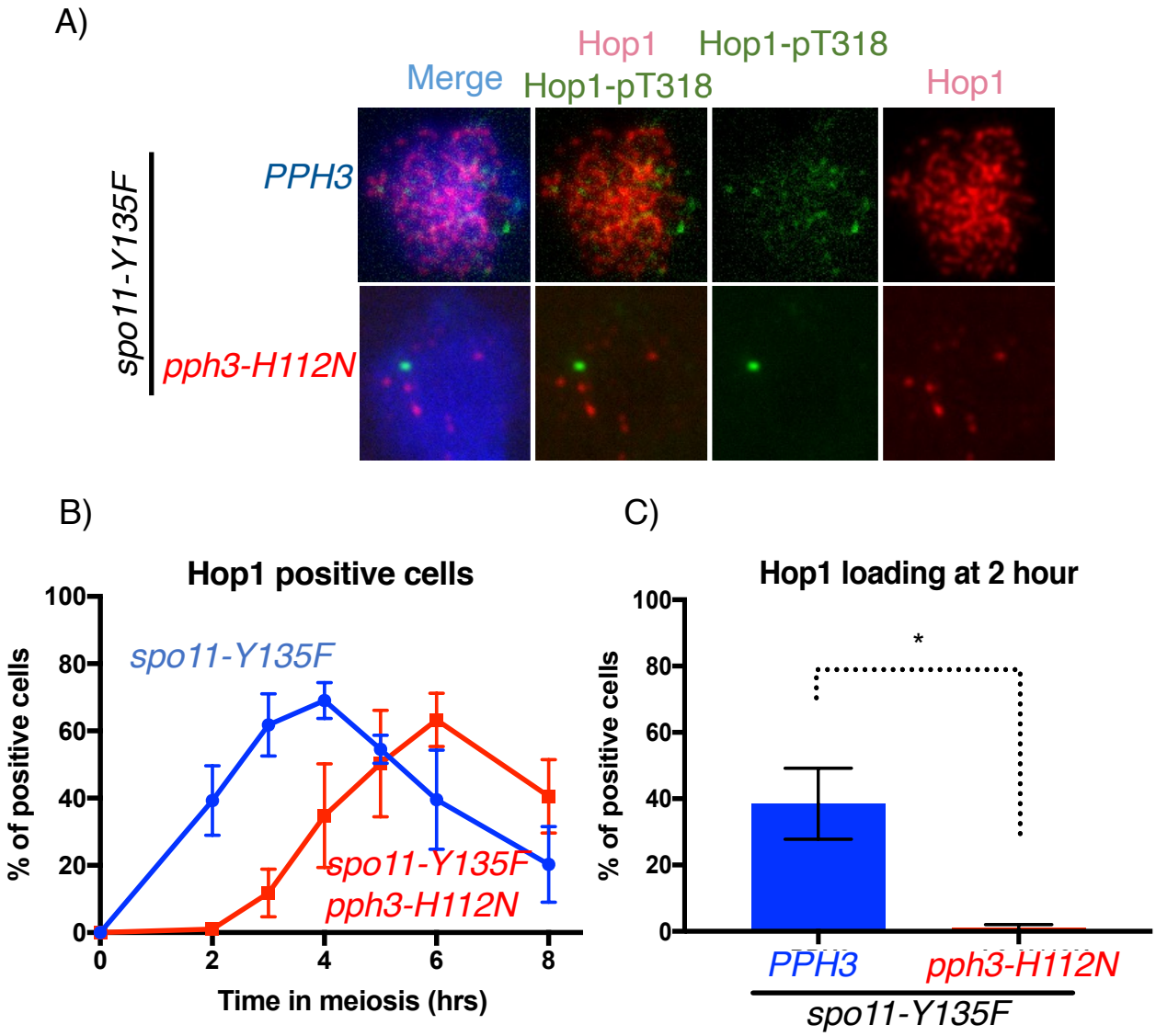
A)
Merge
Hop1
Hop1-pT318
Hop1-pT318
Hop1
spo11-Y135F
PPH3
pph3-H112N
B)
Hop1 positive cells
% of positive cells
spo11-Y135F
spo11-Y135F
pph3-H112N
Time in meiosis (hrs)
C)
Hop1 loading at 2 hour
% of positive cells
*
PPH3
pph3-H112N
spo11-Y135F

Figure 16. The *pph3* mutant showed a significant delay in the loading of Hop1 even in the *spo11-Y135F* mutation background.

A) Immunostaining analysis of Hop1-pT318 and Hop1 with rabbit anti-Hop1-pT318 antibody, guinea pig anti-Hop1 antibody on meiotic nuclear spreads was carried out in *spo11-Y135F* (blue, MSY6345/6346), *spo11-Y135F pph3-H112N* (red, MSY6568/6570) mutants. The representative images overlaid with DAPI (blue), Hop1-pT318 (green) and Hop1 (red) at 3 hour after meiosis entry are showed.

B) Kinetics of Hop1 focus positive cells (cell with more than 5 Hop1 foci) in *spo11-Y135F* (blue, MSY6345/6346), *spo11-Y135F pph3-H112N* (red, MSY6568/6570) mutants. Graph shows the percentage of Hop1 focus positive cells in association with meiosis progress. Error bars indicate the mean ± S.E.M (standard error of the mean) from over 3 times independent trials.

C) Graph re-presents the percentage of Hop1 focus positive cells in *spo11-Y135F* (blue, MSY6345/6346), *spo11-Y135F pph3-H112N* (red, MSY6568/6570) mutants at 2 hour after meiosis entry. Error bars indicate the mean ± S.E.M (standard error of the mean) from over 3 times independent trials. Statistically significant difference was determined by paired t-test using Prism9 software.(*: p value < 0.05)

Figure 17

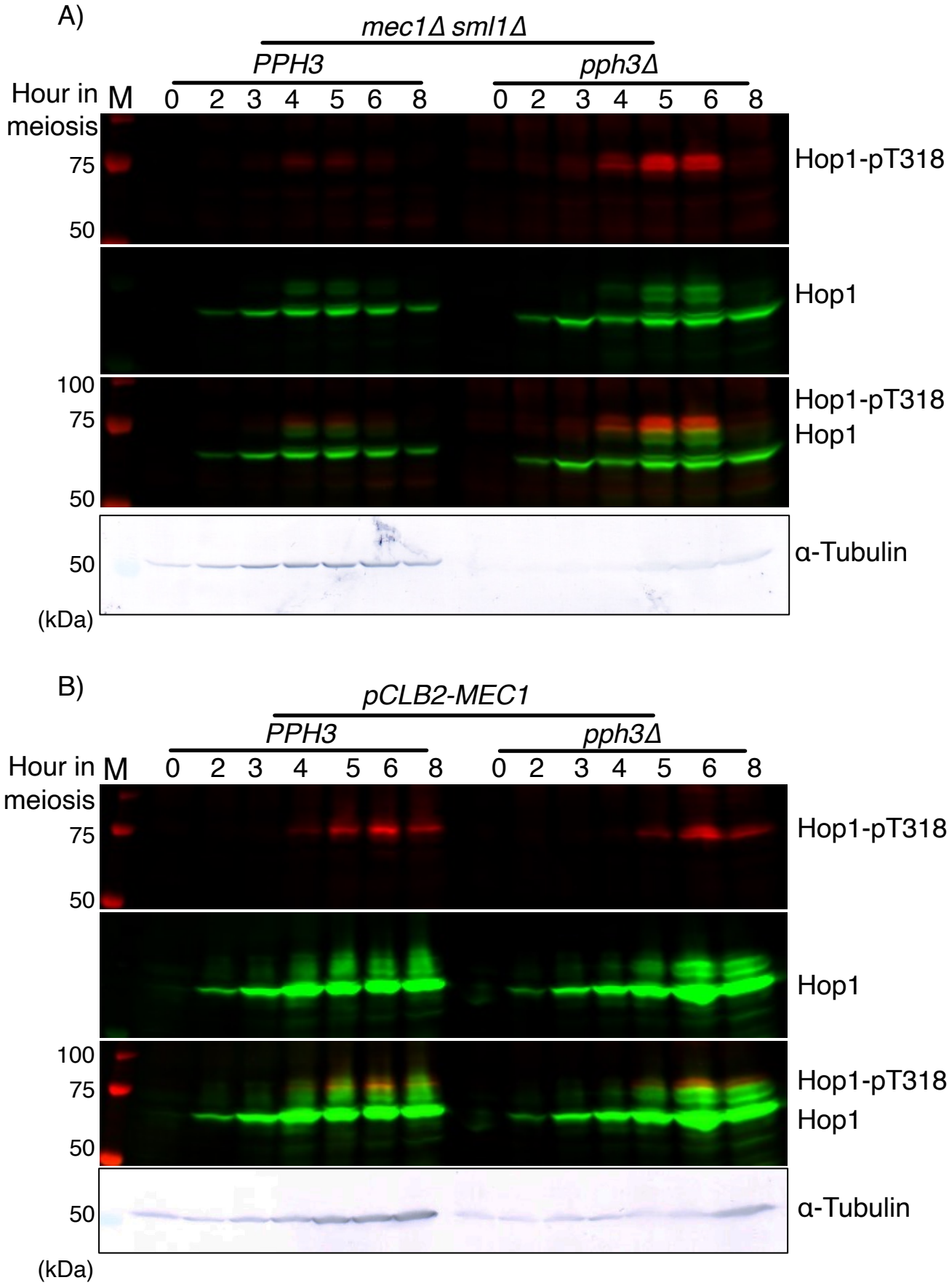
A)
mec1Δ sml1Δ
PPH3
pph3Δ
Hour in meiosis
M
0 2 3 4 5 6 8
0 2 3 4 5 6 8
75
50
Hop1-pT318
Hop1
100
75
50
Hop1-pT318
Hop1
50
α-Tubulin
(kDa)
B)
pCLB2-MEC1
PPH3
pph3Δ
Hour in meiosis
M
0 2 3 4 5 6 8
0 2 3 4 5 6 8
75
50
Hop1-pT318
Hop1
100
75
50
Hop1-pT318
Hop1
50
α-Tubulin
(kDa)

C)

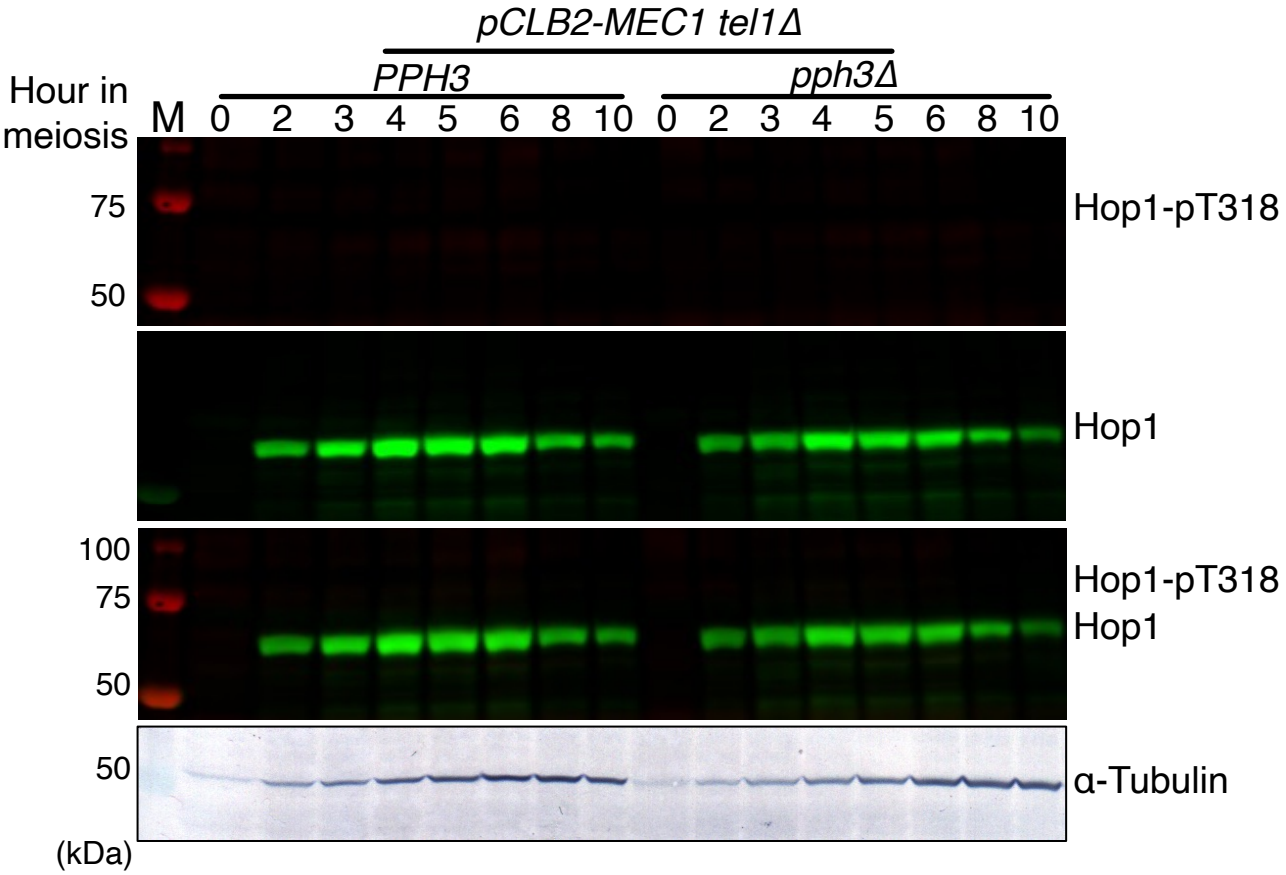
pCLB2-MEC1 tel1Δ
PPH3
pph3Δ
Hour in meiosis
M 0 2 3 4 5 6 8 10 0 2 3 4 5 6 8 10
75
50
Hop1-pT318
Hop1
100
75
50
Hop1-pT318
Hop1
50
α-Tubulin
(kDa)

Figure 17. The activity of Mec1 and Tel1 kinases in meiosis was knockdown in the *pCLB2-MEC1 tel1Δ* background.

A) Representative western blot images of phosphorylated Hop1-T318 (Hop1-pT318), Hop1 and merge Hop1p-T318 (red) and Hop1 (green) in *mec1Δ sml1Δ* (MSY3643/3644) and *mec1Δ sml1Δ pph3Δ* (MSY MSY6560/6565) mutants at the indicated time point during meiosis. The meiotic yeast lysates were subjected to western blotting with rabbit anti-Hop1-pT318 antibody and guinea pig anti-Hop1 antibody. α-Tubulin was also showed bottom as loading control. M denotes molecular weight markers.

B) Representative western blot images of phosphorylated Hop1-T318 (Hop1-pT318), Hop1 and merge Hop1p-T318 (red) and Hop1 (green) in *pCLB2-MEC1* (MSY6551/6552) and *pCLB2-MEC1 pph3Δ* (MSY6574/6576) mutants at the indicated time point during meiosis. The meiotic yeast lysates were subjected to western blotting with rabbit anti-Hop1-pT318 antibody and guinea pig anti-Hop1 antibody. α-Tubulin was also showed bottom as loading control. M denotes molecular weight markers.

C) Representative western blot images of phosphorylated Hop1-T318 (Hop1-pT318), Hop1 and merge Hop1p-T318 (red) and Hop1 (green) in *pCLB2-MEC1 tel1Δ* (MSY5544/5546) and *pCLB2-MEC1 tel1Δ pph3Δ* (MSY5760/5762) mutants at the indicated time point during meiosis. The meiotic yeast lysates were subjected to western blotting with rabbit anti-Hop1-pT318 antibody and guinea pig anti-Hop1 antibody. α-Tubulin was also showed bottom as loading control. M denotes molecular weight markers.

Figure 18

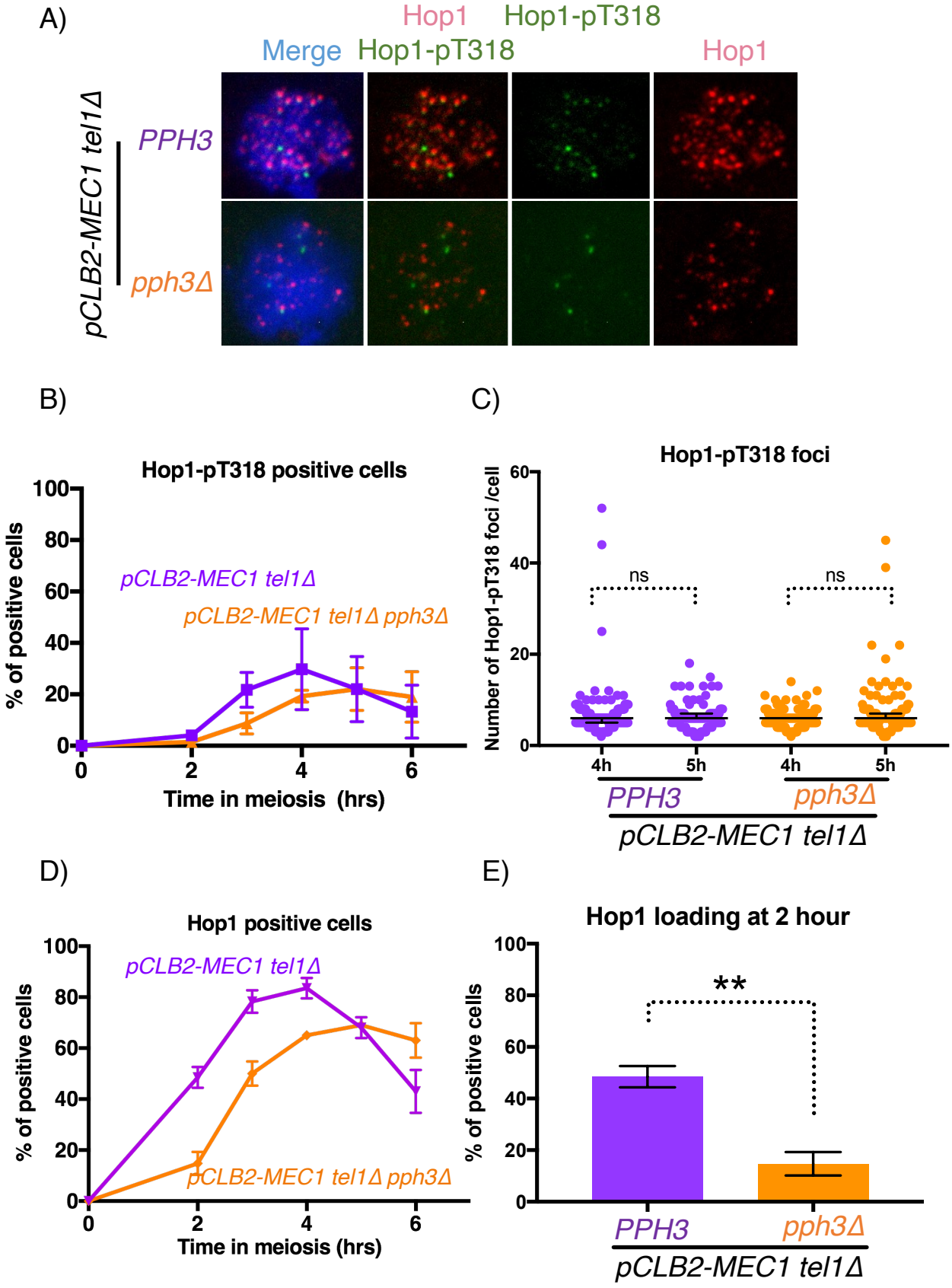
A)
Hop1
Hop1-pT318
Merge
Hop1-pT318
Hop1
pCLB2-MEC1 tel1Δ
PPH3
pph3Δ
B)
Hop1-pT318 positive cells
% of positive cells
pCLB2-MEC1 tel1Δ
pCLB2-MEC1 tel1Δ pph3Δ
Time in meiosis (hrs)
C)
Hop1-pT318 foci
Number of Hop1-pT318 foci /cell
ns
ns
4h
5h
4h
5h
PPH3
pph3Δ
pCLB2-MEC1 tel1Δ
D)
Hop1 positive cells
% of positive cells
pCLB2-MEC1 tel1Δ
pCLB2-MEC1 tel1Δ pph3Δ
Time in meiosis (hrs)
E)
Hop1 loading at 2 hour
% of positive cells
**
PPH3
pph3Δ
pCLB2-MEC1 tel1Δ

Figure 18. The *pph3* mutant showed a significant delay in the loading of Hop1 even in the *pCLB2-MEC1 tel1Δ* background.

A) Immunostaining analysis of Hop1-pT318 and Hop1 with rabbit anti-Hop1-pT318 antibody, guinea pig anti-Hop1 antibody on meiotic nuclear spreads was carried out in *pCLB2-MEC1 tel1Δ* (purple, MSY5544/5546) and *pCLB2-MEC1 tel1Δ pph3Δ* (orange, MSY5760/5762) mutants. The representative images overlaid with DAPI (blue), Hop1-pT318 (green) and Hop1 (red) at 2hour after meiosis entry are showed.

B) Kinetics of Hop1-pT318 focus positive cells (cell with more than 5 Hop1-pT318 foci) in *pCLB2-MEC1 tel1Δ* (purple, MSY5544/5546) and *pCLB2-MEC1 tel1Δ pph3Δ* (orange, MSY5760/5762) mutants. Graph shows the percentage of Hop1-pT318 focus positive cells in association with meiosis progress. Error bars indicate the mean ± S.E.M (standard error of the mean) from over 3 times independent trials.

C) Distributions of Hop1-pT318 foci number per Hop1-pT318 focus positive cell in *pCLB2-MEC1 tel1Δ* (purple, MSY5544/5546) and *pCLB2-MEC1 tel1Δ pph3Δ* (orange, MSY5760/5762) mutants at 4 hour, and 5 hour after meiosis entry. Over 70 nuclei were analyzed in each strain. Error bars indicate the median ± 95% C.I. (Confidence Interval). Statistically significant differences were determined by Mann-Whitney's U-test using Prism9 software.(ns: not significant)

D) Kinetics of Hop1 focus positive cells (cell with more than 5 Hop1 foci) in *pCLB2-MEC1 tel1Δ* (purple, MSY5544/5546) and *pCLB2-MEC1 tel1Δ pph3Δ* (orange, MSY5760/5762) mutants. Graph shows the percentage of Hop1 focus positive cells in association with meiosis progress. Error bars indicate the mean ± S.E.M (standard error of the mean) from over 3 times independent trials.

E) Graph re-presents the percentage of Hop1 focus positive cells in *pCLB2-MEC1 tel1Δ* (purple, MSY5544/5546) and *pCLB2-MEC1 tel1Δ pph3Δ* (orange, MSY5760/5762) mutants at 2 hour after meiosis entry. Error bars indicate the mean ± S.E.M (standard error of the mean) from over 3 times independent trials. Statistically significant difference was determined by paired t-test using Prism9 software.(**: p value < 0.01)

Figure 19

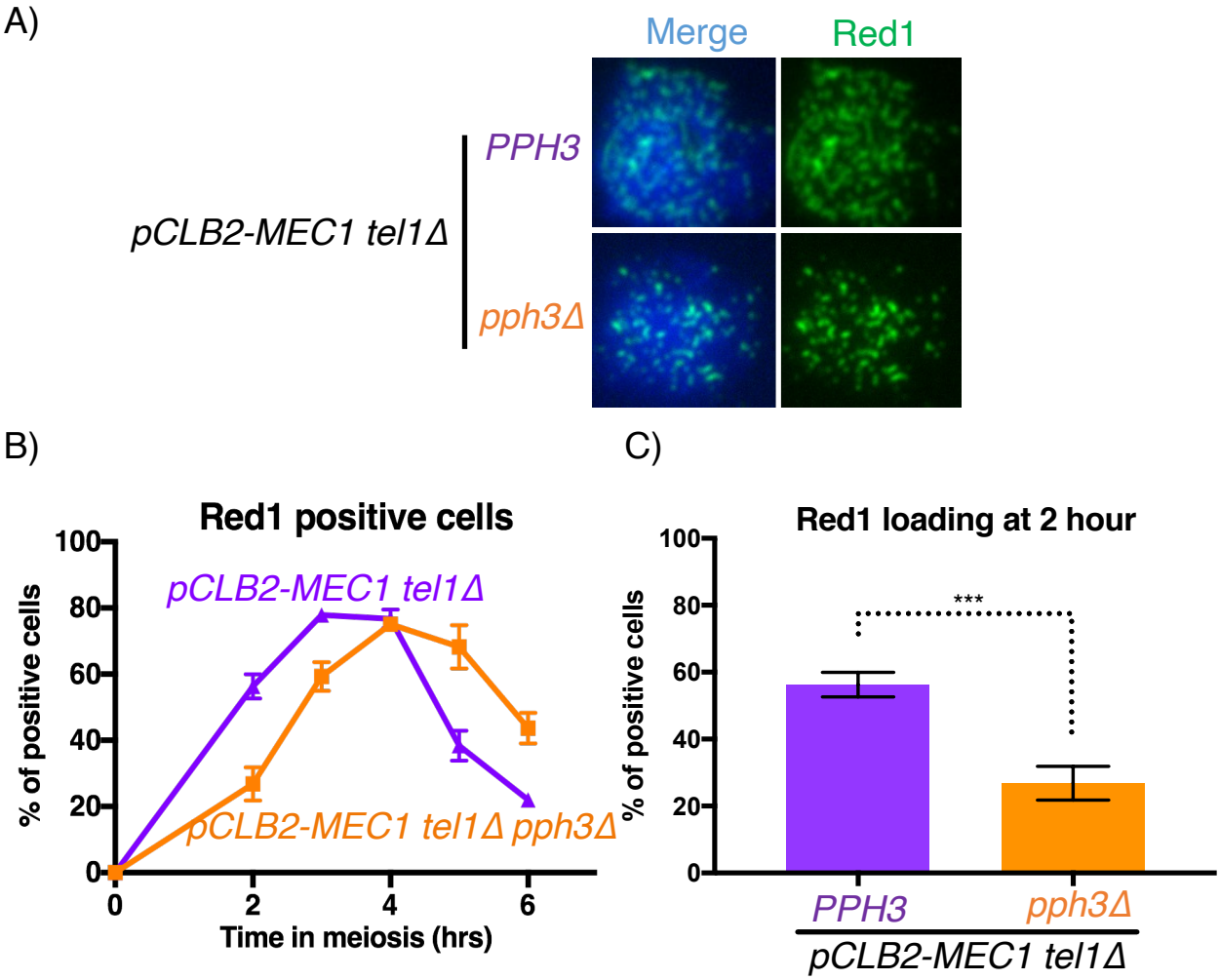

Figure 19. The *pph3* mutant showed a significant delay in the loading of Red1 even in the *pCLB2-MEC1 tel1Δ* background.

A) Immunostaining analysis of Red1 with chick anti-Red1 antibody on meiotic nuclear spreads was carried out in *pCLB2-MEC1 tel1Δ* (purple, MSY5544/5546) and *pCLB2-MEC1 tel1Δ pph3Δ* (orange, MSY5760/5762) mutants. The representative images overlaid with DAPI (blue) and Red1 (green) at 2hour after meiosis entry are showed.

B) Kinetics of Red1 focus positive cells (cell with more than 5 Red1 foci) in *pCLB2-MEC1 tel1Δ* (purple, MSY5544/5546) and *pCLB2-MEC1 tel1Δ pph3Δ* (orange, MSY5760/5762) mutants. Graph shows the percentage of Red1 focus positive cells in association with meiosis progress. Error bars indicate the mean ± S.E.M (standard error of the mean) from over 3 times independent trials.

C) Graph re-presents the percentage of Red1 focus positive cells in *pCLB2-MEC1 tel1Δ* (purple, MSY5544/5546) and *pCLB2-MEC1 tel1Δ pph3Δ* (orange, MSY5760/5762) mutants at 2 hour after meiosis entry. Error bars indicate the mean ± S.E.M (standard error of the mean) from over 3 times independent trials. Statistically significant difference was determined by paired t-test using Prism9 software.(***: p value < 0.001)

Figure 20

A)

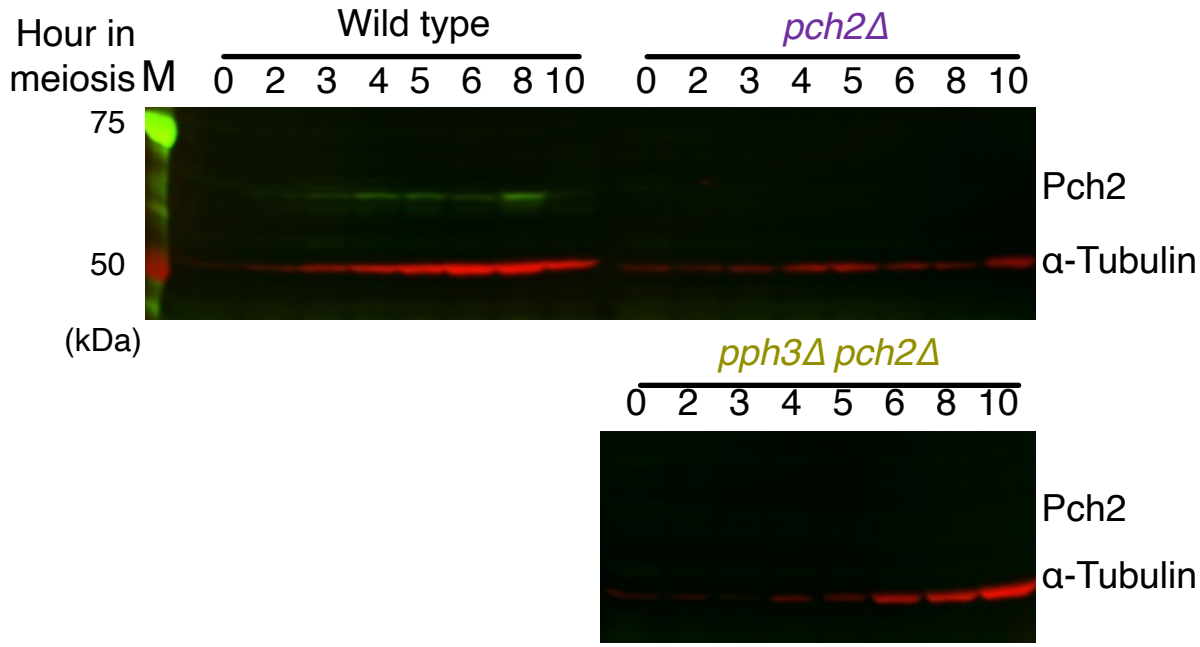
Hour in meiosis
M
Wild type
0 2 3 4 5 6 8 10
pch2Δ
0 2 3 4 5 6 8 10
75
50
(kDa)
Pch2
α-Tubulin
pph3Δ pch2Δ
0 2 3 4 5 6 8 10
Pch2
α-Tubulin

B)

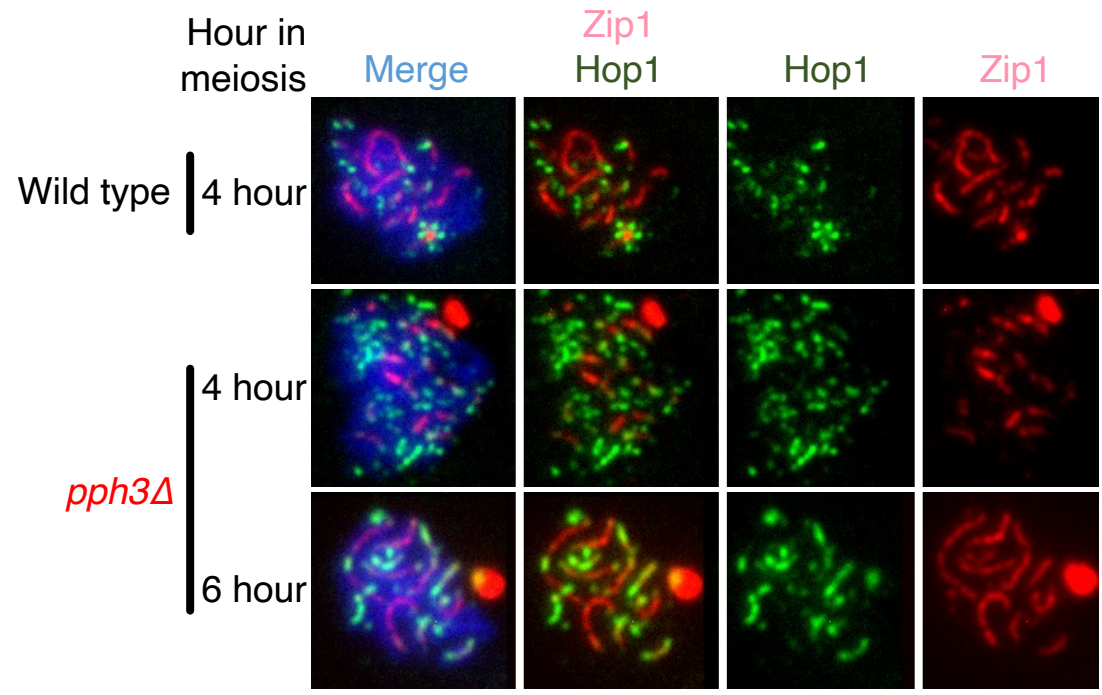
Hour in meiosis
Merge
Zip1
Hop1
Hop1
Zip1
Wild type
4 hour
pph3Δ
4 hour
6 hour

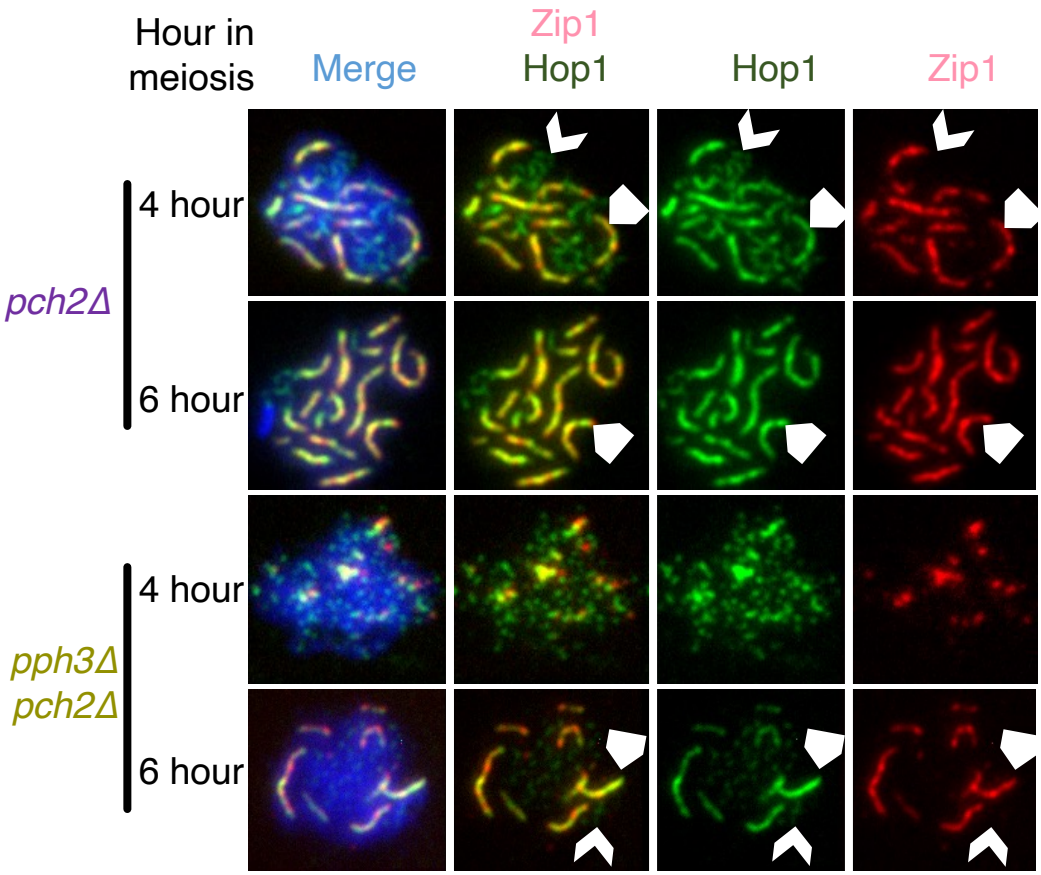
Hour in meiosis
Merge
Zip1
Hop1
Hop1
Zip1
4 hour
6 hour
pch2Δ
4 hour
6 hour
pph3Δ pch2Δ

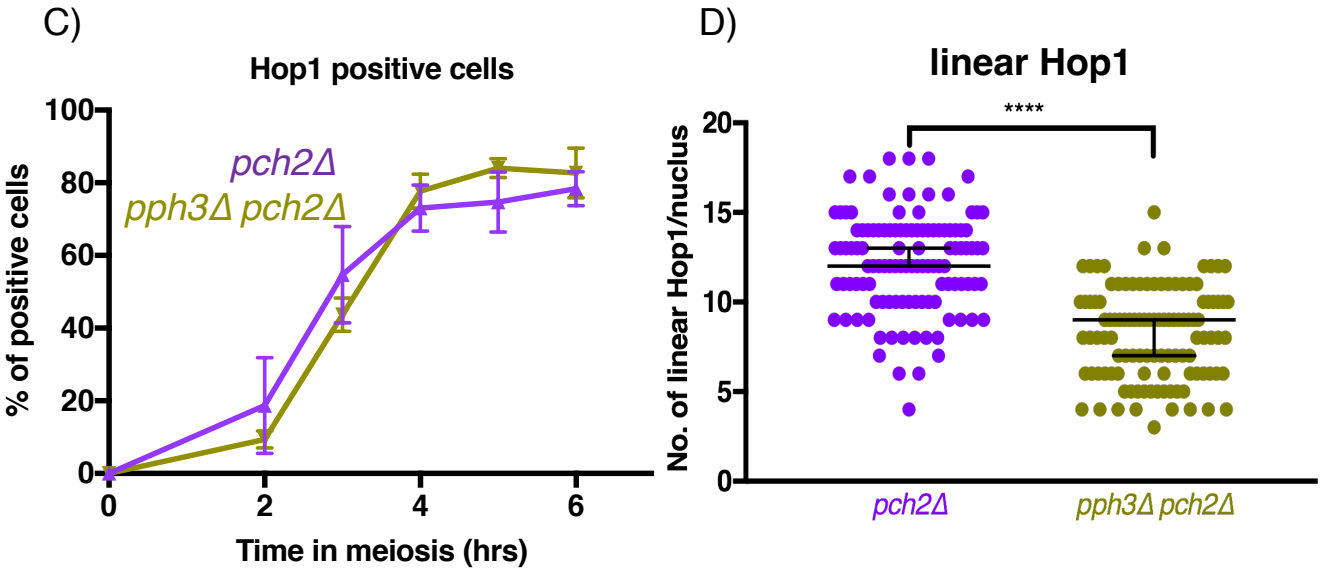
C)
Hop1 positive cells
% of positive cells
100
80
60
40
20
0
0
2
4
6
Time in meiosis (hrs)
pch2Δ
pph3Δ pch2Δ
D)
linear Hop1
****
No. of linear Hop1/nuclus
20
15
10
5
0
pch2Δ
pph3Δ pch2Δ

E)

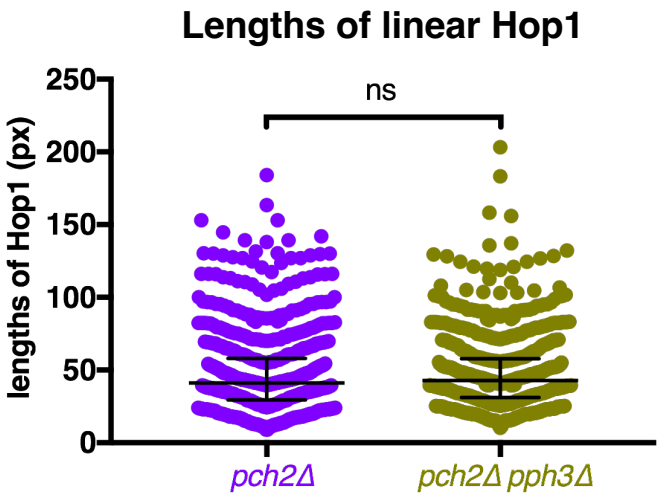
Lengths of linear Hop1
ns
lengths of Hop1 (px)
250
200
150
100
50
0
pch2Δ
pch2Δ pph3Δ

F)

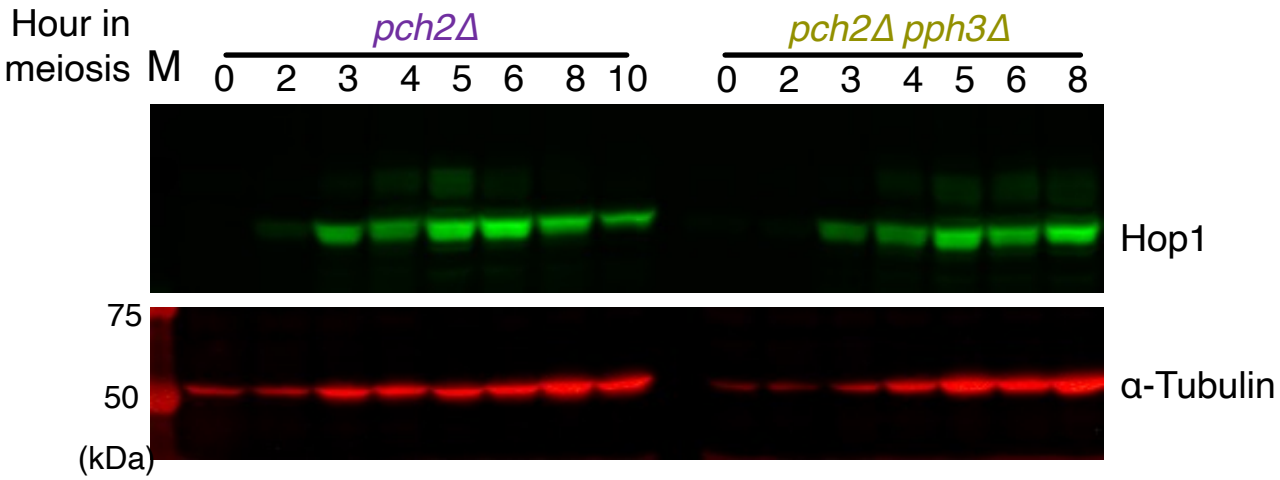
Hour in meiosis
M
pch2Δ
pch2Δ pph3Δ
0 2 3 4 5 6 8 10
0 2 3 4 5 6 8
Hop1
75
50
(kDa)
α-Tubulin

Figure 20. The *pph3* mutant showed a defective assembly of Hop1 on meiotic chromatin in the *pch2Δ* background.

A) Representative western blot images of Pch2 (green) in wild type (black, NKY1303/1543), *pch2Δ* (purple, MSY6446/6448) and *pph3Δ pch2Δ* (dark brown, MSY6417/6419) mutants at the indicated time point during meiosis. The meiotic yeast lysates were subjected to western blotting with rabbit anti-Pch2 antibody. α-Tubulin (red) was also showed merging with Pch2. M denotes molecular weight markers.

B) Immunostaining analysis of Hop1 and Zip1 with rabbit anti-Zip1 antibody, guinea pig anti-Hop1 antibody on meiotic nuclear spreads was carried out in wild type (black, NKY1303/1543), *pph3Δ* (red, MSY5632/5634), *pch2Δ* (purple, MSY6446/6448) and *pph3Δ pch2Δ* (dark brown, MSY6417/6419) mutants. The representative images overlaid with DAPI (blue), Hop1 (green) and Zip1 (red) in wild type (black, NKY1303/1543) at only 4 hour, in *pph3Δ* (red, MSY5632/5634), *pch2Δ* (purple, MSY6446/6448) and *pph3Δ pch2Δ* (dark brown, MSY6417/6419) mutants at 4 and 6 hour after meiosis entry are showed. The ⏠ displays synapsed region, and ^ displays unsynapsed region.

C) Kinetics of Hop1 focus positive cells (cell with more than 5 Hop1 foci) in *pch2Δ* (purple, MSY6446/6448) and *pph3Δ pch2Δ* (dark brown, MSY6417/6419) mutants. Graph shows the percentage of Hop1 focus positive cells in association with meiosis progress. Error bars indicate the mean ± S.E.M (standard error of the mean) from over 3 times independent trials.

D) Distributions of numbers of linear Hop1 per Hop1 focus positive cell at 6 hour after meiosis entry in *pch2Δ* (purple, MSY6446/6448) and *pph3Δ pch2Δ* (dark brown, MSY6417/6419) mutants are shown. Over 100 nuclei were analyzed in each strain. Error bars indicate the median ± 95% C.I. (Confidence Interval). Statistically significant difference was determined by Mann-Whitney's U-test using Prism9 software. (****: p value < 0.0001)

E) Distributions of length of linear Hop1 signal at 6 hour after meiosis entry in *pch2Δ* (purple, MSY6446/6448) and *pph3Δ pch2Δ* (dark brown, MSY6417/6419) mutants are shown. Over 100 nuclei were analyzed in each strain. Error bars indicate the median ± 95% C.I. (Confidence Interval). Statistically significant difference was determined by Mann-Whitney's U-test using Prism9 software. (ns: not significant).

F) Representative western blot images of Hop1 (green) in *pch2Δ* (purple, MSY6446/6448) and *pph3Δ pch2Δ* (dark brown, MSY6417/6419) mutants at the indicated time point during meiosis. The meiotic yeast lysates were subjected to western blotting with guinea pig anti-Hop1 antibody. α-Tubulin (red) is also showed bottom as loading control. M denotes molecular weight markers.

Figure 21

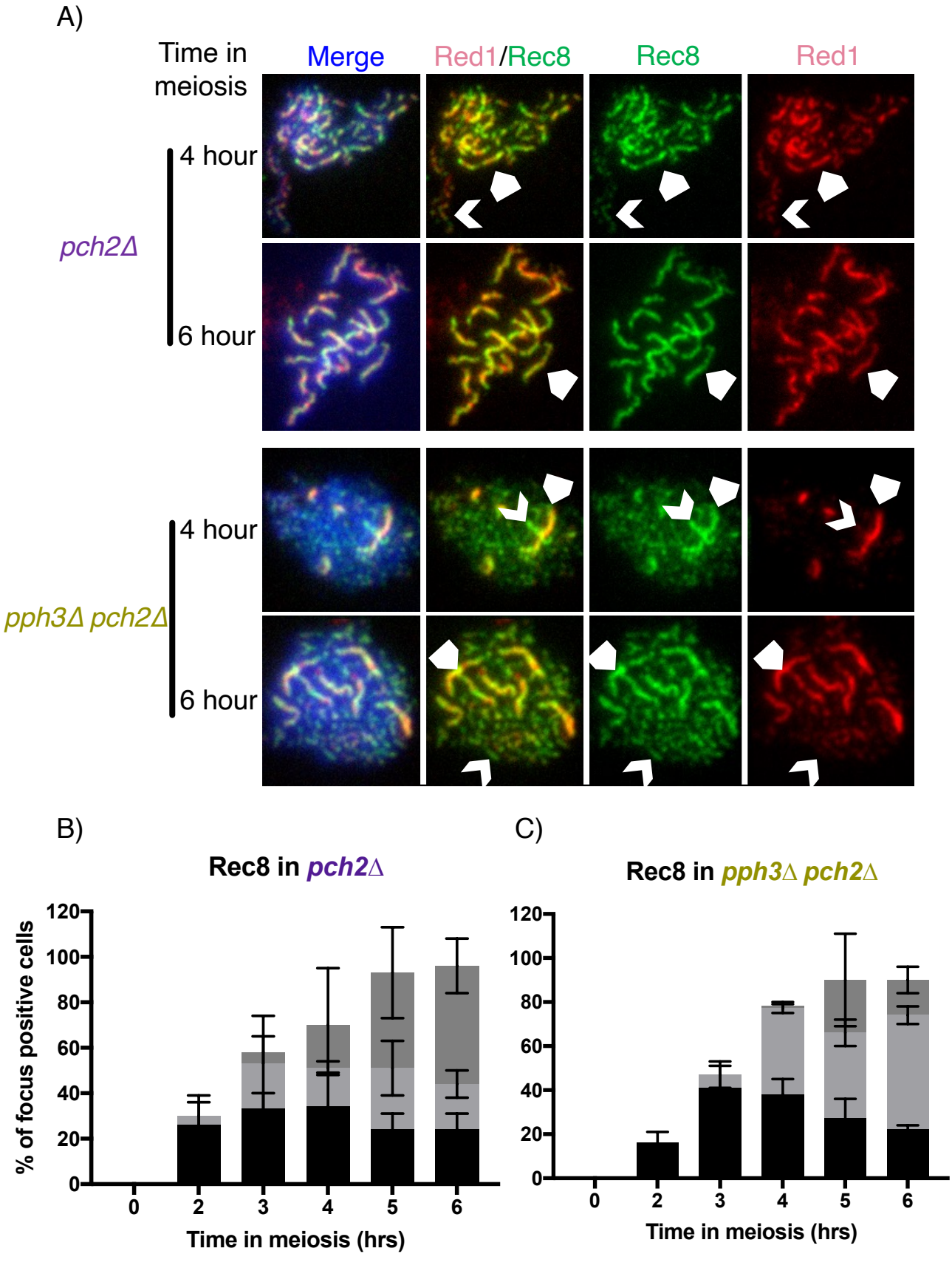
A)
Time in meiosis
Merge
Red1/Rec8
Rec8
Red1
4 hour
pch2Δ
6 hour
4 hour
pph3Δ pch2Δ
6 hour
B)
Rec8 in pch2Δ
% of focus positive cells
120
100
80
60
40
20
0
0
2
3
4
5
6
Time in meiosis (hrs)
C)
Rec8 in pph3Δ pch2Δ
120
100
80
60
40
20
0
0
2
3
4
5
6
Time in meiosis (hrs)

Figure. 21 The *pph3* mutants showed an obvious Red1-related reduction in Rec8 linearization in the *pch2Δ* background.

A) Immunostaining analysis of Red1 and Rec8 with chick anti-Red1 antibody and rabbit anti-Rec8 antibody on meiotic nuclear spreads was carried out in *pch2Δ* (purple, MSY6446/6448) and *pph3Δ pch2Δ* (dark brown, MSY6417/6419) mutants. The representative images overlaid with DAPI (blue), Rec8 (green) and Red1 (red) at 4 and 6 hour after meiosis entry are showed. The ⌂ displays synapsed region, and ^ displays unsynapsed region.

B) Kinetics of Rec8 morphology on meiotic nucleus spread in *pch2Δ* (purple, MSY6446/6448) mutant, which was analyzed by classifying into linear (dark gray), partial (light gray) and dotty (black). A minimum 100 cells were counted at the indicated time point. Error bars indicate the mean ± S.E.M (standard error of the mean) from over 3 times independent trials.

C) Kinetics of Rec8 morphology on meiotic nucleus spread in *pph3Δ pch2Δ* (dark brown, MSY6417/6419) mutant, which was analyzed by classifying into linear (dark gray), partial (light gray) and dotty (black). A minimum 100 cells were counted at the indicated time point. Error bars indicate the mean ± S.E.M (standard error of the mean) from over 3 times independent trials.

Figure 22

A)

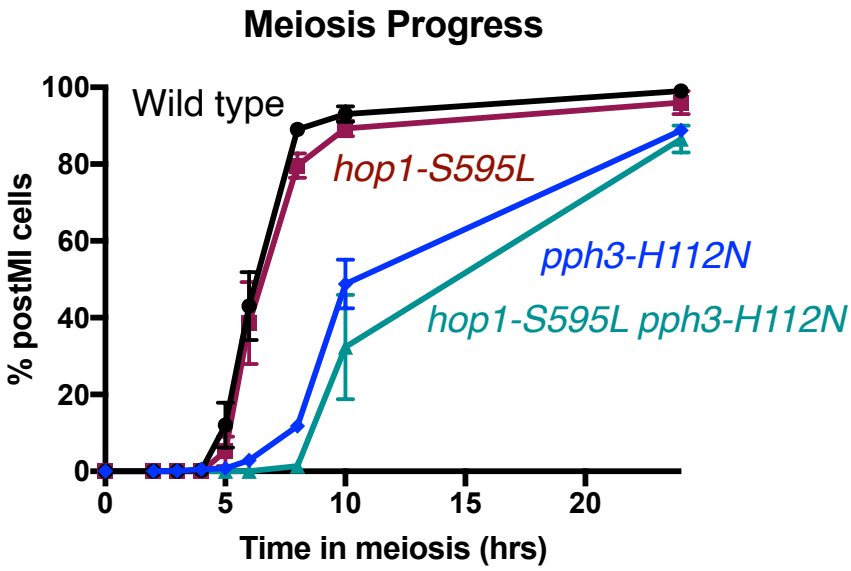

B)

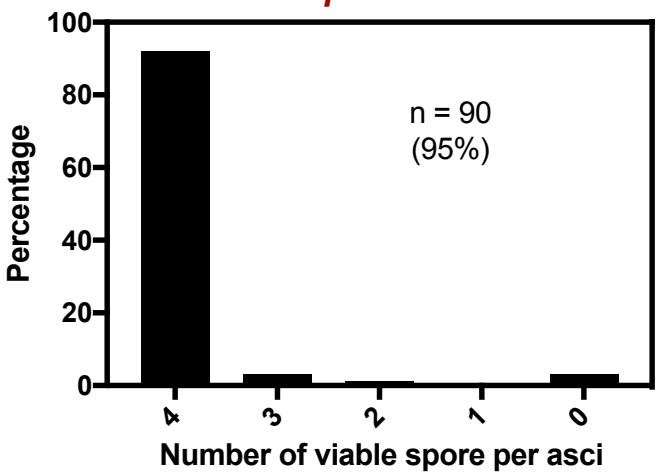

C)

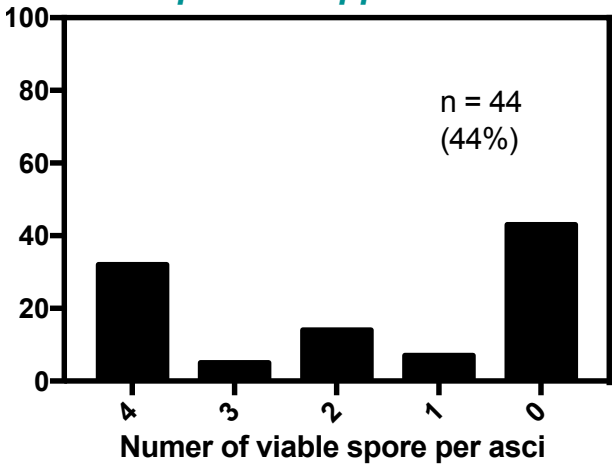

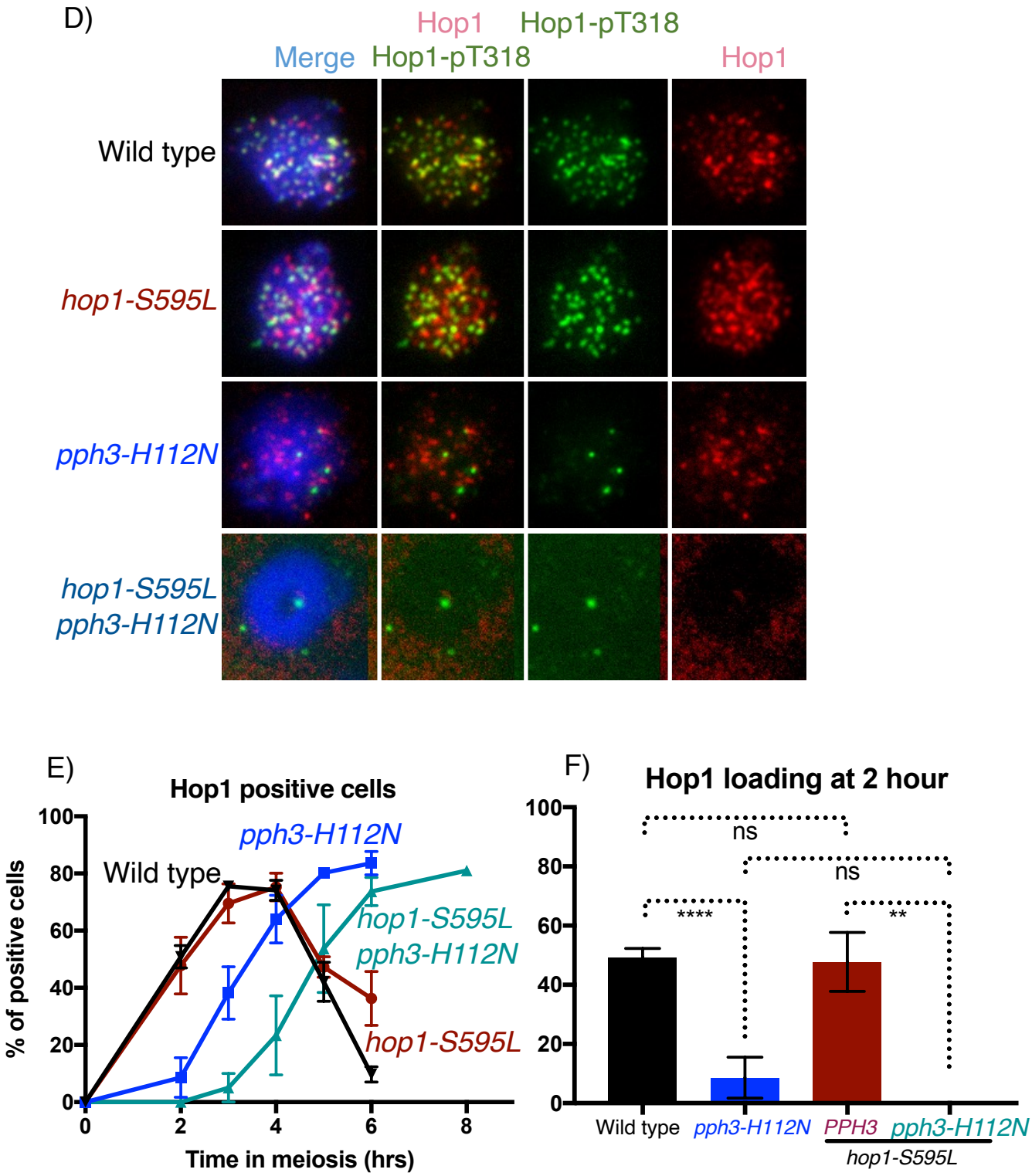
D)
Hop1
Hop1-pT318
Merge
Hop1-pT318
Hop1
Wild type
hop1-S595L
pph3-H112N
hop1-S595L
pph3-H112N
E)
Hop1 positive cells
% of positive cells
100
80
60
40
20
0
0
2
4
6
8
Time in meiosis (hrs)
pph3-H112N
Wild type
hop1-S595L
pph3-H112N
hop1-S595L
F)
Hop1 loading at 2 hour
100
80
60
40
20
0
ns
ns
****
**
Wild type
pph3-H112N
PPH3
pph3-H112N
hop1-S595L

G)

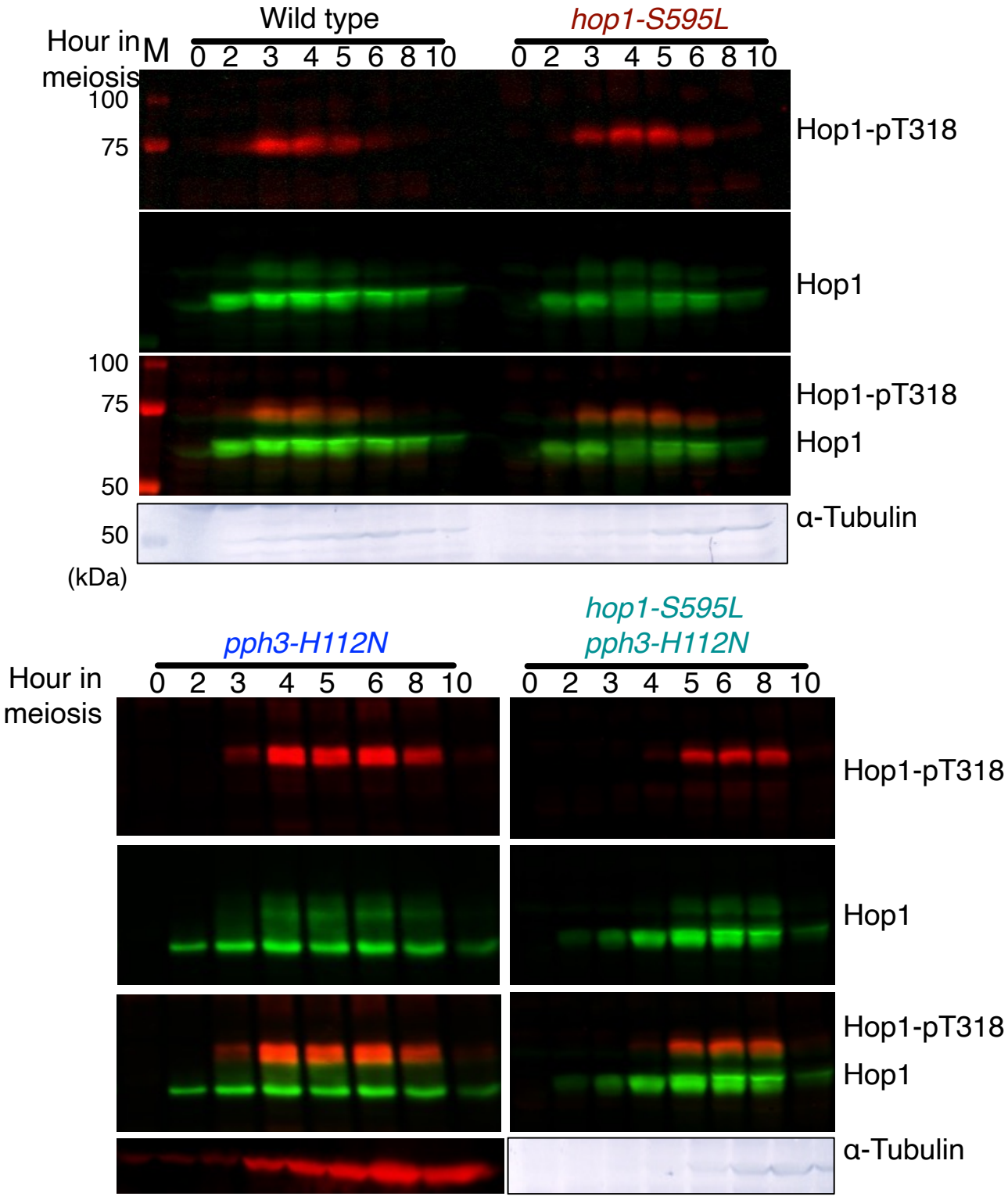
Wild type
hop1-S595L
Hour in meiosis
M
0 2 3 4 5 6 8 10
0 2 3 4 5 6 8 10
100
75
Hop1-pT318
Hop1
100
75
50
Hop1-pT318
Hop1
50
α-Tubulin
(kDa)
pph3-H112N
hop1-S595L pph3-H112N
Hour in meiosis
0 2 3 4 5 6 8 10
0 2 3 4 5 6 8 10
Hop1-pT318
Hop1
Hop1-pT318
Hop1
α-Tubulin

Figure 22. The *pph3* mutants showed a significantly delayed loading of Hop1 onto leptotene chromatin in the *hop1-S595LΔ* background.

A) Meiosis progress was defined by frequency of post-meiosis I (cell with more than 2 DAPI-stained bodies) in wild type (black, NKY1303/1543), *pph3-H112N* (blue, MSY6219/6220) *hop1-S595L* (dark red, MSY6314/6319) and *hop1-S595L pph3-H112N* (light blue, MSY6541/6543) mutants. At least 100 cells were counted at the indicated time point. Error bars show the mean ± S.E.M (standard error of the mean) from over 3 times independent trials.

B) Tetrad analysis of spore viability in *hop1-S595L* (dark red, MSY6314/6319) mutant. The graph shows the respective fraction of 0#, 2#, 3#, 4# viable spore from one asci. n: the number of analyzed asci and the overall spore viability are shown.

C) Tetrad analysis of spore viability in *hop1-S595L pph3-H112N* (light blue, MSY6541/6543) mutant. The graph shows the respective fraction of 0#, 2#, 3#, 4# viable spore from one asci. n: the number of analyzed asci and the overall spore viability are shown.

D) Immunostaining analysis of Hop1-pT318 and Hop1 with rabbit anti-Hop1-pT318 antibody, guinea pig anti-Hop1 antibody on meiotic nuclear spreads was carried out in wild type (black, NKY1303/1543), *pph3-H112N* (blue, MSY6219/6220) *hop1-S595L* (dark red, MSY6314/6319) and *hop1-S595L pph3-H112N* (light blue, MSY6541/6543) mutants. The representative images overlaid with DAPI (blue), Hop1-pT318 (green) and Hop1 (red) at 3 hour after meiosis entry are showed.

E) Kinetics of Hop1 focus positive cells (cell with more than 5 Hop1 foci) in wild type (black, NKY1303/1543), *pph3-H112N* (blue, MSY6219/6220) *hop1-S595L* (dark red, MSY6314/6319) and *hop1-S595L pph3-H112N* (light blue, MSY6541/6543) mutants. Graph shows the percentage of Hop1 focus positive cells in association with meiosis progress. Error bars indicate the mean ± S.E.M (standard error of the mean) from over 3 times independent trials.

F) Graph re-presents the percentage of Hop1 focus positive cells in wild type (black, NKY1303/1543), *pph3-H112N* (blue, MSY6219/6220) *hop1-S595L* (dark red, MSY6314/6319) and *hop1-S595L pph3-H112N* (light blue, MSY6541/6543) mutants at 2 hour after meiosis entry. Error bars indicate the mean ± S.E.M (standard error of the mean) from over 3 times independent trials. Statistically significant difference was determined by paired t-test using Prism9 software.(***: p value < 0.001)

G) Representative western blot images of phosphorylated Hop1-T318 (Hop1-pT318), Hop1 and merge Hop1-pT318 (red) and Hop1 (green) in wild type (black, NKY1303/1543), *pph3-H112N* (blue, MSY6219/6220) *hop1-S595L* (dark red, MSY6314/6319) and *hop1-S595L pph3-H112N* (light blue, MSY6541/6543) mutants at the indicated time point during meiosis. The meiotic yeast lysates were subjected to western blotting with rabbit anti-Hop1-pT318 antibody and guinea pig anti-Hop1 antibody. α-Tubulin is also showed bottom as loading control. M denotes molecular weight markers.

Figure 23

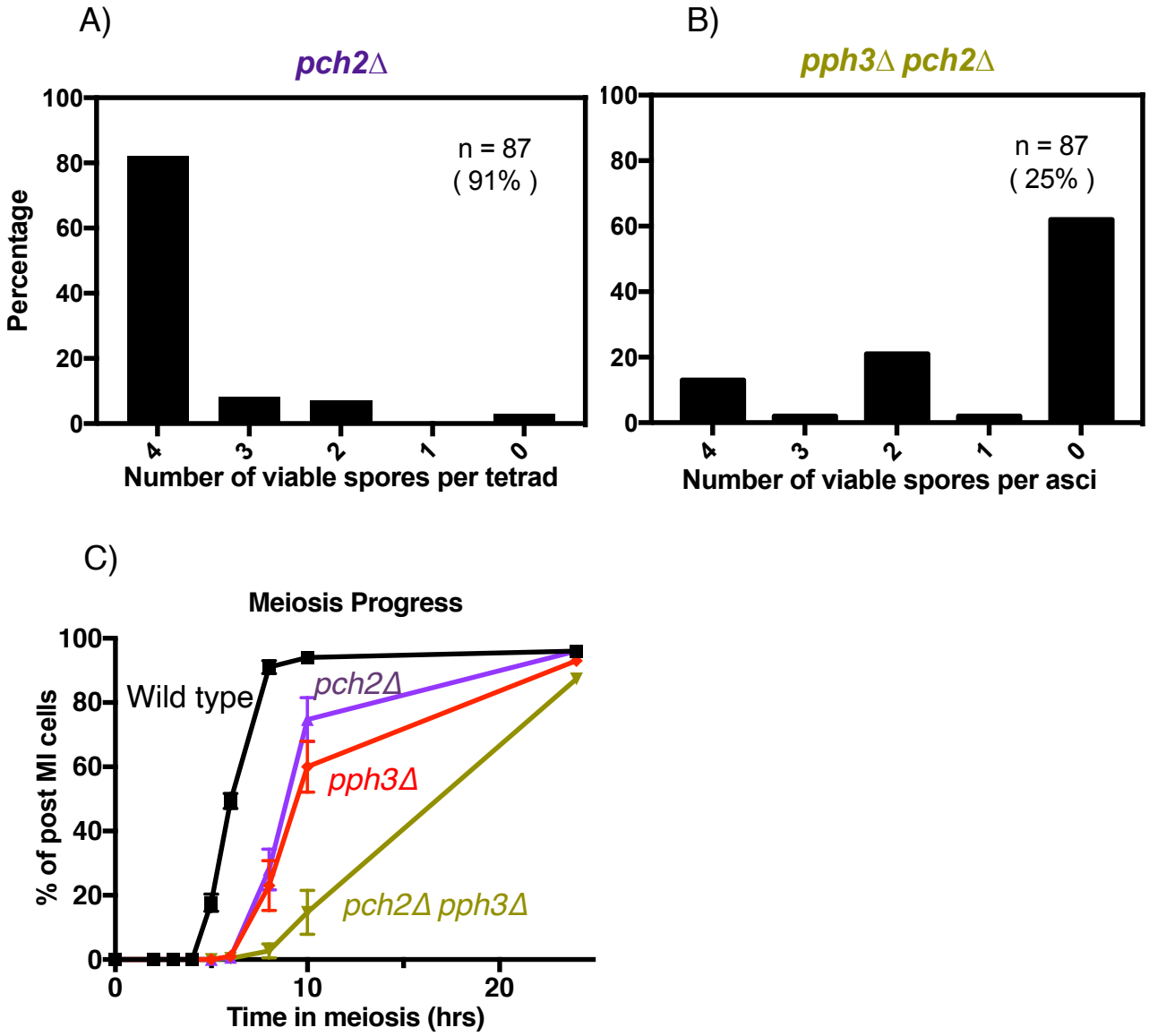

Figure 23. The *pph3Δ* and *pch2Δ* mutations showed synergistic defect in meiotic prophase I.

A) Tetrad analysis of spore viability in *pch2Δ* (purple, MSY6446/6448) mutant. The graph shows the respective fraction of 0#, 2#, 3#, 4# viable spore from one asci. n: the number of analyzed asci and the overall spore viability are shown.

B) Tetrad analysis of spore viability and *pph3Δ pch2Δ* (dark brown, MSY6417/6419) mutant. The graph shows the respective fraction of 0#, 2#, 3#, 4# viable spore from one asci. n: the number of analyzed asci and the overall spore viability are shown.

C) Meiosis progress was defined by frequency of post-meiosis I (cell with more than 2 DAPI-stained bodies) in *pch2Δ* (purple, MSY6446/6448) and *pph3Δ pch2Δ* (dark brown, MSY6417/6419) mutants. At least 100 cells were counted at the indicated time point. Error bars show the mean ± S.E.M (standard error of the mean) from over 3 times independent trials.

Figure 24

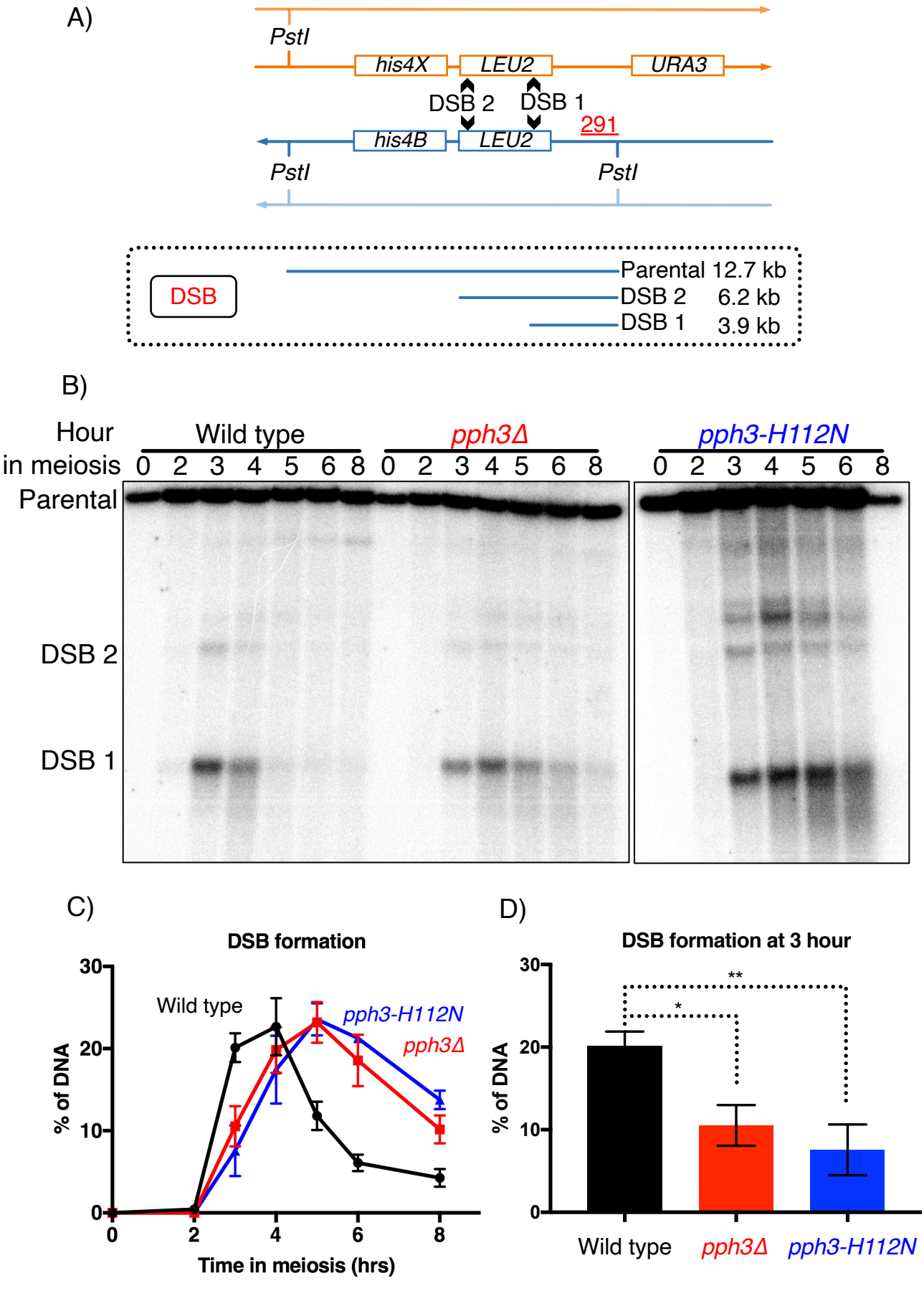
A)
PstI
his4X
LEU2
URA3
DSB 2
DSB 1
291
his4B
LEU2
PstI
PstI
DSB
Parental 12.7 kb
DSB 2 6.2 kb
DSB 1 3.9 kb
B)
Hour in meiosis
Wild type
pph3Δ
pph3-H112N
0 2 3 4 5 6 8
0 2 3 4 5 6 8
0 2 3 4 5 6 8
Parental
DSB 2
DSB 1
C)
DSB formation
% of DNA
30
20
10
0
Wild type
pph3-H112N
pph3Δ
0
2
4
6
8
Time in meiosis (hrs)
D)
DSB formation at 3 hour
% of DNA
30
20
10
0
**
*
Wild type
pph3Δ
pph3-H112N

Figure 24. The *pph3* mutants showed a delay in the formation of DSB at *HIS4-LEU2* hotspot.

A) Schematics of *HIS4-LEU2* recombination hotspot on chromosome III. The sites of diagnostic *PstI* restriction and probe 291 are shown along with the size and identity of diagnostic fragments of DSB 1, DSB 2, parental.

B) Representative images of southern blotting on DSB detection in wild type (black, NKY1303/1543), *pph3Δ* (red, MSY5632/5634), *pph3-H112N* (blue, MSY6219/6220) mutants using probe 291 as shown.

C) Graph shows the quantitative kinetics of DSB I fragment by analyzing the rate of DSB I fragment to total DNA signal at the indicated time point in wild type (black, NKY1303/1543), *pph3Δ* (red, MSY5632/5634), *pph3-H112N* (blue, MSY6219/6220) mutants. Error bars show the mean ± S.E.M (standard error of the mean) from over 3 times independent trials.

D) Graph re-presents the quantity of DSB I fragment in wild type (black, NKY1303/1543), *pph3Δ* (red, MSY5632/5634), *pph3-H112N* (blue, MSY6219/6220) mutants at 2 hour after meiosis entry. Error bars indicate the mean ± S.E.M (standard error of the mean) from over 3 times independent trials. Statistically significant differences were determined by paired t-test using Prism9 software.(**: p value < 0.01; *: p value < 0.05)

Figure 25

A)

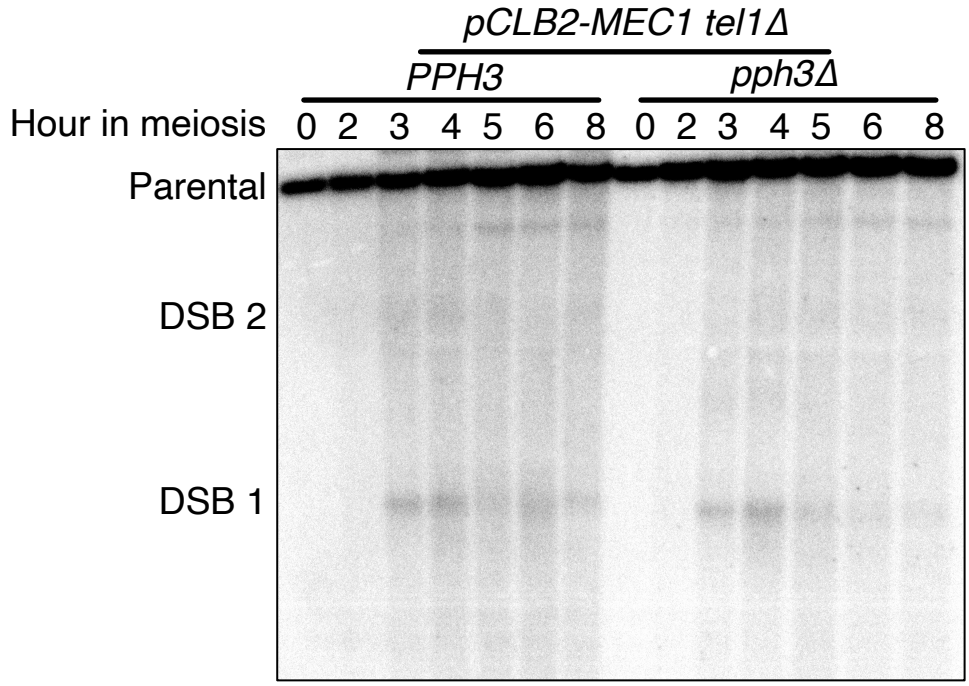

B)

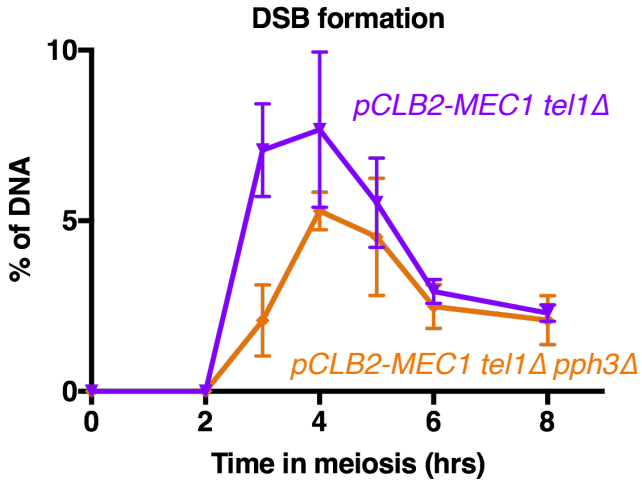

Figure 25. The *pph3* mutants showed a delay in the formation of DSB at *HIS4-LEU2* hotspot even in *pCLB2-MEC1 tel1Δ* background.

A) Representative images of southern blotting on DSB detection in *pCLB2-MEC1 tel1Δ* (purple, MSY5544/5546) and *pCLB2-MEC1 tel1Δ pph3Δ* (orange, MSY5760/5762) mutants using probe 291 as shown.

B) Graph shows the quantitative kinetics of DSB I fragment by analyzing the rate of DSB I fragment to total DNA signal at the indicated time point in *pCLB2-MEC1 tel1Δ* (purple, MSY5544/5546) and *pCLB2-MEC1 tel1Δ pph3Δ* (orange, MSY5760/5762) mutants. Error bars show the mean ± S.E.M (standard error of the mean) from over 3 times independent trials.

Figure 26

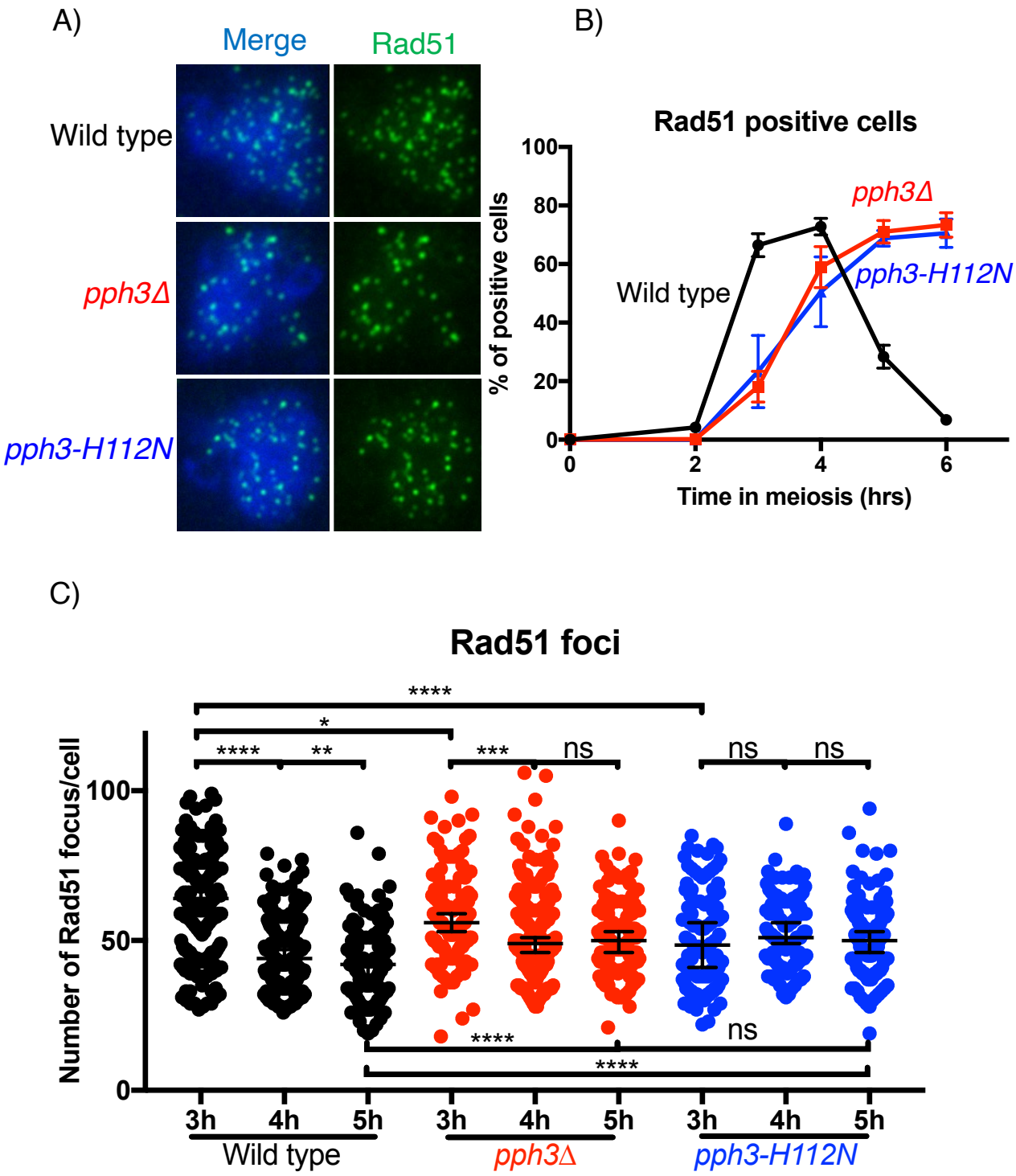
A)
Merge
Rad51
Wild type
pph3Δ
pph3-H112N
B)
Rad51 positive cells
% of positive cells
100
80
60
40
20
0
0
2
4
6
Time in meiosis (hrs)
pph3Δ
pph3-H112N
Wild type
C)
Rad51 foci
Number of Rad51 focus/cell
100
50
0
****
*
****
**
***
ns
ns
ns
****
****
ns
3h
4h
5h
3h
4h
5h
3h
4h
5h
Wild type
pph3Δ
pph3-H112N

Figure 26. The *pph3* mutants showed a delay in the assembly of Rad51 onto meiotic chromatin.

A) Immunostaining analysis of Rad51 with guinea pig anti-Rad51 antibody on meiotic nuclear spreads was carried out in wild type (black, NKY1303/1543), *pph3Δ* (red, MSY5632/5634), *pph3-H112N* (blue, MSY6219/6220) mutants. The representative images overlaid with DAPI (blue) and Rad51 (green) at 4 hour after meiosis entry are showed.

B) Kinetics of Rad51 focus positive cells (cell with more than 5 Rad51 foci) in wild type (black, NKY1303/1543), *pph3Δ* (red, MSY5632/5634), *pph3-H112N* (blue, MSY6219/6220) mutants. Graph shows the percentage of Rad51 focus positive cells in association with meiosis progress. Error bars indicate the mean ± S.E.M (standard error of the mean) from over 3 times independent trials.

C) Distributions of Rad51 foci number per Rad51 focus positive cell in wild type (black, NKY1303/1543), *pph3Δ* (red, MSY5632/5634), *pph3-H112N* (blue, MSY6219/6220) mutants at 3 hour, 4 hour, and 5 hour after meiosis entry. Over 100 nuclei were analyzed at the indicated time point in each strain. Error bars indicate the median ± 95% C.I. (Confidence Interval). Statistically significant differences were determined by Mann-Whitney's U-test using Prism9 software.(****: p value < 0.0001; ***: p value < 0.001; **: p value < 0.01; *: p value < 0.05; ns: not significant)

Figure 27

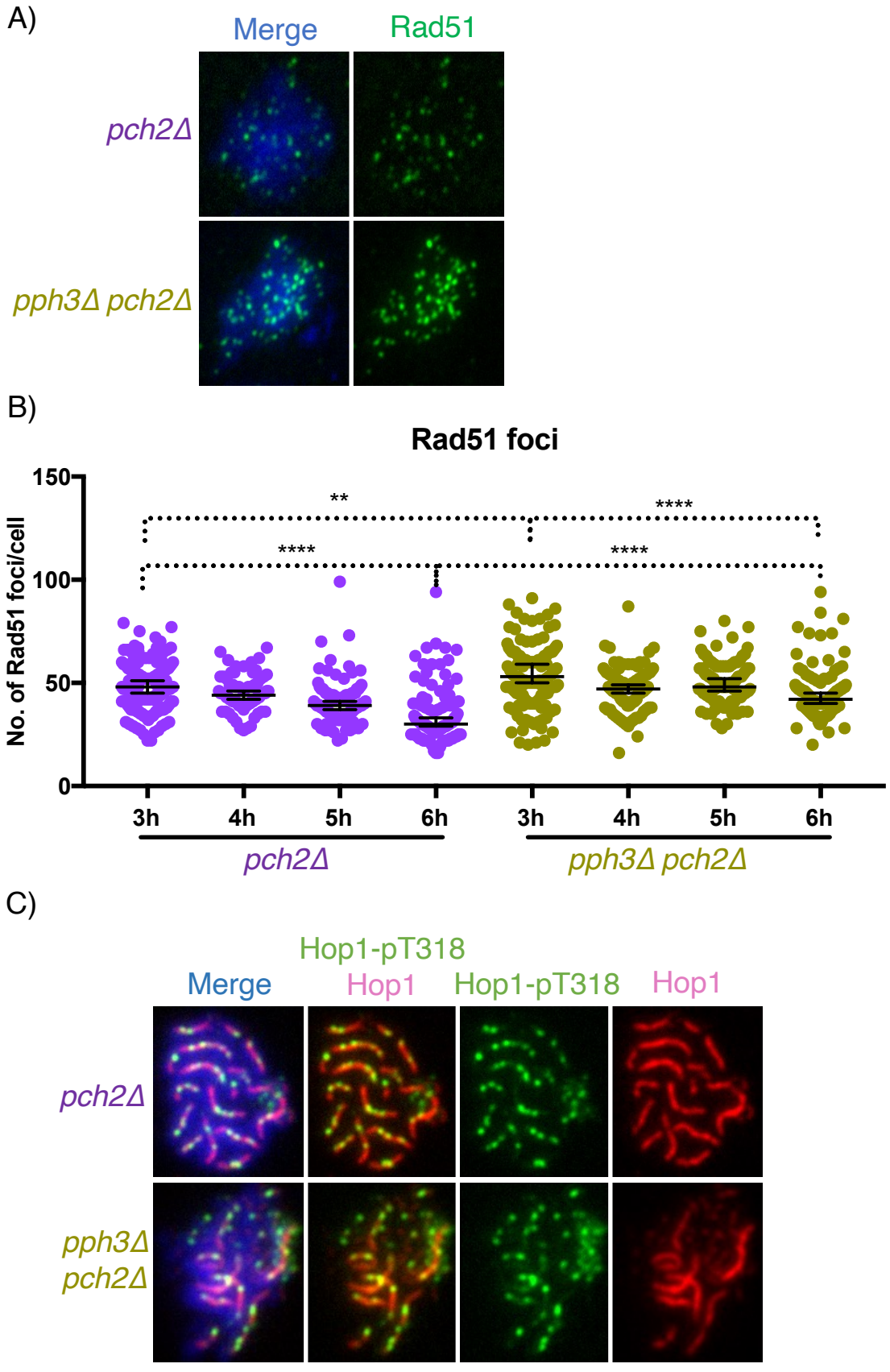
A)
Merge
Rad51
pch2Δ
pph3Δ pch2Δ
B)
Rad51 foci
No. of Rad51 foci/cell
150
100
50
0
**
****
****
****
3h
4h
5h
6h
3h
4h
5h
6h
pch2Δ
pph3Δ pch2Δ
C)
Hop1-pT318
Merge
Hop1
Hop1-pT318
Hop1
pch2Δ
pph3Δ
pch2Δ

Figure 27. The *pph3Δ pch2Δ* mutant showed comparable numbers of Rad51 foci per cell with the *pch2Δ* mutant.

A) Immunostaining analysis of Rad51 with guinea pig anti-Rad51 antibody on meiotic nuclear spreads was carried out in *pch2Δ* (purple, MSY6446/6448) and *pph3Δ pch2Δ* (orange, MSY6417/6419) mutants. The representative images overlaid with DAPI (blue) and Rad51 (green) at 4 hour after meiosis entry were showed.

B) Distributions of Rad51 foci number per Rad51 focus positive cell in *pch2Δ* (purple, MSY6446/6448) and *pph3Δ pch2Δ* (orange, MSY6417/6419) mutants at 3 hour, 4 hour, 5 hour and 6 hour after meiosis entry. Over 100 nuclei were analyzed in each strain at the indicated time point. Error bars indicate the median ± 95% C.I. (Confidence Interval). Statistically significant differences were determined by Mann-Whitney's U-test using Prism9 software. (****: p value < 0.0001; **: p value < 0.01)

C) Immunostaining analysis of Hop1-pT318 and Hop1 with rabbit anti-Hop1-pT318 antibody, guinea pig anti-Hop1 antibody on meiotic nuclear spreads was carried out in *pch2Δ* (purple, MSY6446/6448) and *pph3Δ pch2Δ* (orange, MSY6417/6419) mutants. The representative images overlaid with DAPI (blue), Hop1-pT318 (green) and Hop1 (red) at 5 hour after meiosis entry are showed.

Figure 28

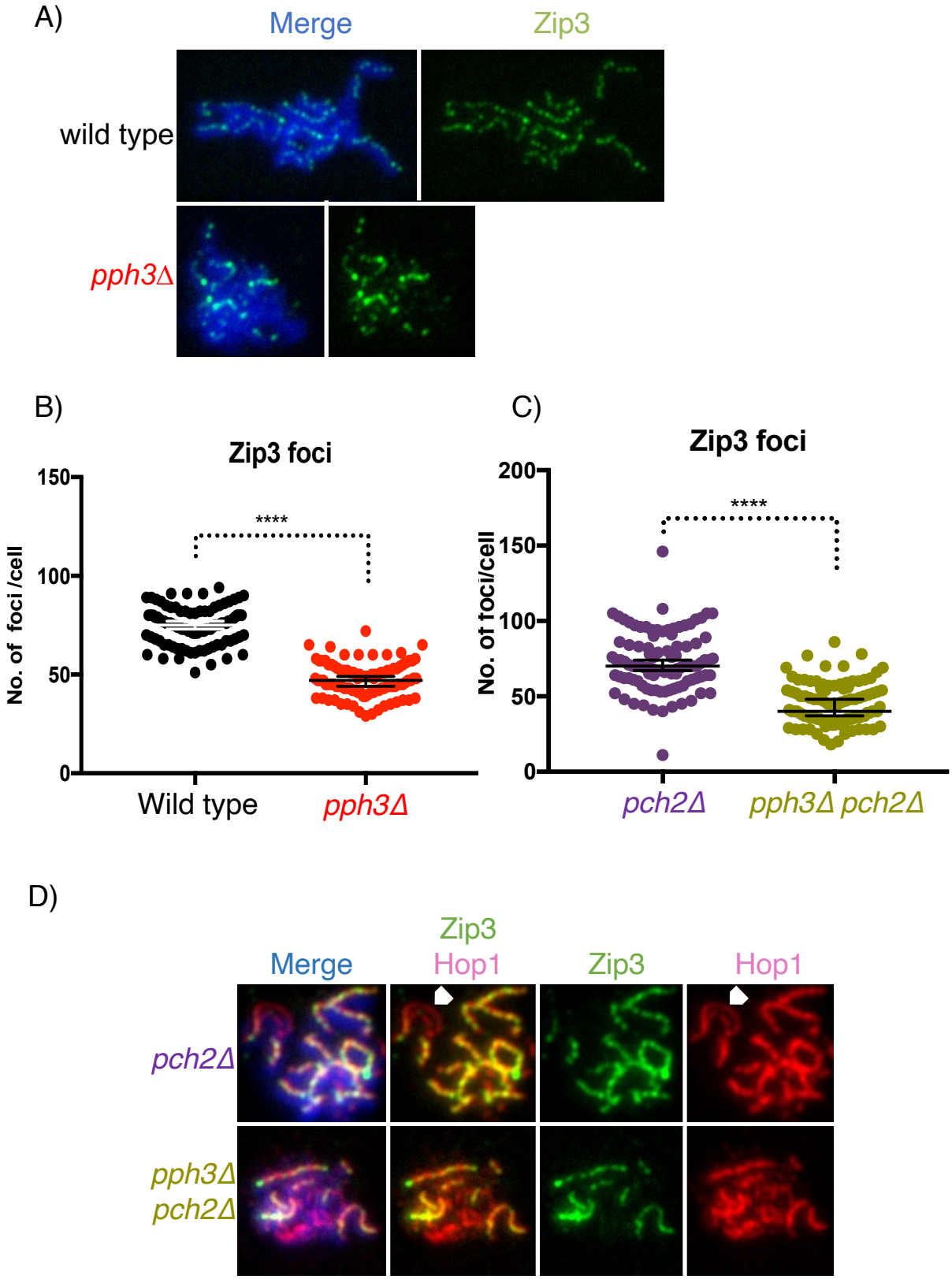
A)
Merge
Zip3
wild type
pph3Δ
B)
Zip3 foci
No. of foci /cell
150
100
50
0
****
Wild type
pph3Δ
C)
Zip3 foci
No. of foci/cell
200
150
100
50
0
****
pch2Δ
pph3Δ pch2Δ
D)
Merge
Zip3
Hop1
Zip3
Hop1
pch2Δ
pph3Δ
pch2Δ

Figure 28. The *pph3* mutants showed a Pch2-independent decrease in the assembly of Zip3 on chromatin.

A) Immunostaining analysis of Zip3 with rabbit-Zip3 antibody on meiotic nuclear spreads was carried out in wild type (black, NKY1303/1543), *pph3Δ* (red, MSY5632/5634) mutants. The representative images overlaid with DAPI (blue), Zip3 (green) at 4 hour after meiosis entry are showed.

B) Distributions of Zip3 foci number per Zip3 focus positive cell in wild type (black, NKY1303/1543), *pph3Δ* (red, MSY5632/5634) mutants at 4 hour after meiosis entry. Over 80 nuclei were analyzed in each strain. Error bars indicate the median ± 95% C.I. (Confidence Interval). Statistically significant difference was determined by Mann-Whitney's U-test using Prism9 software. (****: p value < 0.0001)

C) Distributions of Zip3 foci number per Zip3 focus positive cell in *pch2Δ* (purple, MSY6446/6448) and *pph3Δ pch2Δ* (orange, MSY6417/6419) mutants at 6 hour after meiosis entry. Over 80 nuclei were analyzed in each strain. Error bars indicate the median ± 95% C.I. (Confidence Interval). Statistically significant difference was determined by Mann-Whitney's U-test using Prism9 software. (****: p value < 0.0001)

D) Immunostaining analysis of Zip3 and Hop1 with rabbit anti-Zip3 antibody and guinea pig anti-Hop1 antibody on meiotic nuclear spreads was carried out in *pch2Δ* (purple, MSY6446/6448) and *pph3Δ pch2Δ* (orange, MSY6417/6419) mutants. The representative images overlaid with DAPI (blue), Zip3 (green) and Hop1 (red) at 6 hour after meiosis entry are showed. The ⬟ displays ribosomal DNA region.

Figure 29

A)

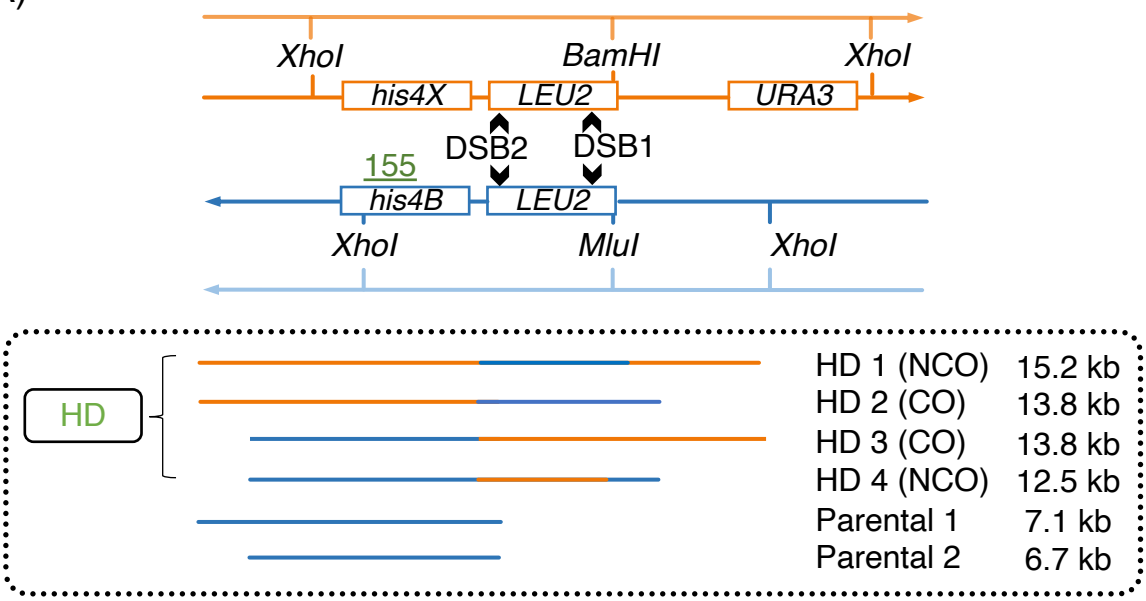
XhoI
BamHI
XhoI
his4X
LEU2
URA3
DSB2
DSB1
155
his4B
LEU2
XhoI
MluI
XhoI
HD
HD 1 (NCO) 15.2 kb
HD 2 (CO) 13.8 kb
HD 3 (CO) 13.8 kb
HD 4 (NCO) 12.5 kb
Parental 1 7.1 kb
Parental 2 6.7 kb

B)

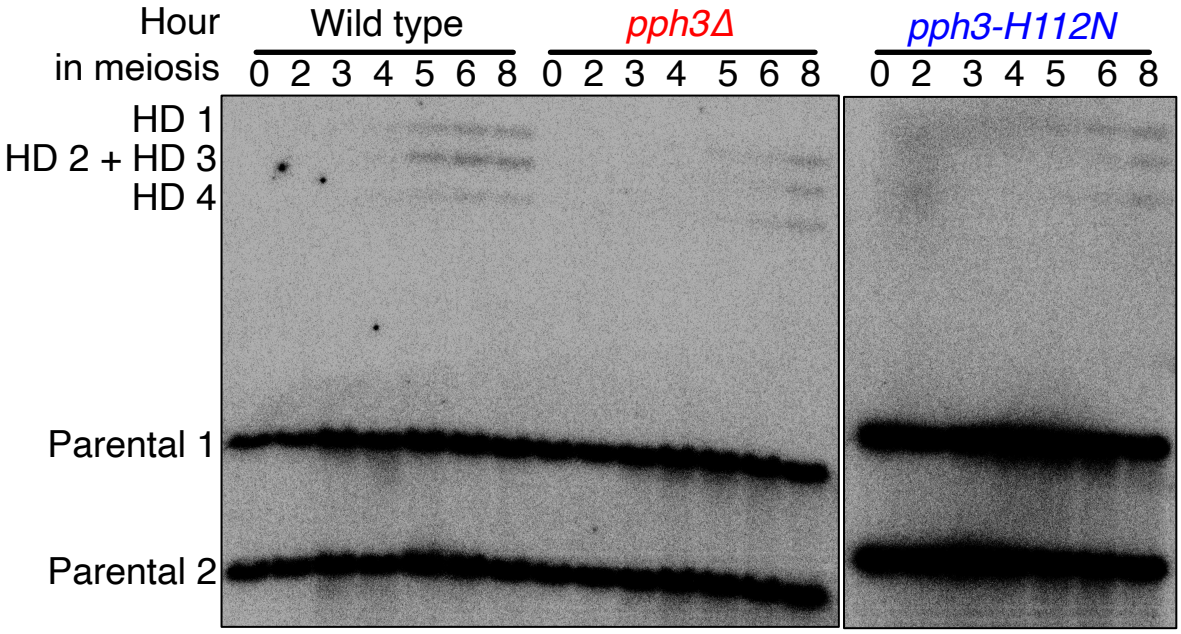
Hour
in meiosis
Wild type
pph3Δ
pph3-H112N
0 2 3 4 5 6 8
0 2 3 4 5 6 8
0 2 3 4 5 6 8
HD 1
HD 2 + HD 3
HD 4
Parental 1
Parental 2

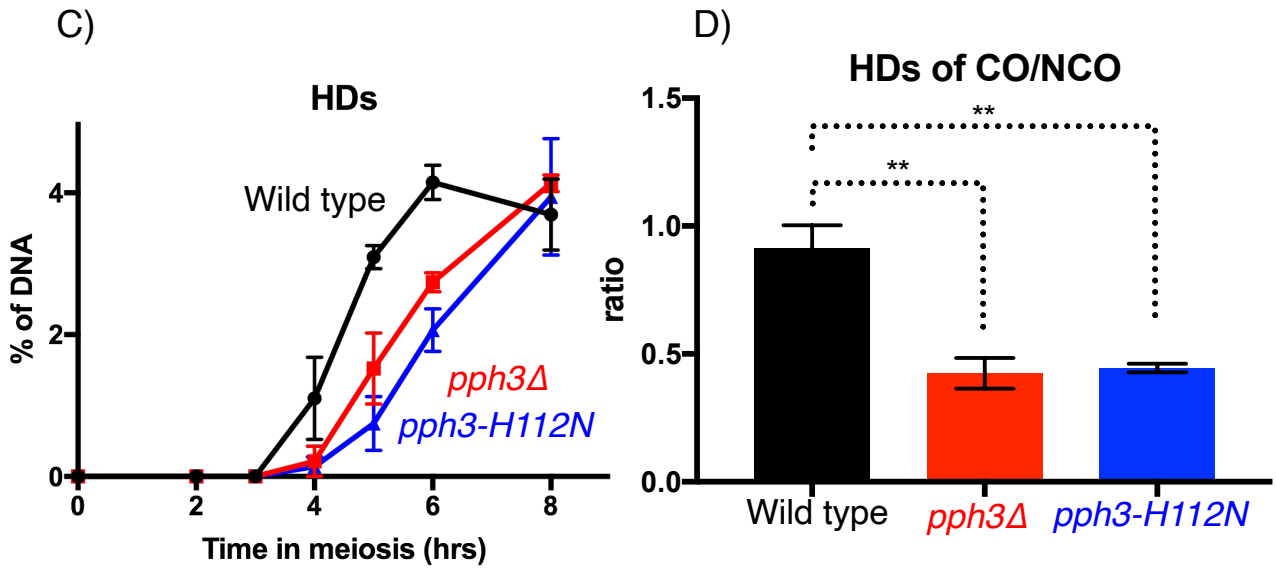

Figure 29. The *pph3* mutants showed decreased crossover formation and increased noncrossover formation in meiotic recombination.

A) Schematics of *HIS4-LEU2* recombination hotspot on chromosome III. The sites of diagnostic *XhoI*, *BamHI* and *MluI* restriction and probe 155 are showed along with the size and identity of diagnostic fragments of heteroduplexes (HDs), parental 1 and Parental 2. The HDs associated with the intermediators of crossover recombination (HD2 and HD3) and noncrossover recombination (HD1 and HD4).

B) Representative images of southern blotting on the detection of HD-associated crossover recombination and noncrossover recombination in wild type (black, NKY1303/1543), *pph3Δ* (red, MSY5632/5634), *pph3-H112N* (blue, MSY6219/6220) mutants *us*ing probe 155 as shown.

C) Graph shows the quantity of total HDs by analyzing the rate of HDs fragments to total DNA signal at the indicated time point in wild type (black, NKY1303/1543), *pph3Δ* (red, MSY5632/5634), *pph3-H112N* (blue, MSY6219/6220) mutants. Error bars show the mean ± S.E.M (standard error of the mean) from over 3 times independent trials.

D) Graph shows the quantitative ratios of crossover-HDs to noncrossover-HDs at peak time point in wild type (black, NKY1303/1543) at 6 hour, *pph3Δ* (red, MSY5632/5634) and *pph3-H112N* (blue, MSY6219/6220) mutants at 8 hour. Error bars indicate the mean ± S.E.M (standard error of the mean) from over 3 times independent trials. Statistically significant differences were determined by paired t-test using Prism9 software. (**: p value < 0.01)

Figure 30

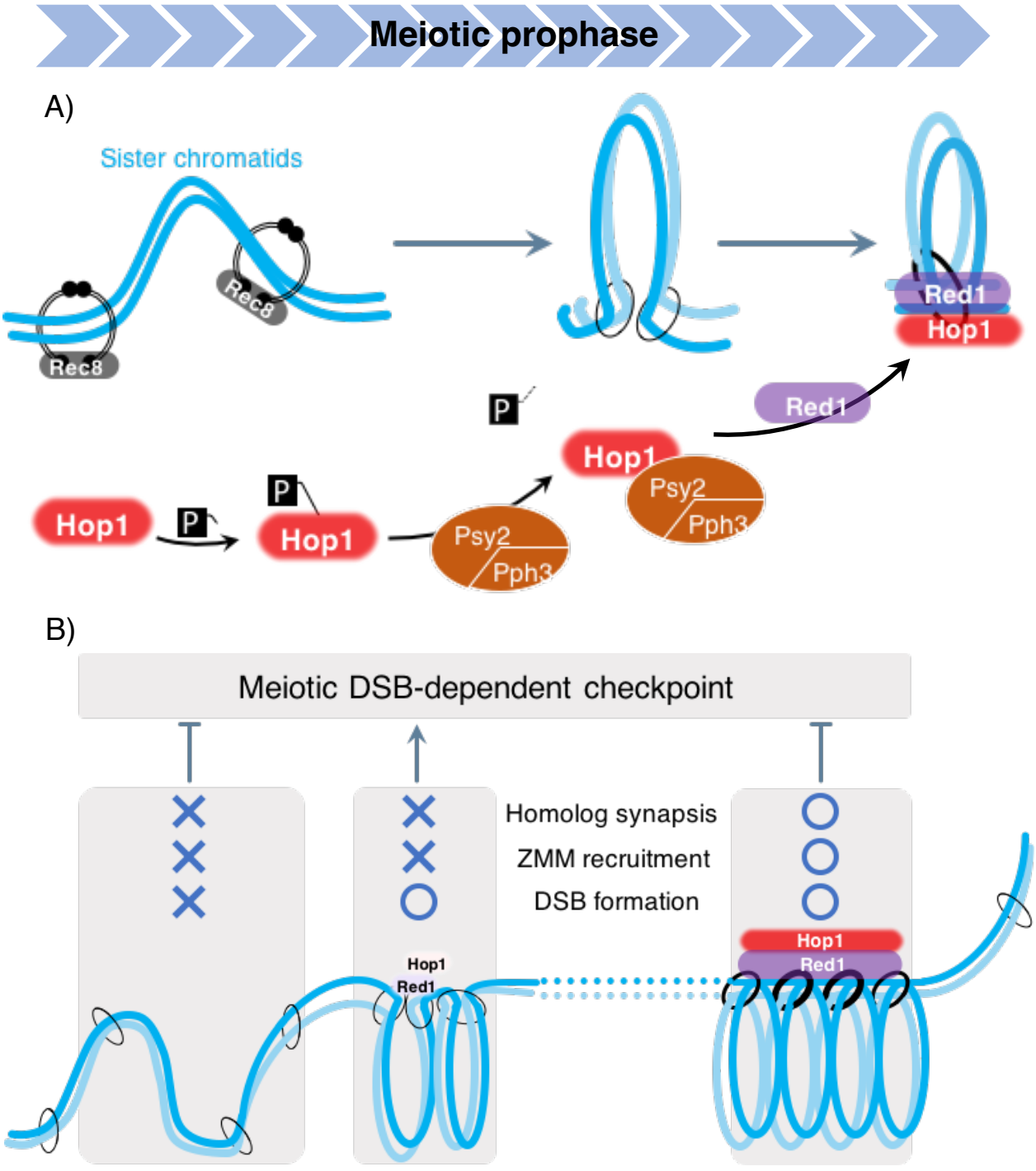

Figure 30. Model of PP4 function in promoting the formation of chromosome axes.

A) A model shows the novel role of PP4 activity in promoting Hop1 and Red1 loading.

B) A model shows defect in *pph3Δ pch2Δ* double mutants. The decreased assembly of Hop1-Red1 caused a defect in the recruitment of ZMM proteins resulting in incomplete synapsis, which activates meiotic checkpoint.